Masterarbeit

Battery Modeling By Means Of Statistical Models

Maria Sendlhofer-Schag

Institut für Signalverarbeitung und Sprachkommunikation
Technische Universität Graz
Vorstand: Univ.-Prof. Dipl.-Ing. Dr. techn. Gernot Kubin

Betreuer und Begutachter: Franz Pernkopf

Graz, im Oktober 2020

Kurzfassung

Bei Hybridfahrzeugen ist die genaue Schätzung des Ladezustandes der Batterie von besonders großer Bedeutung. Im Gegensatz zu reinen Elektrofahrzeugen wird bei Hybridantrieben während des Betriebs die Batterie ständig geladen und entladen. Das Management System der Batterie hat die Aufgabe, die einzelnen Zellen der Batterie in einem ausgeglichenen Ladezustand zu halten um übermäßiges Laden beziehungsweise Entladen zu vermeiden, was einen großen sicherheitsrelevanten Aspekt darstellt. Da der Ladezustand aber keine Größe ist, die direkt messbar ist, muss sie geschätzt werden, was mittels Systemmodellierung erreicht werden kann.

Bei der Systemmodellierung versucht man das Verhalten einer einzelnen Zelle abzubilden. Die Batterie selbst besteht aus vielen solcher Zellen in paralleler und serieller Schaltung. Den Ansatz der statistischen Modellierung mit Hilfe eines Kalman-Filters hat bereits Gregory L. Plett verfolgt, und seine Ergebnisse für Lithium-Ionen-Polymer Batterien sind vielversprechend.

Bei diesem Ansatz wird die Zelle durch ein Zustandsraummodell dargestellt, das sowohl Verhalten als auch dynamische Effekte wie den Hysterese-Effekt modellieren kann. Der Ladezustand der Zelle wird dabei als Systemzustand betrachtet. Ist das Modell mit seinen Parametern ermittelt, kann mit Hilfe des Kalman Filters im ersten Schritt der Systemzustand vorausgesagt und geschätzt werden und in einem zweiten Schritt wird dieser Schätzwert mit Hilfe aktueller Messwerte korrigiert. Für die Berechnungen sind lediglich die Werte des vorhergehenden Zeitschrittes notwendig. Es ist nicht erforderlich, einen umfangreichen zeitlichen Verlauf zu speichern, was ebenfalls ein großer Vorteil ist.

In der vorliegenden Arbeit wird untersucht, ob diese Art der Zellmodellierung auch für andere Arten von Zellchemie-Typen in Lithium-Ionen-Batterien vergleichbare Ergebnisse liefern kann.

Die Daten für Systemidentifikation und Zellmodellierung stammen von Standard Zell-Tests, durchgeführt auf Prüfständen der Magna E-Car (Graz).

Die verschiedenen Zellchemie-Typen eignen sich je nach der Ausprägung der charakteristischen Kennlinie besser oder weniger gut für diese Art der Zustandsschätzung. Wie gut der Kalman-Filter arbeiten kann hängt hauptsächlich davon ab, wie genau sich im Vorfeld die Parameter ermitteln lassen. Die Qualität der geschätzten Parameter wiederum hängt von der Qualität der Testdaten ab - diese sollten möglichst genau und fehlerfrei aufgezeichnet sein, da Fehler bei der Systemidentifikation sonst indirekt in den Parametern mitgeschätzt werden und somit zu systematischen Fehlern bei der späteren Zustandsschätzung führen.

Abstract

An accurate value of a cell's state (i.e. its State of Charge (SOC)) is very important in the field of Hybrid Electric Vehicles (HEVs), since in contrast to Electric Vehicles (EVs) the battery is constantly charged and discharged during use and losing track of the SOC would lead to serious problems within the battery management unit. Unfortunately, SOC cannot be measured directly and therefore has to be estimated. This leads to a point where system modeling plays a role.

The variety of approaches to cell modeling is wide, ranging from simple statistical models to neural nets to complex, physics based models. Using a Kalman Filter (KF) to estimate a systems state has already been tested by Gregory L. Plett and his results working with lithium-ion polymer cells are promising.

This modeling approach is based on state space representations that model behavior and dynamics of the system (i.e. the cell). Detailed insights of the cell are not necessary, dynamic effects like hysteresis and relaxation can easily be taken into account. By taking SOC as a system state, once the model and its parameters are determined, a KF (or an Extended Kalman Filter (EKF) in the case of nonlinear state space equations) is used to predict the state of the system while running and corrects the estimate by exploiting the actual measurements. This only requires the values of the previous time step, there is no need to store more history.

This thesis investigates whether using different kinds of lithium-ion cell chemistries results in similar outcomes. Data for system identification and testing was obtained from standard cell tests performed at Magna E-Car (Graz). The models proposed by Plett were used and nonlinear system identification was done by applying an EKF.

It appears that the KF considered by itself works well but system identification is crucial. Accurate estimates of the system parameters are absolutely essential for satisfying state estimation. Thus carefully determined experimental data is necessary. Otherwise system identification leads to faulty parameters which in turn cause inaccurate state estimation of the model.

STATUTORY DECLARATION

I declare that I have authored this thesis independently, that I have not used other than the declared sources / resources, and that I have explicitly marked all material which has been quoted either literally or by content from the used sources.

....
date (signature)

Acknowledgement

I suppose this page will be the most widely read of the whole work, so I want to use this opportunity to share some thoughts.

It took me years to finally finish this work. And probably it was me who had least faith in myself to do so. Family and close friends kept encouraging me, above all my husband who was often reaping my bad mood in turn (sorry for that!). I feel deep gratitude for you to do so. I know it was exhausting and you felt like fighting windmills. Good news: it's over. Thank you all for having my back.

I also want to thank my supervisor Franz Pernkopf for his support and patience. I know it's not for granted to be allowed to show up after years and find an open door.

To whom I really owe the most are my parents. They always kept focus on good education and I could count on their support whatever studies I would choose. Being raised in a family where this is a very important value, can be hard sometimes but on the long run it facilitates life lot.

We are all privileged to live in a country where education is easy to access, affordable and of high quality. From my experience as a woman in the working world, I am equally paid and I will always find a good job thanks to my education at TUGraz. I know this isn't for granted either and I really do appreciate it.

And last but not least I should be thankful for the lack of places in day nurseries which forced me into educational leave and got me to where I am now.

Graz, 3th october 2020 Maria Sendlhofer-Schag

Contents

List of Figures

List of Tables

Abbreviations

BMS	Battery-Management System
DOD	Depth of Discharge
ECM	Equivalent Circuit Model
EKF	Extended Kalman Filter
ESCM	Enhanced Self-Correcting Model
EV	Electric Vehicle
HEV	Hybrid Electric Vehicle
KF	Kalman Filter
LIB	Lithium-Ion Battery
LiFePO	Lithium-Iron-Phosphate
LiPB	Lithium-Ion Polymer Battery
LiTi	Lithium-Titanate
LUT	Look-Up Table
OCP	Open-Circuit Potential
OCV	Open-Circuit Voltage
OSHM	One-State Hysteresis Model
PPC	Pulse Power Characterization
SCiB	Super Charge Ion Battery
SM	Simple Model
SOC	State of Charge
ZSHM	Zero-State Hysteresis Model

Chapter 1

Introduction

Batteries can not be imagined away these days. They are prevalent in mobile phones, notebooks or other portable devices that ease and comfort our everyday lives. But even more complex applications like an Hybrid Electric Vehicle (HEV) make use of portable power supplies. From perspective of the user, running out of power can range from annoying disruptions of phone calls to loss of work as well as to stranding by the side of the road. Thus knowing the current State of Charge (SOC) is essential, the more precise the better. In the case of hybrid or electric vehicles the information on the current SOC resembles the fuel gauge and the estimate is required as exact as possible.

However, the measurement of a fluid level is much easier than an educated guess of the remaining charge of a battery. But SOC does not only represent the electric fuel gauge, it is also relevant for the battery pack management and safety issues which is even more crucial though not obvious to the user.
Since it can not be measured directly SOC is needed to be estimated. While a rough guesstimate would be sufficient for appliances like mobile phones, the Battery-Management System (BMS) of an HEV makes use of various models to compute an (still inexact) estimate of that quantity.
Those models range from simple statistical models to neural nets to complex, physics-based models [18]. Physics-based models are for instance electrochemical models or equivalent circuit-based models.

In automotive applications the preferred type of battery at this time is the Lithium-Ion Battery (LIB) [1]. Those batteries have the best energy-to-weight ratios, low self-discharge

[1] LIBs are intercalation-based batteries, where intercalation is the term for ions moving in and out of an interstitial site in a lattice structure.

rates when not in use and exhibit no memory effect [2]. The application in an HEV demands large amounts of energy, safe operations, reliability and durability. The BMS that controls the battery is composed of hardware and software to control the charging and discharging processes. This is critical for safety, since LIBs can ignite and burst into flames when incorrectly (over)charged or damaged [5].

1.1 Motivation

The focus of this work is on cell modeling by means of statistical models, in particular based on the principles of the Extended Kalman Filter (EKF). It closely follows the work of Gregory L. Plett who has already successfully built such models for Lithium-Ion Polymer Battery (LiPB) packs (see: Plett [14, 15, 16]). LiPB uses a polymer gel as electrolyte. This type of battery cell is mostly used in handheld devices since it provides high energy density but within the cost of a higher risk of inflammation in case of damage. Those cell types also come with neat cell characteristics, which makes modeling fairly easy. The shape of the Open-Circuit Voltage (OCV) characteristic has big influence on the later estimate. A flat curve may lead to more inaccurate estimates and makes the model prone to errors.

The aim was to achieve comparable results with two different cell chemistries (Lithium-Titanate (LiTi): $Li_4Ti_5O_{12}$ and Lithium-Iron-Phosphate (LiFePO): $LiFePO_4$) which offer lower energy density but are also less likely to explode. The Lithium-Titanate (LiTi)-cells on the one hand show only little hysteresis effect which is good for modeling, the LiFePO-cells on the other hand show high polarization values and moreover the Open-Circuit Voltage (OCV)-characteristic has plateaus and is only linearly increasing within an interval of approximately 12% to 35% SOC. Usually batteries are operated within the range of 20% to 80% of SOC so in the latter case, the shape of the OCV characteristic poses a challenge for the estimate of the SOC. Moreover the data of the LiFePO-pack is highly affected by drift.

Data used for the experiments is drawn from various standard tests of the battery packs on test plants, the packs itself are to be implemented in HEV applications.

[2] Memory effect - also known as lazy battery effect, observed in NiCd (Nickel-Cadmium) rechargeable batteries. The term refers to the loss of capacity when NiCd-cells are repeatedly recharged after being partially discharged (which causes changes in the metallic structure of the charged portions of the nickel electrode), see Cope and Podrazhansky [6].

1.2 Related Work

1.2.1 Approaches to Cell Modeling

There is a wide range of approaches to this topic. Generally speaking modeling means reproducing the relevant parts of a real system to build up an abstract copy of it which can be used for diagnostics and prognostics. The advantage of a model compared to the real system is that since it is an abstraction, it is less complex but accurate enough to investigate the main parameters.

One distinguishes between *white-box* models, *black-box* models and the hybrid form called *grey-box* models.

White-box modeling refers to modeling, where the system and it's structure are well-known but of too complex nature. So the complexity is reduced willingly through abstraction. On the other hand there are systems, where the inner structure is unknown and only the performance and input-/output variables can be monitored. The background and context of the system's interaction are often hard or not to understand. Drawing models from observations, respectively from experimental data is called black-box modeling.

Since the world itself is not only black-and-white, the most common type of model is the grey-box model, where parts of the system are well-known and others are not, nor can every interaction be entirely explained. The resulting model therefore is based on experimental data as well as on insights into the system.

A good overview of various approaches is provided in [13]. The main representatives for modeling cells are briefly explained in the following:

1.2.2 Equivalent Circuit-Based Modeling

Usually in an Equivalent Circuit Model (ECM) the OCV is represented by a high-valued capacitor and the SOC-value is inferred via a OCV-SOC Look-Up Table (LUT) (OCV can be regarded as 'state' of the system). The remainder of the circuit represents the internal resistance of the cell and effects like terminal voltage relaxation. ECMs are based on the physical understanding of the cell structure and chemistry as well as they require a few parameters (like resistance values) which can easily be obtained from experimental data. It is obvious that ECMs are kind of grey-box models. The benefits of this approach is that complicated and intensive computing can be minimized and thus results are obtained quickly. As a drawback, those models can not adapt to influences like cell aging.

Yann Liaw developed a simple ECM [12] for LIBs which is shown in Figure 1.1. R_1 unites all ohmic resistant components and the non-linear components are modeled as the R_2C-circuit, where R_2 unites all non-linear, faradic behavior (charge transfer, redox-related properties, ...). The source and load serve for charging and discharging conditions.

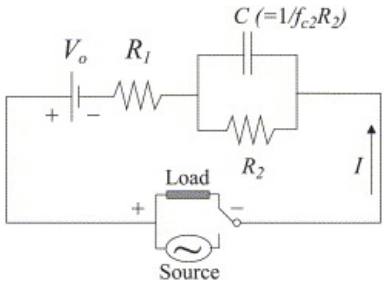

Figure 1.1: Example of a simple ECM (from Liaw et al. [12]).

This model is mainly used for simulation of cell impedance response and discharge behavior.

1.2.3 Electrochemical Modeling

This modeling approach is based on electrochemical principles and is therefore physics-based (based on the insights), although it also requires some offline estimated parameters which are obtained by experimental data. Electrochemical models are supposed to predict the spatially distributed behavior of the cell, like the concentration of lithium ions or the potentials in the electrolyte and the solid electrode. For simplification usually one-dimensional (1D)-spatial models are derived, that represent the dynamics along the horizontal X-axis (see Figure 2.1).

Lithium can be considered to appear in two disjoint states also called *phases*, namely dissolved in the electrolyte and intercalated in the electrode material. Hence lithium occurs at every point along the X-axis either in phase 1 or 2. The dynamics of those phases are described by a set of differential equations where the state parameters at the position x at time t are the current and the electric potential (in the solid electrode as well as in the electrolyte), the molar flux of lithium, the concentration of the electrolyte and the concentration of the solid-phase lithium [5].

1.2.4 Statistical Modeling

Statistical modeling is the object of this work. The methods are based on Kalman Filter (KF) theory. To be able to make use of KFs a discrete-time state-space model of the cell itself is needed. The state-space model consists of two equations: the *state equation* and the *output equation*, i.e:

$$x_k = f(x_{k-1}, u_{k-1}) + w_{k-1} \qquad \text{state equation} \qquad (1.1)$$

$$y_k = g(x_k, u_k) + v_k \qquad \text{output equation} \qquad (1.2)$$

The state of the system x_k at a certain time k is a function of the exogenous system input u_{k-1} and system state x_{k-1} at the previous time step $k-1$ as well as of unmeasured *process noise* w_{k-1}. The corresponding output y_k at time k then is a function of the actual system state x_k and input u_k with additional *measurement noise* v_k.

In contrast to other modeling methods, the cell's SOC is considered to be a fundamental state of the system, not an output variable.

Within a simple basic model the present electric current represents the system's exogenous input and the loaded terminal voltage (note, not the Open-Circuit Voltage (OCV) at rest) is regarded as the system's output. The process noise models the current-sensor error and inaccuracies of the state equation, whereas the measurement noise represents errors of the voltage sensor and inaccuracies of the output equation. SOC is denoted as system state x_k.

But also more complex models are feasible, they only differ in the definitions of x_k, u_k, $f(\ldots)$ and $g(\ldots)$. For example may the vector u_k also contain cell temperature T_k, an estimate of the cell capacity C or an estimate of the cell's internal resistance R_k. Also additional system states can be taken into account, like the level of hysteresis which is typically slowly changing. Adding a hysteresis state to the state equation models these slow transitions. Both functions $f(\ldots)$ and $g(\ldots)$ can be linear as well as non-linear.

Basically the output of a causal system depends on past and present inputs. Considering a system state like in our case SOC, it reflects a summary of all impacts that past inputs had on the system. Hence, the present system output can be regarded as a functional relation of the present system input and present system state only. Its advantage is, that no past input values need to be stored.

A Kalman Filter (KF) is an algorithm used to estimate the time-varying inner states of a dynamic system. It comprises a set of recursive equations that are evaluated at every time step as the system is running. Mainly two computation steps are performed: First a *time update* is calculated to predict the expected state value for the following time index (see Equation 1.1). Second, during the *measurement update* (see Equation 1.2), the estimated output based on the state-estimate of the time update is compared to the physical system output and the difference is seen as output error. More precisely it is named *innovation*, because it is used to adapt the model's state estimate in order to minimize the error and thus it innovates the estimate of the time update. The influence of the correction term itself is adjusted by the *Kalman gain* which can be regarded as the weighing of the innovation.

Since the KF tracks its own error, it provides dynamic error-bounds for the state estimates. This allows an extensive use of the system within save limits. In case of a battery that stands for save operations without over-stressing of the cells.

1.3 Organization of the Work

After a short introduction in Chapter 1, Chapter 2 gives a quick overview of what a Lithium-Ion Battery (LIB) is and clarifies naming conventions. Also a short review on the Discrete Kalman Filter (KF) is provided in Chapter 3.

Chapter 4 discusses the different models used in this work in detail as well as methods for system identification an parameter determination.

Cell Testing and the recorded data are topics of Chapter 5, discussed for both cell chemistries used. The necessary preprocessing of the data is explained as well as the composition of test and training data sets.

Chapter 6 sets focus on the hysteresis effect and how the cell characteristic i.e. OCV curve and hysteresis loops are derived from the given data.

The results of the implementation are finally shown and discussed in Chapter 7.

Chapter 2

Fundamentals

2.1 Principle of a Lithium-Ion Battery

Naming Conventions are important to be clear about frequently-used terms, therefore according to Andrea [1, chap. 1.1] the definitions are:

- Cell: basic element of a battery
- Block: collection of cells (wired parallel, providing greater amount of ampere hours)
- Battery: collections of cells or blocks (wired in series, providing higher voltage)
- Pack (or battery pack): collection of batteries arranged in any series and/or parallel combination

The principle of intercalation-based cells is explained as follows[1]: the four main components are the porous negative electrode, the porous positive electrode, the separator and the electrolyte. The negative electrode is connected to the negative terminal of the cell (contains usually graphite as intercalation material) and the positive electrode is connected to the positive terminal. This electrode can be made of various chemistries, but metal oxides or a blend of multiple metal oxides (like $LiMnO_2$) from which the naming of the cell is derived are most commonly used. The separator is the electrical insulator and is a thin porous medium that inhibits electrons to flow between the positive and negative electrode. The electrolyte is a concentrated solution which serves as an ionic conduction medium where both electrodes and the separator are immersed. Since the separator is porous, ions can pass through it by means of the electrolyte. The Li^+ ions move in response to an electrochemical potential gradient.

[1] Algorithms for Advanced BMS-systems [5]

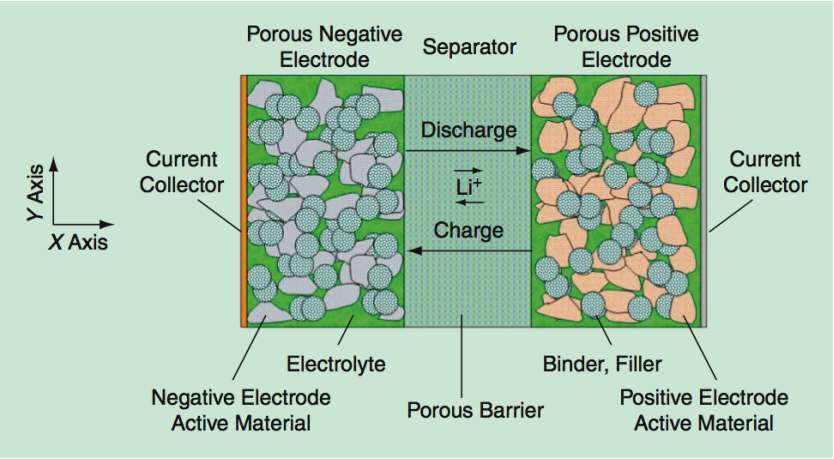

Figure 2.1: The anatomy of an intercalation cell: additional conductive and binder materials in the electrodes hold the electrode together and improve its conductivity (from Chaturvedi et al. [5]).

Figure 2.1 shows the main components of a cell. During discharge, ions are extracted from the negative electrode and intercalate the positive electrode. During charge, the reverse process occurs. The free energy of the lithium inserted in the negative electrode differs from the free energy when placed in interstitials sites of the positive electrode. In fact, the energy of lithium stored in the negative electrode is much higher. Those free energies are known as electrochemical potentials (in $[J/mol]$). Using these potentials, the electrostatic potential (also called the electric potential or electric field potential, in $[J/C]$ or $[V]$) of an electrode can be expressed as a function of the amount of lithium stored in the material or to be more precise as a function of the *utilization* of the electrode, where the term utilization denotes the ratio of the actual to the maximum possible lithium concentration.

The electrostatic potential is also referred to as Open-Circuit Potential (OCP). Both electrodes show OCPs, where the difference between them denotes the OCP of the complete cell. It relates to the rest voltage which is measured between the current collectors, assuming no charging or discharging currents. Alternatively the OCP of a cell is also called OCV.

Intercalation cells show different equilibrium potentials at the same SOC, depending on its recent history - i.e. whether the battery was previously charged (intercalated) or discharged (deintercalated). The OCV following charge is higher than following a discharge pulse at the same SOC. When doing a full discharge followed by a charge cycle the legs of the main hysteresis loop can be measured. These mark the maximum limits of polarization. When cycling round a certain level of SOC, the hysteresis loop takes accordingly smaller shape.

2.2 Relevance of the State Of Charge

In Andrea [1, chap. 1.4] the State of Charge (SOC) of a cell or a battery at a given time is the proportion of the charge available at that point, compared to the total charge available when it is fully charged. It is expressed in percent, from 100% when full to 0% when empty.

It is important to emphasize, that every cell of a battery pack has its own SOC, whereupon the resulting capacity of the whole pack can also be denoted as SOC. In this work the term SOC is mainly used for a single cell since the modeling concerns the cell itself and not the cell compound i.e. the whole battery pack.

When charging or discharging a battery, the battery's ability of accepting or releasing charge is limited by the cell which first reaches a SOC of 100% or 0%. Hence, the charging or discharging process is triggered by the SOC-levels of the single cells instead of the whole pack in order to avoid over-discharge and over-charge, which would harm the cells and pose a risk to the user. More precisely, the cells' voltages are monitored and if the voltage of a cell meets a certain threshold (both for charge and discharge), the cell is assumed to be fully charged or discharged.

It is clear to see, that the battery's capacity depends on the capacities of the cells. If there are severe cell-to-cell imbalances of SOC, the resulting capacity of the battery is very low, up to the extreme case that it becomes nearly useless. In order to maximize the battery's capacity one tends to equalize the SOC-levels of the cells. This is done by so-called balancing algorithms that are implemented within the BMS (Cao et al. [4]):

- Charge Shuttling among the cells (Active Balancing)
- Wasting Energy of the mostly charged cell with dissipative resistors (Passive Balancing)
- Selectively Shunting the charging current around already fully charged cells via shunt resistors (End-Of-Charge Method)

Electric Vehicle (EV) batteries tend to be fully charged between the use cycles in contrast to HEV-applications, where a fully charged battery would diminish the charge acceptance capability (e.g. through regenerative braking). On the other hand a system at a level close to 0% SOC, which is definitely ready to accept energy, is not able to deliver any. Therefore in HEVs the battery pack is usually maintained at some intermediate SOC-level around 40% to 80%. That marks save boundaries providing enough headroom to accept regenerative power on the one hand and on the other hand the lower limit assures high power discharge capabilities for boosting and moreover lengthens the battery life since too deep Depth of Discharge (DOD) is avoided.

Another reason for keeping the pack in the medium range of SOC is that in this region most cell chemistries show nearly linear relations between the open circuit terminal voltage and the SOC. The OCV-characteristic (OCV vs. SOC) can be seen as the fingerprint of a cell's chemistry and plays a very important role in cell modeling (for detailed explanation see chapter 6). When a cell is allowed to rest for a longer period of time, its terminal voltage decays to the OCV, therefore a simple approach for getting a rough SOC estimate would be using the OCV- characteristic as a LUT.

2.2.1 Benefits of an accurate State Of Charge estimation

A battery pack takes several advantages of an accurate SOC estimate [Plett [14]]:

- *Longevity* of the battery pack, due to avoidance of over-discharge and over-charge (taking account of the differing SOC-levels of the cells).
- *Performance,* by knowing the constraints for over-discharge and over-charge, one can aggressively use the entire pack capacity.
- *Reliability,* good SOC estimators are independent of the driving profile.
- *Density,* smaller and lighter packs are feasible, since, due to accurate information on battery state and SOC, extensive use within design limits becomes possible (no "over-engineering" is needed).
- *Economy,* costs can be reduced due to small and reliable systems.

2.2.2 Influences on State Of Charge

One may think that simple coulomb counting, current integration or voltage metering (OCV characteristic as LUT) alone could provide a satisfying SOC estimate. But SOC is also highly influenced by other quantities than the input current, which must not be neglected. In order to achieve accurate estimates of the SOC it is necessary to pay attention to these influencing factors, both during extensive testing of the pack and during cell modeling.

The most important factors that have an impact on the cell's capacity and further on its SOC are discussed in the following:

First of all capacity varies significantly with *temperature* and *cell aging* causes a decrease of the capacity over time.

Charge and discharge rates have an impact on the SOC because of the electrochemical actions inside the cell: it takes them finite time to complete. This is apparent when

considering short term charging and discharging pulses. By the time the discharge pulse occurs, the chemical effect of the preceding charging pulse may not be completed yet.

Last but not least are LIBs subject to *hysteresis effects*: The OCV following a charge is higher than the OCV following a discharge pulse at the same SOC (see also Chapter 6).

Self discharge at rest due to the drain of built-in voltage monitoring circuits and the chemical constituent parts is very low for LIBs and can therefore be neglected. Moreover battery packs in HEVs are unlikely to rest for weeks or months.

Chapter 3

Introduction Of Discrete Kalman Filter

3.1 Short Review

Greg Welch and Gary Bishop are well-known for their seminal paper titled 'An Introduction to the Kalman Filter' [19]. In this section a short review on that topic is given. The notations are coincident, but in contrast to Welch and Bishop the driving input u_k is also accounted for in the output equation which is similar to the definition of [14].

In case of a linear system, Equations (1.1) and (1.2) can be rewritten in matrix notation as:

$$x_k = Ax_{k-1} + Bu_{k-1} + w_{k-1} \tag{3.1}$$

$$y_k = Cx_k + Du_k + v_k \tag{3.2}$$

w_k and v_k are white Gaussian noise, assumed to be independent and show normal probability distributions. Q and R represent the *process noise covariance* and *measurement noise covariance*, i.e.:

$$p(w) \sim \mathcal{N}(0, Q),$$
$$p(v) \sim \mathcal{N}(0, R).$$

The matrices A and B relate the previous state and input to the current state, C maps the state to the measurement (output of the system) and D relates the input directly to the output, all matrices together describe the dynamics of the system. Note, that these matrices may possibly change within time but for better readability the subscript k is neglected.

As already mentioned in 1.2.4, a KF consists of two major computing parts at a time step k: the *time update* and the *measurement update* which are also named *prediction step* and *correction step*. This can be regarded as a form of feedback control: First, a system state is estimated. Afterwards the filter gets a feedback in form of the (noisy) measurement and based on that feedback the filter corrects its estimate. This is shown in Figure 3.1.

In order to be able to distinguish between these estimates, the terms *a priori* estimate i.e. the estimate of x_{k-1} and the measurement y_{k-1} are known, and *a posteriori* estimate, i.e. y_k is known, are established. The a priori estimates are denoted by a super minus, whereas the a posteriori estimates are denoted by a super plus: $\hat{x}_k^-$, $\hat{x}_k^+$. The hat itself indicates that the value is an estimate.

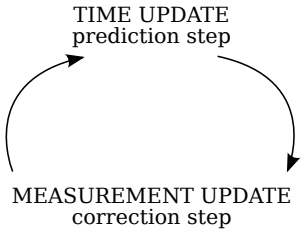

Figure 3.1: The KF iterates through prediction and correction step.

We define the estimate errors e_k^-, e_k^+ and the corresponding covariances P_k^-, P_k^+ as:

$$e_k^- \equiv x_k - \hat{x}_k^-, \quad P_k^- = E[e_k^-, e_k^{-T}], \tag{3.3}$$

$$e_k^+ \equiv x_k - \hat{x}_k^+, \quad P_k^+ = E[e_k^+, e_k^{+T}], \text{ where } E \text{ denotes the expected value.} \tag{3.4}$$

The *Kalman gain* or *blending factor* K is a factor that minimizes the a posteriori error covariance (3.4) in order to improve the estimate. The derivation of K is not trivial and there are more than one possible resulting forms. A common one is given by:

$$K_k = \frac{P_k^- C^T}{C P_k^- C^T + R}. \tag{3.5}$$

The gain K is later used to weigh the *innovation* (see Equation (3.9)) i.e. the difference between the actual measurement y_k and the measurement prediction $Cx_k^- + Du_k$. It is easy to see that the weighting depends on the measurement noise covariance R: if R approaches zero, which allows the assumption of a very accurate measurement, K increases and therefore weights the innovation more heavily. This can be interpreted as that the measurement becomes more trustworthy and the predicted value is trusted less. On the other hand, if the a priori error covariance P_k^- approaches zero, this would indicate a very

accurate estimate and therefore the estimate is trusted more while the impact of the actual measurement decreases.

The five equations of the discrete KF-algorithm resemble a predictor-corrector algorithm, initial estimates for $\hat{x}_{k-1}^{+}$ and P_{k-1}^{+} are required:

$$\hat{x}_k^- = A\hat{x}_{k-1}^+ + Bu_{k-1}, \tag{3.6}$$
$$P_k^- = AP_{k-1}^+A^T + Q, \tag{3.7}$$
$$K_k = {}^{P_k^-C^T}/_{CP_k^-C^T+R}, \tag{3.8}$$
$$\hat{x}_k^+ = \hat{x}_k^- + K_k[y_k - (C\hat{x}_k^- + Du_k)], \tag{3.9}$$
$$P_k^+ = (I - K_kC)P_k^-. \tag{3.10}$$

Equations (3.6) and (3.7) constitute the time update (predictor step) and equations (3.8) - (3.10) form the measurement update (correction step). The filter cycles through the steps in a recursive manner. But no actual recursion needs to be computed, neither past state nor input values need to be stored since they are indirectly available through the a posteriori estimates which are projected to the next iteration. This makes implementations of the KF very feasible A, B, C and D are taken from (3.1) and (3.2), Q and R are the covariances of the noise processes. The actual measurement is taken before computing the a posteriori estimate $\hat{x}_k^+$. A detailed and profound derivation of the KF and its equations based on the probabilistic origins and principles of system theory can be found in [3].

3.2 Extended Kalman Filtering for Nonlinear Processes

If the state and/or the output equations are non-linear, Kalman filtering as presented above can not be applied. Linearization has to be done for the current estimate using the partial derivatives of the non-linear functions $f(\ldots)$ and $g(\ldots)$ with respect to x. State and output equation are defined as in (1.1) and (1.2):

$$x_k = f(x_{k-1}, u_{k-1}) + w_{k-1},$$
$$y_k = g(x_k, u_k) + v_k.$$

$f(\ldots)$ and $g(\ldots)$ can be approximated by a first order Taylor series expansion[1]

$$f(x_k, u_k) \approx f(\hat{x}_k, u_k) + \left.\frac{\partial f(x_k, u_k)}{\partial x_k}\right|_{x_k=\hat{x}_k} (x_k - \hat{x}_k), \text{ and} \tag{3.11}$$

$$g(x_k, u_k) \approx g(\hat{x}_k, u_k) + \left.\frac{\partial g(x_k, u_k)}{\partial x_k}\right|_{x_k=\hat{x}_k} (x_k - \hat{x}_k). \tag{3.12}$$

The partial derivates are defined as $\hat{A}_k$ and $\hat{C}_k$ (which are Jacobian matrices):

$$\hat{A}_k = \left.\frac{\partial f(x_k, u_k)}{\partial x_k}\right|_{x_k=\hat{x}_k}, \tag{3.13}$$

$$\hat{C}_k = \left.\frac{\partial g(x_k, u_k)}{\partial x_k}\right|_{x_k=\hat{x}_k}. \tag{3.14}$$

Substituting Equation (1.1) and (1.2) into (3.11) and (3.12) and using $\hat{A}_k$ and $\hat{C}_k$ leads to:

$$x_k \approx \hat{A}_{k-1}x_{k-1} + \underbrace{f(\hat{x}_{k-1}, u_{k-1}) - \hat{A}_{k-1}\hat{x}_{k-1}}_{I} + w_{k-1}, \tag{3.15}$$

$$y_k \approx \hat{C}_k x_k + \underbrace{g(\hat{x}_k, u_k) - \hat{C}_k\hat{x}_k}_{II} + v_k. \tag{3.16}$$

The marked terms I and II are not functions of x_k but of its estimate and they replace the terms Bu_{k-1} and Du_k in comparison to the Equations in (3.1) and (3.2), which were used to deduce the standard KF from.

The whole algorithm adapted for the EKF is summarized as follows:

$$\hat{x}_k^- = f(\hat{x}_{k-1}^+, u_{k-1}) \tag{3.17}$$

$$P_k^- = \hat{A}_{k-1}P_{k-1}^+\hat{A}_{k-1}^T + Q \tag{3.18}$$

$$K_k = {}^{P_k^-\hat{C}_k^T}/_{\hat{C}_k P_k^- \hat{C}_k^T + R} \tag{3.19}$$

$$\hat{x}_k^+ = \hat{x}_k^- + K_k[y_k - g(\hat{x}_k^-, u_k)] \tag{3.20}$$

$$P_k^+ = (I - K_k\hat{C}_k)P_k^- \tag{3.21}$$

The definitions are very similar to (3.6) - (3.10). For the state and output estimate the non-linear functions are used and the matrices A and C are replaced by $\hat{A}_k$ and $\hat{C}_k$.

[1] assumed $f(x)$ is differentiable at the point x_0, the Taylor series expansion is:
$f(x) = f(x_0) + \frac{f'(x_0)}{1!}(x - x_0)^1 + \frac{f''(x_0)}{2!}(x - x_0)^2 + \ldots + \frac{f^{(n)}(x_0)}{n!}(x - x_0)^n + R_n(x)$.
The linearization of the function $y = f(x)$ at an operation point $P_0(x_0, y_0)$ (which is from the geometrical point of view the approximation of the function by its first derivate) is denoted as:
$f(x) \approx f(x_0) + f'(x_0)(x - x_0)$, [2, chap. 15.1.3].

3.3 Extended Kalman Filtering for System Identification

In this work, EKF is used to identify parameters of the models if the parameters are not linear. If the parameters are linear the problem can be solved straightforward by least-squares estimation [15]. At this point this kind of application of EKF is discussed in general, independently of any concrete system model. The appliance to a certain model depends basically on the adaptation of Equation (3.24).

For system identification the EKF is used as an observer of the parameters of the system models. The parameters are denoted by Θ and the non-linear state-space model is adapted in a way, that Θ becomes the 'state' i.e. vector of states which has to be estimated:

$$\Theta_k = \Theta_{k-1} + r_{k-1}, \tag{3.22}$$

$$d_k = g(x_k, u_k, \Theta_k) + e_k. \tag{3.23}$$

r_k is fictitious white Gaussian noise and represents small perturbations, since model parameters might change slowly over time. Moreover by adding noise, the established uncertainty of the estimate (even if the parameters are assumed constant) allows the algorithm to adapt to $\hat{\Theta}$. Function $g(\ldots)$ is the (non-linear) output equation of the system model, e_k again models sensor noise as well as modeling errors and d_k is the system output which, computed with regard to the estimated parameters $\hat{\Theta}$, is compared to the measured cell output y_k in order to adapt the parameters and minimize the estimation error. The functionality of the algorithm is the same as before, merely some equations slightly change in their definition. For easier legibility the error covariance matrices of r_k and e_k are denoted according to the previous derivation of the EKF as $\tilde{Q}$ and $\tilde{R}$.

According to (3.14):

$$\hat{C}_k^{\Theta} = \left.\frac{dg(x_k, u_k, \Theta)}{d\Theta}\right|_{\Theta=\hat{\Theta}_k^-}. \tag{3.24}$$

Similar as in (3.17) to (3.21) we have the equations for the EKF for system identification as follows:

$$\hat{\Theta}_k^- = \hat{\Theta}_{k-1}^+, \tag{3.25}$$

$$P_k^- = P_{k-1}^+ + \tilde{Q}, \tag{3.26}$$

$$K_k^{\Theta} = {}^{P_k^-(\hat{C}_k^{\Theta})^T}/_{\hat{C}_k^{\Theta} P_k^- (\hat{C}_k^{\Theta})^T + \tilde{R}}, \tag{3.27}$$

$$\hat{\Theta}_k^+ = \hat{\Theta}_k^- + K_k^{\Theta}[y_k - g(x_k, u_k, \hat{\Theta}_k^-)], \tag{3.28}$$

$$P_k^+ = (I - K_K^{\Theta}\hat{C}_k^{\Theta})P_k^-. \tag{3.29}$$

Chapter 4

Statistical Approach for Cell Modeling

As already mentioned in this work we focus on the papers of Gregory L. Plett [14, 15, 16]. We are interested in applying these models for different cell chemistries and investigate their performance. The models are left unchanged in order to be able to compare the results directly. All models are equal in the sense that they are state-space models, where SOC is (amongst others) regarded as a state of the system. In Table 4.1 on page 34 the state-space equations of the models that were evaluated are listed and summarized.
But before, each model is introduced in detail in the following sections.

4.1 Simple Model

The Simple Model (SM) is specified as:

$$z_k = z_{k-1} - \left(\frac{\eta \Delta t}{C_n}\right) i_{k-1}, \tag{4.1}$$

$$y_k = \mathrm{OCV}(z_k) - R i_k, \tag{4.2}$$

where z_k denotes the *system state (SOC)*, i_k represents the *system input (current)*, η describes *coulombic efficiency* and C_n: *nominal capacity*, y_k represents the *system output (predicted cell terminal voltage)*, R describes the *internal resistance* of the cell.

The Simple Model (SM) is the most basic model and may be intuitively understood. The state equation (4.1) is based on the formula that states, that the electric charge which is transferred in the period t_1 to t_2 equals the integral of the current $i(t)$ over that period: $Q = \int_{t_1}^{t_2} I \, \mathrm{d}t$ (see [9, chap M.2]). Assuming an adequate small sampling period and within that a constant current i_k, the expression can be discretized by the following rectangular

approximation [2, chap. 12]: $Q_k = i_k \Delta t$.

The second term of Equation (4.1) calculates the charge weighted by the coulombic efficiency η which indicates the efficiency of the transferred charge with which the chemical reaction inside the cell is caused. Both, LiTi-cells and LiFePO-cells have a coulombic efficiency of 0.9999 for charging as well as for discharging currents[1]. In order to obtain an expression of SOC the value is related to the nominal capacity C_n. Therefore the overall state value comprises the state value of the previous time step added up with the estimated value of the current sampling interval Δt.

The output equation (4.2) simply uses the OCV-characteristic as a LUT. This rough first estimate is corrected by the term Ri_k where R denotes the inner resistance of the cell.

It might contradict intuition that the correcting term in (4.2) as well as the second term in (4.1) are actually subtracted from the first terms. This is because Plett's definition of the instantaneous cell current is negative for charging and positive for discharging. Therefore in the case of charging considering a negative signed i_k the SOC increases as one expects and the estimated output voltage becomes greater than the estimate taken from the LUT, which also fully complies with what we know about the hysteresis.

4.2 Zero-State Hysteresis Model

The Zero-State Hysteresis Model (ZSHM) is specified as:

$$z_k = z_{k-1} - \left(\frac{\eta \Delta t}{C_n}\right) i_{k-1}, \tag{4.3}$$

$$y_k = \mathrm{OCV}(z_k) - Ri_k - s_k M(z_k), \tag{4.4}$$

where again as in Section 4.1 the variables denote the following: z_k: *system state (SOC)*, i_k: *system input (current)*, η: *coulombic efficiency*, C_n: *nominal capacity*, y_k: *system output (predicted cell terminal voltage)*, R: *internal resistance of cell*. In addition s_k describes the *signum* of i_k and $M(\cdot)$ marks the *maximum polarization*.

The drawback of the SM is the fact that it doesn't factor-in the impact of the hysteresis[2]. A simple approach to tackle this issue is to check the sign of the instantaneous current and switch to the corresponding function i.e. 'leg' of the major hysteresis loop (for example the major hysteresis loop of LiFePO-cells is shown in Figure 6.5). This is accounted for in Zero-State Hysteresis Model (ZSHM). Since no additional state for hysteresis is introduced, the model is named *Zero*-State Hysteresis Model (in contrast to the One-State Hysteresis Model (OSHM) in Section 4.3).

[1] personal conversation with Klaus Hochgatter, chemist at Magna E-Car, 2011.
[2] For a detailed explanation of the hysteresis effect and its origins see Chapter 6.

The state equation of the ZSHM is the same as for the SM, since no additional state is required. Merely the output equation is modified by adding the term $s_k M(z_k)$ which represents the offset due to hysteresis. s_k is the sign of i_k, therefore its value is 1 for positive (discharging) and -1 for negative currents (charging). In the case of rest periods $s_k = s_{k-1}$, which means it is kept in mind whether the current of the preceding time step was a charging or discharging one. $M(\cdot)$ denotes the maximum hysteresis, more precisely half the difference between the two legs of the major hysteresis loop. This is also called the cell's *polarization voltage*. Thus the polarization voltage is added or subtracted to the estimated cell voltage depending on the sign of the current.

4.3 One-State Hysteresis Model

The polarization voltage as introduced in Section 4.2 leads to a kind of worst case estimate since it refers to the maximum deviance of the output voltage due to hysteresis effects. The real deviation of the terminal voltage is more likely to be smaller, since the cells are charged and discharged continuously and the hysteresis can not be expected to develop to its maximum at each time step. In fact the major hysteresis loop only takes its shape in the case of a full charge followed by a full discharge. Under everyday conditions shorter periods of partial charge are followed by periods of partial discharge and vice versa. Therefore instead of the major loop, minor hysteresis loops occur. Furthermore supposing the polarization to flip its sign according to the input current is a crude assumption. It rather decays slowly from one leg to the other. Therefore the hysteresis effect suggests itself to rather influence the output as a system state depending on the previous time step than to have an impact as a fixed value which is summed up to the output measurement. Considering the hysteresis value as additional system state distinguishes the OSHM from the ZSHM (Section 4.2) although both are designed to model hysteretic behavior. The therefore introduced hysteresis state $h(z,t)$ is not a differential equation in time, but in SOC, where $\dot{z} = dz/dt$. Then the hysteresis state can be expressed as

$$\frac{dh(z,t)}{dz} = \gamma \, sgn(\dot{z})(M(z,\dot{z}) - h(z,t)), \tag{4.5}$$

where $M(z,\dot{z})$ is a function which describes the maximum polarization with regard to hysteresis as a function of SOC and the rate-of-change of SOC. Note, within the ZSHM of the previous Section 4.2, the maximum polarization is considered to be a constant value. The term $M(z,\dot{z}) - h(z,t)$ relates to the characteristic that the rate-of-change of the hysteresis voltage is proportional to the distance from the major hysteresis loop, i.e. an exponential decay of voltage to the major loop. This rate of decay is tuned by γ (the *hysteresis rate constant*), a positive constant where the *signum* function ensures the equation

to be stable for both, charge and discharge. Since the state space models are differential equations in time (not SOC), the hysteresis state has to be modified by multiplying both sides of Equation 4.5 with $\frac{dz}{dt}$:

$$\frac{\mathrm{d}h(z,t)}{\mathrm{d}z}\frac{\mathrm{d}z}{\mathrm{d}t} = \gamma\ sgn(\dot{z})(M(z,\dot{z}) - h(z,t))\frac{\mathrm{d}z}{\mathrm{d}t}. \tag{4.6}$$

The change of SOC with respect to t, $\frac{\mathrm{d}z}{\mathrm{d}t}$, is nothing else than $-(\eta\, i(t)/C_n)$ (see also the discussion of Equation (4.1) in section 4.1). Using $\dot{z}\ sgn(\dot{z}) = |\dot{z}|$, equation (4.6) can be rewritten to

$$\dot{h}(t) = \left|\frac{\eta\ i(t)\gamma}{C_n}\right| M(z,\dot{z}) - \left|\frac{\eta\ i(t)\gamma}{C_n}\right| h(t). \tag{4.7}$$

Assuming $i(t)$ and $M(z,\dot{z})$ are constant over the sample period Δt, equation (4.7) can be discretized using standard techniques[3] to

$$h_{k+1} = exp\left(-\left|\frac{\eta\ i_k\gamma\ \Delta t}{C_n}\right|\right) h_k + \left(1 - exp\left(-\left|\frac{\eta\ i_k\gamma\ \Delta t}{C_n}\right|\right)\right) M(z,\dot{z}). \tag{4.8}$$

For better readability Equation (4.8) is shortened by substituting $F(i_k)$ for the term $exp(\cdot)$, with

$$F(i_k) = exp\left(-\left|\frac{\eta\ i_k\gamma\ \Delta t}{C_n}\right|\right), \tag{4.9}$$

where η describes the *coulombic efficiency*, C_n the *nominal capacity*, γ refers to the *hysteresis rate constant* and Δt is the *sampling interval*. This is pasted into the state equation (Equation 4.10) and the output equation is extended by the actual hysteresis state (which replaces the rough hysteresis voltage estimate of the ZSHM), see Equation 4.11.

Thus the One-State Hysteresis Model (OSHM) is specified as:

$$\begin{bmatrix} h_k \\ z_k \end{bmatrix} = \begin{bmatrix} F(i_{k-1}) & 0 \\ 0 & 1 \end{bmatrix} \begin{bmatrix} h_{k-1} \\ z_{k-1} \end{bmatrix} + \begin{bmatrix} 0 & (1 - F(i_{k-1})) \\ -\frac{\eta\Delta t}{C_n} & 0 \end{bmatrix} \begin{bmatrix} i_{k-1} \\ M(z,\dot{z}) \end{bmatrix}, \tag{4.10}$$

$$y_k = \mathrm{OCV}(z_k) - Ri_k + h_k, \tag{4.11}$$

where within the vector containing the system states z_k denotes SOC and h_k the *hysteresis voltage*. i_k refers to the *system input (current)*, $F(i_k)$ is defined as in Equation (4.9). $M(\cdot,\cdot)$

[3] Plett [15] doesn't go into detail which techniques have been used, but I suppose the matrix exponential $\frac{d}{dt}e^{At} = Ae^{At} = e^{At}A$ has been applied, such that $\dot{x}(t) = Ax(t) + Bu(t)$ by premultiplying can be rewritten to $e^{-At}\dot{x}(t) = e^{-At}Ax(t) + e^{-At}Bu(t)$. Then integrating leads to the solution of the continuous equation: $x(t) = e^{At}x(0) + \int_0^t e^{A(t-\tau}Bu(\tau)d\tau$ which can be discretized assuming u constant during each time step to $x[k+1] = e^{AT}x[k] + A^{-1}(e^{AT} - I)Bu[k]$.

denotes the *maximum polarization* as a function of SOC, η describes *coulombic efficiency* and C_n *nominal capacity*. The predicted cell terminal voltage is described by the *system output* y_k, R shows the *internal resistance of the cell*.

4.4 Enhanced Self-Correcting Model

What is referred to as relaxation effect describes the phenomenon that when a cell is allowed to rest (time constants between pulsed currents), it takes some time for the voltage to completely relax to its rest voltage, i.e. convergence to its steady-state level. Those time constants can be described as rest periods where the output voltages y_k converges to OCV as well as constant current charge or discharge periods.
The relaxation effect can be implemented as low-pass filter on i_k. The aim is to achieve a model that forces y_k to converge to OCV for rest or OCV $-Ri_k$ for a constant charging / discharging current.

Meeting this requirements, the output equation needs to have the form

$$y_k = \underbrace{\mathrm{OCV}(z_k)}_{fn(z_k)} + \underbrace{h_k}_{fn(z_k,i_k)} + \underbrace{filt(i_k) - Ri_k}_{fn(i_k)}, \tag{4.12}$$

where $fn(z_k)$ and $fn(z_k, i_k)$ describe the long-term DC-level like a bias to the output and $fn(i_k)$ contribute the short-term variation around the long-term level.

From this, two criteria can be deduced for the filter:

1. The output of the filter $filt(i_k)$ has to be zero after a long rest period i.e. $y_k \to \mathrm{OCV} + h_k$.

2. The output of the filter $filt(i_k)$ has to converge to zero during constant charge / discharge i.e. that $y_k \to \mathrm{OCV} + h_k - Ri_k$.

The first criterion is met by using a stable linear filter[4]. To satisfy the second criterion the filter should have zero DC-gain.

The state-space form of the filter itself is

$$f_k = A^{\mathrm{f}} f_{k-1} + B^{\mathrm{f}} i_{k-1}, \tag{4.13}$$

$$y_k^{\mathrm{f}} = G^{\mathrm{f}} f_k, \tag{4.14}$$

[4]For asymptotic stability the eigenvalues (i.e. the poles of the system) have to be located inside the unit circle, see [10, chap. 7.6.2]

where f_k is the filter state, A^{f} denotes the state-transition matrix, B_{f} the input matrix and G_{f} the output matrix of the filter. The above equations can easily be integrated into the state-space equations of the model as shown in Equations (4.15) and (4.16).

The state-space equations of the Enhanced Self-Correcting Model (ESCM) are specified as:

$$\begin{bmatrix} f_k \\ h_k \\ z_k \end{bmatrix} = \begin{bmatrix} diag(\alpha) & 0 & 0 \\ 0 & F(i_{k-1}) & 0 \\ 0 & 0 & 1 \end{bmatrix} \begin{bmatrix} f_{k-1} \\ h_{k-1} \\ z_{k-1} \end{bmatrix} + \begin{bmatrix} 1 & 0 \\ 0 & (1 - F(i_{k-1})) \\ -\frac{\eta \Delta t}{C_n} & 0 \end{bmatrix} \begin{bmatrix} i_{k-1} \\ M(z, \dot{z}) \end{bmatrix}, \tag{4.15}$$

$$y_k = \mathrm{OCV}(z_k) - Ri_k + h_k + Gf_k. \tag{4.16}$$

The additional system state f_k denotes the *relaxation filter state* z_k and h_k remain the system states *SOC* and *hysteresis voltage*, i_k represents the *system input (current).* α contains the *filter poles*, $F(i_k)$ is explained in Equation 4.9. $M(\cdot, \cdot)$ shows *maximum polarization*, η marks the *coulombic efficiency* and C_n the *nominal capacity.* y_k again represents the *system output (predicted cell terminal voltage)* and R marks the *internal resistance* of the cell, G states the *filter gain matrix* as introduced in Equation 4.14.

4.4.1 Filter Poles

The poles of the filter are found via the eigenvalues of A^{f} [5]. The filter is stable if all poles are located within the unit circle, i.e. $max\left|eig(A^{\mathrm{f}})\right| < 1$. Poles close to +1 tend to show slowly decaying dynamics whereas poles close to zero decay quickly. Negative poles oscillate and so may complex-conjugate poles. Thus it is adequate to define the state-transition matrix such that $A^{\mathrm{f}} = diag(\alpha),\ -1 < \alpha_j < 1$, where α is a vector containing the eigenvalues of A, i.e. the poles.

The input matrix B^{f} can be chosen arbitrarily under the constraint that no entry is zero. By selecting A^{f} and B^{f} as described above, the first criterion is met which states $y_k \to \mathrm{OCV} + h_k$ for long rest periods.

The output matrix G^{f}, also referred to as the weighting of the filter or *gain*, has to be chosen in a way that satisfies the second criterion i.e. $y_k \to \mathrm{OCV} + h_k - Ri_k$ for constant input currents. In our case G^{f} is a vector of length n^{f}, where n^{f} is the number of filter

[5] The eigenvalues of A are the solutions λ to the *characteristic equation:* $det(A - \lambda I) = 0$ of A, where I is the identity matrix. In case that A is a diagonal matrix, the eigenvalues are the entries of the main diagonal. The eigenvalues of the system matrix correspond to the poles of the systems's transfer function.

states, defined as follows:

$$G^{\mathrm{f}}(I - A^{\mathrm{f}})^{-1}B^{\mathrm{f}} = 0,$$
$$G^{\mathrm{f}}\left[diag(\frac{1}{1-\alpha})\right]B^{\mathrm{f}} = 0.$$

Assuming $B^{\mathrm{f}} = [1 \dots 1]^T$, the above equation can be rewritten as a sum, i.e.:

$$\sum_{j=1}^{n_{\mathrm{f}}} \frac{g_j}{1-\alpha_j} = 0. \tag{4.17}$$

To fix the zero DC-gain constraint one element of the G^{f} vector has to be dependent on the others in a way that the overall sum in (4.17) equals zero. This is met by defining the $n^{\mathrm{f}} - th$ element of G^{f} as the negative sum over the others, i.e. the elements g_1 to $g_{n^{\mathrm{f}}-1}$ are determined during system identification and $g_{n^{\mathrm{f}}}$ is

$$g_{n^{\mathrm{f}}} = -\sum_{j=1}^{n^{\mathrm{f}}-1} g_j \frac{1-\alpha_{n^{\mathrm{f}}}}{1-\alpha_j}. \tag{4.18}$$

4.5 Overview of Models

Table 4.1 allows a direct comparison of the state-space equations of the examined models. From top to bottom more complexity is added to the models which is obvious when opposing the equations to each other. The state equations can be intuitively understood as system states are only added but not modified. For example the state equation for z_k as defined within the Simple Model (SM) can directly be read out of the state equation from One-State Hysteresis Model (OSHM) or Enhanced Self-Correcting Model (ESCM). The output equations reflect the enhancement of the output estimate by adding additional terms to the OCV-bias.

Examined models (brought up by G. L. Plett [16])

Simple Model (SM):

$$\begin{aligned} z_k &= z_{k-1} - \left(\tfrac{\eta\Delta t}{C_n}\right) i_{k-1} \\ y_k &= \mathrm{OCV}(z_k) - Ri_k \end{aligned}$$

Zero-State Hysteresis Model (ZSHM):

$$\begin{aligned} z_k &= z_{k-1} - \left(\tfrac{\eta\Delta t}{C_n}\right) i_{k-1} \\ y_k &= \mathrm{OCV}(z_k) - Ri_k - s_k M(z_k) \end{aligned}$$

One-State Hysteresis Model (OSHM):

$$\begin{aligned} \begin{bmatrix} h_k \\ z_k \end{bmatrix} &= \begin{bmatrix} F(i_{k-1}) & 0 \\ 0 & 1 \end{bmatrix} \begin{bmatrix} h_{k-1} \\ z_{k-1} \end{bmatrix} + \begin{bmatrix} 0 & (1 - F(i_{k-1})) \\ -\frac{\eta\Delta t}{C_n} & 0 \end{bmatrix} \begin{bmatrix} i_{k-1} \\ M(z, \dot{z}) \end{bmatrix} \\ y_k &= \mathrm{OCV}(z_k) - Ri_k + h_k \end{aligned}$$

Enhanced Self-Correcting Model (ESCM):

$$\begin{aligned} \begin{bmatrix} f_k \\ h_k \\ z_k \end{bmatrix} &= \begin{bmatrix} diag(\alpha) & 0 & 0 \\ 0 & F(i_{k-1}) & 0 \\ 0 & 0 & 1 \end{bmatrix} \begin{bmatrix} f_{k-1} \\ h_{k-1} \\ z_{k-1} \end{bmatrix} + \begin{bmatrix} 1 & 0 \\ 0 & (1 - F(i_{k-1})) \\ -\frac{\eta\Delta t}{C_n} & 0 \end{bmatrix} \begin{bmatrix} i_{k-1} \\ M(z, \dot{z}) \end{bmatrix} \\ y_k &= \mathrm{OCV}(z_k) - Ri_k + h_k + Gf_k \end{aligned}$$

Table 4.1: Overview of the models examined in this work.

4.6 System Identification

To be able to use the models for predicting state and output variables, first the model parameters need to be identified. These unknown quantities can be estimated by system identification procedures, where a set of N input/output triples $\{y_k, i_k, z_k\}$ is given.

If parameters occur linearly in the output equation, the model is said to be *linear in the parameters*. Thus offline least-squares estimation in closed form is a feasible approach for determining the parameters of such models [11, chap. 18.5], like in the case of SM and ZSHM. If a model is not linear in the parameters, like in the case of OSHM and Enhanced Self-Correcting Model (ESCM), an alternative method is needed. A possible way to tackle this problem is using an EKF for estimating the parameters as already introduced in Section 3.3 on page 26.

4.6.1 System Identification using Least Squares

In order to be able to use least squares estimation three matrices have to be formed first:

OCV does not have impact on any of the parameters, only directly on the output. Therefore computation can be simplified by not using the output voltage values for system identification but define the vector $Y = [y1 - \mathrm{OCV}(z_1)\ \ y2 - \mathrm{OCV}(z_2)\ \ \ldots\ \ y_N - \mathrm{OCV}(z_N)]^T$ which contains the measured output subtracted by the corresponding value selected from the OCV LUT [6]

This leads to a simplified output Equation 4.19.
Matrix $H = [h_1\ h_2\ \ldots\ h_N]^T$ contains the parameter's coefficients of the output equation: each row h_j equals a whole parameter set. The unknown parameters are collected in the vector $\Theta = [\theta_1\ \ \theta_2\ \ldots\ \ \theta_k]^T$.

$$Y = H\Theta. \tag{4.19}$$

Assuming that the k columns of H are linearly independent, Equation (4.19) can be solved for Θ using the pseudo inverse. This results in the desired values of the models' parameters:

$$\Theta = \underbrace{(H^T H)^{-1} H^T}_{\text{pseudo inverse}}\ Y. \tag{4.20}$$

[6] For information on how to generate such LUTs, see Chapter 6, Section 6.4 and 6.5 and Section 5.4.1.

Parameter estimation for the Simple Model:

The unknown parameter of the SM is the internal resistance R of the cell. Since the internal resistance under charging conditions does not equal the internal resistance under discharging conditions, we introduce R^+ and R^- respectively, i.e.:

$$\Theta = \begin{bmatrix} R^+ & R^- \end{bmatrix}^T.$$

The superscript indicates whether the resistance is valid for positive or negative input currents. Thus the rows of H are $h_j = \begin{bmatrix} i_j^+ & i_j^- \end{bmatrix}$, also compare the output equation of the SM (4.2). Y is defined as shown on page 35.

Parameter estimation for the Zero-State Hysteresis Model:

Again Y is used as before. According to Equation (4.4) the unknown parameters then are R^+, R^- and M appearing with its coefficients $\pm\, i_j$ and s_j. Thus

$$\Theta = \begin{bmatrix} R^+ & R^- & M \end{bmatrix}^T$$

and the rows of H are formed by $h_j = \begin{bmatrix} i_j^+ & i_j^- & s_j \end{bmatrix}$. Note, within ZSHM there doesn't exist any dependency of M on z_k i.e. the SOC, M is considered to be a constant value, see Section 4.2. Otherwise ZSHM wouldn't be linear in its parameters.

4.6.2 System Identification using the Extended Kalman Filter

How the Extended Kalman Filter (EKF) can be used for system identification is already explained in Section 3.3. Here the specific details for applying this method to the models which are not linear in parameters is discussed.

$C_k^\Theta = \frac{d\, g(\cdot,\cdot,\cdot)}{d\, \Theta}\Big|_{\Theta=\hat{\Theta}_k^-}$ needs to be calculated for every single model (see Equation (3.24)). For that the following derivatives are required, where $g(\cdot,\cdot,\cdot)$ is the output equation of the system model (see Equation 3.23). Equation 4.22 is the calculation of the term $\mathrm{d}x_k/\mathrm{d}\Theta$ from Equation 4.21, where $f(\cdot,\cdot,\cdot)$ represents the state equation of the system model (see Equation 3.22):

$$\frac{\mathrm{d}g(x_k,u_k,\Theta)}{\mathrm{d}\Theta} = \frac{\partial g(x_k,u_k,\Theta)}{\partial \Theta} + \frac{\partial g(x_k,u_k,\Theta)}{\partial x_k}\frac{\mathrm{d}x_k}{\mathrm{d}\Theta}, \tag{4.21}$$

$$\frac{\mathrm{d}x_k}{\mathrm{d}\Theta} = \frac{\partial f(x_{k-1},u_{k-1},\Theta)}{\partial \Theta} + \frac{\partial f(x_{k-1},u_{k-1},\Theta)}{\partial x_{k-1}}\frac{\mathrm{d}x_{k-1}}{\mathrm{d}\Theta}. \tag{4.22}$$

Apparently, Equations (4.21) and (4.22) are of recursive nature and evolve over time. For initialization purposes, the term $\mathrm{d}x_0/\mathrm{d}\Theta$ is set to zero except that side information which

would lead to a better estimate of the initial state is available.

Parameter estimation for the One-State Hysteresis Model (OSHM) :

In the case of OSHM the unknown parameter vector is

$$\Theta = \begin{bmatrix} R^+ & R^- & M & \gamma \end{bmatrix}^T .$$

Again $\pm\ R$ is the cell's internal resistance, M the maximum polarization voltage and γ as part of $F(i_k)$ the hysteresis rate constant.

$f(\cdot)$ and $g(\cdot)$ are according to Equations (4.10) and (4.11):

$$f(x_k, u_k, \Theta) = \begin{bmatrix} F(i_k)h_k \ + \ (1 - F(i_k))\ M(z, \dot{z}) \\ z_k \ + \ \left(-\frac{\eta\ \Delta t}{C_n} i_k\right) \end{bmatrix}$$
$$g(x_k, u_k, \Theta) = \mathrm{OCV}(z_k) \ - \ Ri_k \ + \ h_k$$

with $F(i_k) = exp(-|\frac{\eta\ i_k\ \gamma\ \Delta t}{C_n}|)$ or in short F_k.

In order to solve Equations (4.21) and (4.22) the partial derivatives have to be calculated:

$$\begin{aligned} \frac{\partial g(x_k, u_k, \Theta)}{\partial \Theta} &= \begin{bmatrix} \frac{\partial g(\cdot)}{\partial R^+} & \frac{\partial g(\cdot)}{\partial R^+} & \frac{\partial g(\cdot)}{\partial M} & \frac{\partial g(\cdot)}{\partial \gamma} \end{bmatrix} \\ &= \begin{bmatrix} -i^+ & -i^- & 0 & 0 \end{bmatrix} \\ \frac{\partial g(x_k, u_k, \Theta)}{\partial x_k} &= \begin{bmatrix} \frac{\partial g(\cdot)}{\partial h_k} & \frac{\partial g(\cdot)}{\partial z_k} \end{bmatrix} \\ &= \begin{bmatrix} 1 & \frac{\partial \mathrm{OCV}(z_k)}{\partial z_k} \end{bmatrix} \end{aligned}$$

$$\begin{aligned} \frac{\partial f(x_{k-1}, u_{k-1}, \Theta)}{\partial \Theta} &= \begin{bmatrix} \frac{\partial f(h_{k-1}, u_{k-1}, \Theta)}{\partial R^+} & \frac{\partial f(h_{k-1}, u_{k-1}, \Theta)}{\partial R^-} & \frac{\partial f(h_{k-1}, u_{k-1}, \Theta)}{\partial M} & \frac{\partial f(h_{k-1}, u_{k-1}, \Theta)}{\partial \gamma} \\ \frac{\partial f(z_{k-1}, u_{k-1}, \Theta)}{\partial R^+} & \frac{\partial f(z_{k-1}, u_{k-1}, \Theta)}{\partial R^-} & \frac{\partial f(z_{k-1}, u_{k-1}, \Theta)}{\partial M} & \frac{\partial f(z_{k-1}, u_{k-1}, \Theta)}{\partial \gamma} \end{bmatrix} \\ &= \begin{bmatrix} 0 & 0 & (1 - F_{k-1}) sgn(i_{k-1}) & (M - h_{k-1}) \left|\frac{\eta\ i_{k-1}\ \Delta t}{C_n}\right| F_{k-1} \\ 0 & 0 & 0 & 0 \end{bmatrix} \\ \frac{\partial f(x_{k-1}, u_{k-1}, \Theta)}{\partial x_{k-1}} &= \begin{bmatrix} \frac{\partial f(h_{k-1}, u_{k-1}, \Theta)}{\partial h_{k-1}} & \frac{\partial f(h_{k-1}, u_{k-1}, \Theta)}{\partial z_{k-1}} \\ \frac{\partial f(z_{k-1}, u_{k-1}, \Theta)}{\partial h_{k-1}} & \frac{\partial f(z_{k-1}, u_{k-1}, \Theta)}{\partial z_{k-1}} \end{bmatrix} \\ &= \begin{bmatrix} F_{k-1} & 0 \\ 0 & 1 \end{bmatrix} \end{aligned}$$

In Equation (4.21) the terms $\frac{\partial g(\cdot)}{\partial x_k}$ and $\frac{\mathrm{d}x_k}{\mathrm{d}\Theta}$ are multiplied. Since the second row's entries of $\frac{\partial f}{\partial \Theta}$ are zero, the term $\frac{\partial \mathrm{OCV}(z_k)}{\partial z_k}$ is always multiplied by zero and therefore never used. Thus the resulting equations corresponding to (4.21) and (4.22) simplify to:

$$\frac{\mathrm{d}g(x_k, u_k, \Theta)}{\mathrm{d}\Theta} = \begin{bmatrix} -i^+ & -i^- & 0 & 0 \end{bmatrix} + [1]\frac{\mathrm{d}h_k}{\mathrm{d}\Theta}$$

$$\frac{\mathrm{d}h_k}{\mathrm{d}\Theta} = \begin{bmatrix} 0 & 0 & (1-F_{k-1})sgn(i_{k-1}) & (M-h_{k-1})\left|\frac{\eta\ i_{k-1}\ \Delta t}{C_n}\right| F_{k-1} \end{bmatrix} + F_{k-1}\frac{\mathrm{d}h_{k-1}}{\mathrm{d}\Theta}$$

Parameter estimation for the Enhanced Self-Correcting Model :

Assuming n^{f} filter states the unknown parameter vector then is

$$\Theta = \begin{bmatrix} R^+ & R^- & g_1 & \dots & g_{n^{\mathrm{f}}-1} & \beta_1 & \dots & \beta_{n^{\mathrm{f}}} & M & \gamma \end{bmatrix}^T,$$

where β is defined as

$$\beta = tanh(\alpha), \tag{4.23}$$

and α is the vector which contains the location of the filter poles. This definition produces the benefit that its inverse function forces α to stay within values[7] of $\pm$ 1 which is required for the filter to be asymptotically stable.

The elements of $G^{\mathrm{f}} = [g_1 \quad g_2 \quad \dots \quad g_{n^{\mathrm{f}}}]$ are only estimated up to $g_{n^{\mathrm{f}}-1}$ since the $n^{\mathrm{f}^{th}}$ element depends on the other entries to achieve zero DC-gain as mentioned in Equation (4.17). This also causes the derivatives to be a bit more complicated.

$f_k = [f_{k_1} \quad f_{k_2} \quad \dots \quad f_{k_{n^{\mathrm{f}}}}]^T$ is a column vector of length n^{f} and let $n^{\mathrm{f}} = 3$. The third term of the filter output equation is computed using the sum from Equation (4.18) in order to fulfill the second criterion of zero DC-gain (Section 4.4):

$$\begin{aligned} \mathrm{y}^{\mathrm{f}} &= G^{\mathrm{f}} f \\ &= g_1 f_1 + g_2 f_2 + \underbrace{\left(-g_1\frac{1-\alpha_3}{1-\alpha_1} - g_2\frac{1-\alpha_3}{1-\alpha_2}\right)}_{g_{n^{\mathrm{f}}}} f_3 \end{aligned}$$

Then for instance

$$\frac{\partial \mathrm{y}^{\mathrm{f}}}{\partial g_1} = f_1 - f_3\frac{1-\alpha_3}{1-\alpha_1}.$$

[7] $\alpha = tanh^{-1}(\beta) = artanh(\beta)$, the areatangens hyperbolicus is defined as: $artanh(x) := \frac{1}{2}ln(\frac{1+x}{1-x})$, $|x| < 1$ and its derivative is $\frac{\mathrm{d}}{\mathrm{d}x}artanh(x) = \frac{1}{1-x^2}$, $|x| < 1$.

Therefore

$$\frac{\partial g(x_k, u_k, \Theta)}{\partial g_i} = f_{k_i} - f_{k_{n^\mathrm{f}}} \frac{1-\alpha_{n^\mathrm{f}}}{1-\alpha_i}, \quad \text{for } i = \{1,\ \ldots,\ (n^\mathrm{f}-1)\}. \tag{4.24}$$

$f(\cdot)$ and $g(\cdot)$ according to (4.15) and (4.16) and with respect to Equation (4.23) are:

$$\begin{aligned} f(x_k, u_k, \Theta) &= \begin{bmatrix} diag(artanh(\beta))f_k \ + \ i_k \\ F(i_k)h_k \ + \ (1-F(i_k))\ M(z,\dot{z}) \\ z_k \ + \ \left(-\frac{\eta\ \Delta t}{C_n} i_k\right) \end{bmatrix} \\ g(x_k, u_k, \Theta) &= \mathrm{OCV}(z_k) \ - \ Ri_k \ + \ h_k \ + \ G^\mathrm{f} f_k \\ &= \mathrm{OCV}(z_k) \ - \ Ri_k \ + \ h_k \ + \ g_1 f_{k_1} \ + \ g_2 f_{k_2} \ + \ \ldots \ + \ g_{n^\mathrm{f}} f_{k_{n^\mathrm{f}}} \end{aligned}$$

Hence the partial derivatives evolve as follows:

$$\begin{aligned} \frac{\partial g(\cdot)_k}{\partial \Theta} &= \begin{bmatrix} -i^+ & -i^- & f_{k_1} - f_{k_{n^\mathrm{f}}} \frac{1-\alpha_{n^\mathrm{f}}}{1-\alpha_1} & \cdots & f_{k_{n^\mathrm{f}-1}} - f_{k_{n^\mathrm{f}}} \frac{1-\alpha_{n^\mathrm{f}}}{1-\alpha_{n^\mathrm{f}-1}} & 0 & \ldots & 0 \end{bmatrix} \\ \frac{\partial g(\cdot)_k}{\partial x_k} &= \begin{bmatrix} G_\mathrm{f} & 1 & \dfrac{\partial \mathrm{OCV}(z_k)}{\partial z_k} \end{bmatrix} \\ \frac{\partial f(\cdot)_{k-1}}{\partial \Theta} &= \begin{bmatrix} 0 & \ldots & 0 & diag\left(\frac{1}{1-\beta^2}\right) f_{k-1} & 0 & 0 \\ 0 & \ldots & 0 & 0 & (1-F_{k-1})sgn(i_{k-1}) & (M-h_{k-1}) \left|\frac{\eta\ i_{k-1}\ \Delta t}{C_n}\right| F_{k-1} \\ 0 & \ldots & 0 & 0 & 0 & 0 \end{bmatrix} \\ \frac{\partial f(\cdot)_{k-1}}{\partial x_{k-1}} &= \begin{bmatrix} diag(artanh(\beta)) & 0 & 0 \\ 0 & F_{k-1} & 0 \\ 0 & 0 & 1 \end{bmatrix} \end{aligned}$$

As in the case of OSHM, the term $\frac{\partial \mathrm{OCV}(z_k)}{\partial z_k}$ multiplies to zero and the simplified equations for (4.21) and (4.22) are:

$$\begin{aligned} \frac{\mathrm{d}g(x_k, u_k, \Theta)}{\mathrm{d}\Theta} &= \begin{bmatrix} -i^+ & -i^- & f_{k_1} - f_{k_{n^\mathrm{f}}} \frac{1-\alpha_{n^\mathrm{f}}}{1-\alpha_1} & \cdots & f_{k_{n^\mathrm{f}-1}} - f_{k_{n^\mathrm{f}}} \frac{1-\alpha_{n^\mathrm{f}}}{1-\alpha_{n^\mathrm{f}-1}} & 0 & \ldots & 0 \end{bmatrix} + \\ &\quad \ldots + \begin{bmatrix} G^\mathrm{f} & 1 \end{bmatrix} \frac{\mathrm{d}\tilde{x}_k}{\mathrm{d}\Theta} \\ \frac{\mathrm{d}\tilde{x}_k}{\mathrm{d}\Theta} &= \begin{bmatrix} 0 & \ldots & 0 & diag\left(\frac{1}{1-\beta^2}\right) f_{k-1} & 0 & 0 \\ 0 & \ldots & 0 & 0 & (1-F_{k-1})sgn(i_{k-1}) & (M-h_{k-1}) \left|\frac{\eta\ i_{k-1}\ \Delta t}{C_n}\right| F_{k-1} \end{bmatrix} + \\ &\quad \ldots + \begin{bmatrix} diag(artanh(\beta)) & 0 \\ 0 & F_{k-1} \end{bmatrix} \frac{\mathrm{d}\tilde{x}_{k-1}}{\mathrm{d}\Theta} \end{aligned}$$

Chapter 5

Cell Testing and Data Preprocessing

All cell tests were performed on a test plant at Magna E-Car (Graz) in 2010/2011.

5.1 Testing the Lithium-Titanate - cells

The Lithium-Titanate (LiTi)-pack[1] is a Toshiba Super Charge Ion Battery (SCiB) with twelve cells in series.

5.1.1 Open-Circuit Voltage - Test

The test started with a fully charged pack, then the pack was discharged in steps of 5% of SOC each until fully discharged and afterwards charged with the same procedure until fully charged again. Between each pulse the pack was allowed to rest for three hours to relax to the open current voltage at the current reference point. It took more than 120 hours (5 days) to complete the test.

The pack was tested at a temperature of 25°C as well as of 40°C. Besides other variables, voltage, current and time as well as the amount of electric charge $Q[Ah]$ (via an ampere-hour meter) were recorded at a sampling rate of $10s$, except during the occurrence of current pulses the sampling rate was higher with $5ms$. Figure 5.1 shows the current pulses and the corresponding amount of ampere hours of collected data at a temperature of 25°C.

The initial condition of the pack was set to $Q = 0Ah$ and it was discharged with $3A$-pulses that last for $207s$. When fully discharged, the pack's state reached a state of $-3.345Ah$. For charging pulses of $10A$ with a duration of $62s$ were used. When fully charged again the pack showed a capacity of $0.116Ah$ due to a longer rest period before the test. This equals 3.3% of the (measured) capacity and lies within the known range of

[1] Molecular Formula: $Li_4Ti_5O_{12}$

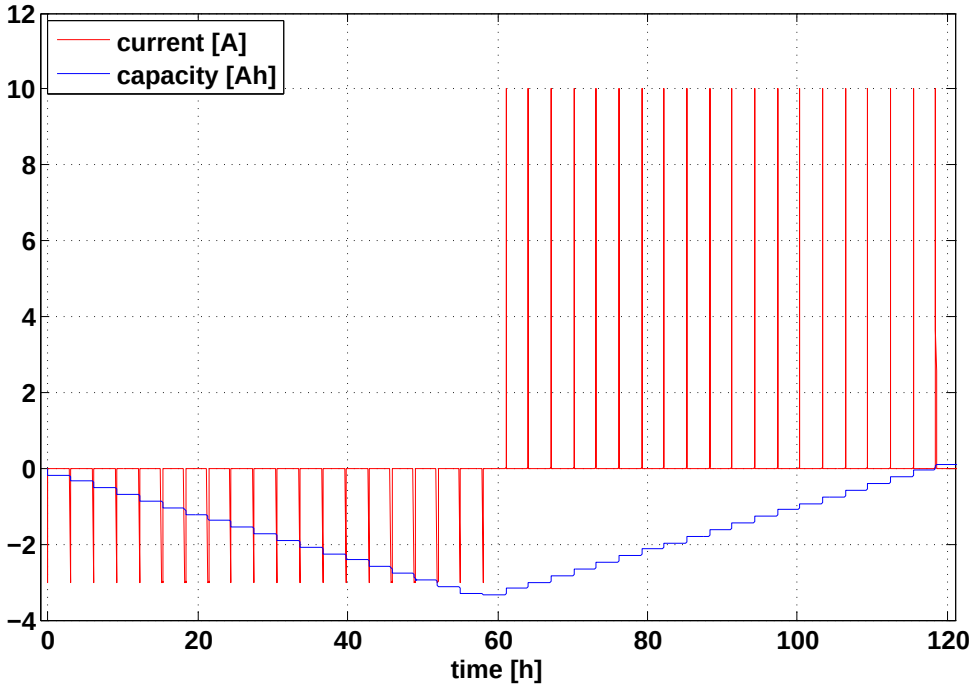

Figure 5.1: Example of raw data measured during an OCV-test at 25°C. The charging and discharging pulses (red) correspond exactly to the edges of the curve of the measured capacity (blue).

self-discharge rates. Therefore, the overall measured nominal capacity is $3.345 + 0.116 \approx 3.46Ah$.

The corresponding SOC[%]-values can be calculated from the recorded Q[Ah]-data:

$$\mathrm{SOC} = \frac{Q - Q_{\min}}{C_n} \cdot 100, \tag{5.1}$$

where C_n denotes the nominal capacity of the pack.

We used the data obtained by the OCV - test to determine the OCV characteristic and hysteresis curve.

5.1.2 Pulse Power Characterization - Test

In general the Pulse Power Characterization (PPC) - test serves to determine the charging and discharging performance of the pack at a certain level of SOC.

Similar to the OCV-test the pack was fully charged and discharged in steps of 10% of the measured nominal capacity. After reaching a defined SOC-level, the pack rested for $90min$, then a charging or discharging pulse was turned on followed by another $30min$ of

rest. Before turning to the next reference point of SOC, a correction pulse with 75% of the preceding pulse was used to avoid artifacts from the previous step.

In contrast to the OCV-test, the cells are only allowed to rest for $30min$ after the onset of the current pulse, yet not completely relaxed when heading for the next reference point. To encounter that, the correction pulse is needed.

This test was executed within two different settings: With charging and discharging pulses of $100A$ as well with charging pulses of $50A$ and discharging pulses of $80A$. Both settings were tested at 25°C and at 40°C. All pulses (also the correction pulses) lasted for a period of $10s$.

Unfortunately in the case of discharging the test stand also used 75% of the charging pulse as correction pulse instead of 75% of the discharging pulse which in the latter case of different amplitudes lead to errors of the succeeding location of the reference point (the SOC was too low).

I also used this data to determine both the OCV characteristic and hysteresis curve but since the internal resistance of a cell depends on the current pulses (amplitude and duration) this lead to higher resistance values and a greater polarization within the hysteresis legs which is more unlikely than the results obtained through OCV-data. Considering the fact that current pulses like in the Pulse Power Characterization (PPC)-test do not occur in the 'real life' (i.e. the driving profile) of a battery, adhering to OCV-data seemed to be more plausible.

5.1.3 Test-Cycle - Test

The cycle used in the test-cycle-tests as well as in the life-cycle-tests is a certain load profile specified by the client. It lasts about $4200s$ and consists of three sub-cycles. Correction pulses are used to keep the SOC-level neutral. Started at a desired initial condition of SOC the cycle is supposed to end at the same level (due to drift the SOC increases slightly) followed by two reference pulses of $31A$ which last $10s$ each. Since within the entire cycle the sub-cycles start at different SOC-levels diversity of the data is given.

In the case of the test-cycle two cycles in series were examined. The first test runs were done with the coolant at 42°C, an initial condition of $1.33Ah$ which equals 43% SOC and not only the packs' voltage and temperature were recored but the voltage and temperature of every single cell. Figure 5.1.3 shows how the cells' temperatures evolve over time. Later on the test was repeated for a temperature of the coolant from 20°C to 40°C in steps of 5°C. For each temperature the data was collected for three different initial states namely 33%, 43% as well as 53% SOC. During these test runs only the minimum and maximum temperature of the cells and the minimum and maximum cell voltage was recorded.

From a previous test[2] a nominal capacity of $3.1Ah$ was determined (the pack has had aged in the mean while). Firstly the pack was fully discharged until its first cell reached the minimum of $1.8V$ (specified by the manufacturer). The ampere-hour meter was reset to zero[3] and the pack was charged to the initial condition. Two entire cycles were executed consecutively and afterwards the pack was discharged again to the threshold of $1.8V$. From these reference points of full discharge the drift of the ampere-hour meter was calculated.

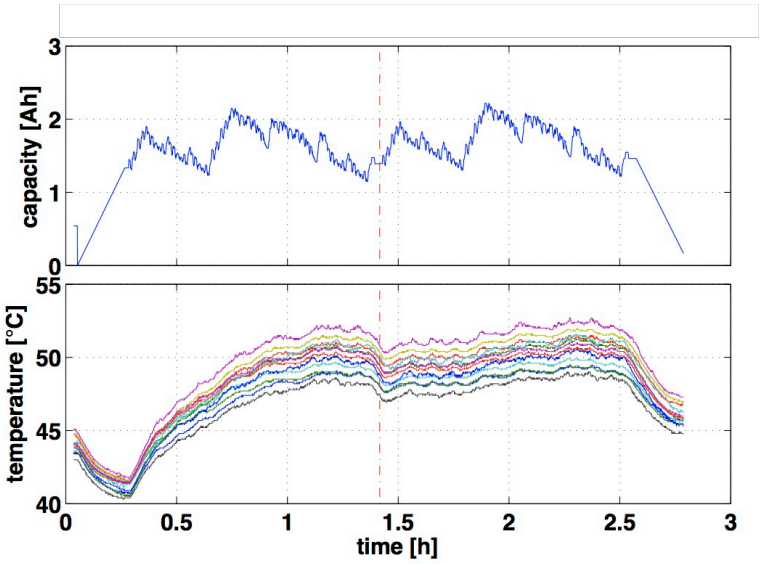

Figure 5.2: Temperatures of the single cells and corresponding developing of Ah-values measured during a test-cycle-test at 42°C which is the temperature of the coolant. The two cycles are separated by a red dashed line. It can be seen that it almost takes the whole first cycle to bring the cells to operating temperature. Their temperatures differ from each other since they are mounted separately on the coolant.

This data was used for system identification as well as for testing. Since the temperatures of the second cycle didn't vary as much as during the first cycle, data samples of the first cycle were omitted when estimating the parameters.

5.1.4 Life-Cycle - Test

The life-cycle-test is similar to the test-cycle test except that seven cycles are executed one after another, each followed by two reference pulses of $31A$ for $10s$. This test was only performed at a temperature of 42°C. It is used for testing purposes with parameters

[2] A shortened PPC-test was used as reference test to determine the remaining nominal capacity after 2000 operating hours.

[3] If the ampere-hour meter is reset and therefore not calibrated, one cannot calculate the corresponding SOC-values directly from the Ah-measurements as proposed in section 5.1.1 but has to compute the integral over the input current (cumulative sum).

determined by system identification with test-cycle data of the same temperature. As in the case of the test-cycle test it is obvious that drift is an issue. It is primarily caused by the ampere-hour meter and can be assumed linear[4]. Figure 5.3 shows the measured Ah data and the same data corrected by its drift. When using Ah-values computed by integrating the current, the same correction is needed and as a consequence by that procedure the SOC-values are pruned too. Of course this also holds true for data of the test-cycle tests.

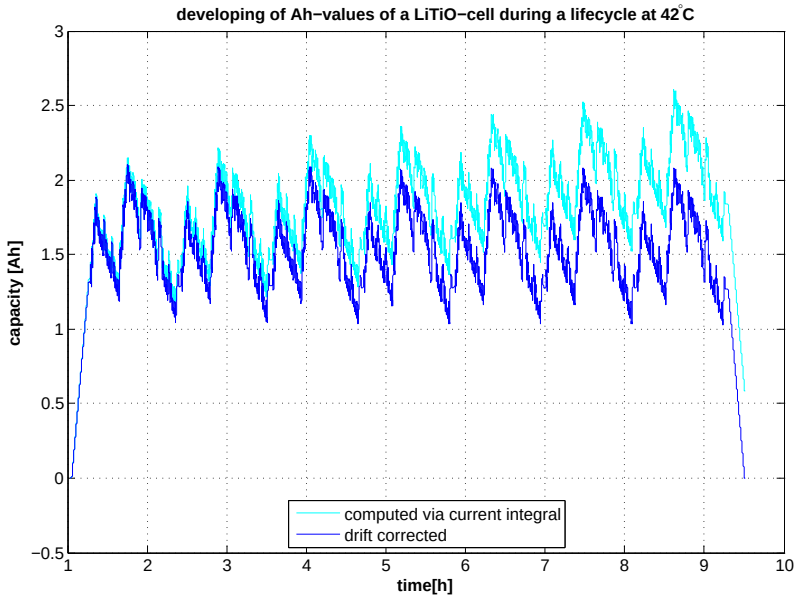

Figure 5.3: Life-cycle test of seven cycles. The Ah-values computed via the integral of the input current before (cyan) and after drift-correction (blue).

[4]personal conversation with Dr. Stefan Doczy

5.2 Testing the Lithium-Iron-Phosphate - cells

The Lithium-Iron-Phosphate (LiFePO)-pack[5] consists of 66 cells of $4.5Ah$ capacity with every two cells forming a block summing up to a total capacity of $8.5Ah$[6]

5.2.1 Open-Circuit Voltage - Test

Testing differs from the test of the LiTi-pack which has such little hysteretic behavior that it was possible to neglect current pulses usually used for leading the pack back to OCV-level. These short pulses of $\pm 60A$ for charge and $\pm 80A$ for discharge are necessary for the LiFePO-pack and are set directly before the onset of the next charging / discharging step ($4,2A$ charging / discharging pulse). This guarantees that the pack's voltage returns to OCV from the hysteresis leg it has relaxed to. Figure 5.4 shows the input current together with the resulting SOC. This test was realized for 23°C as well as for 40°C.

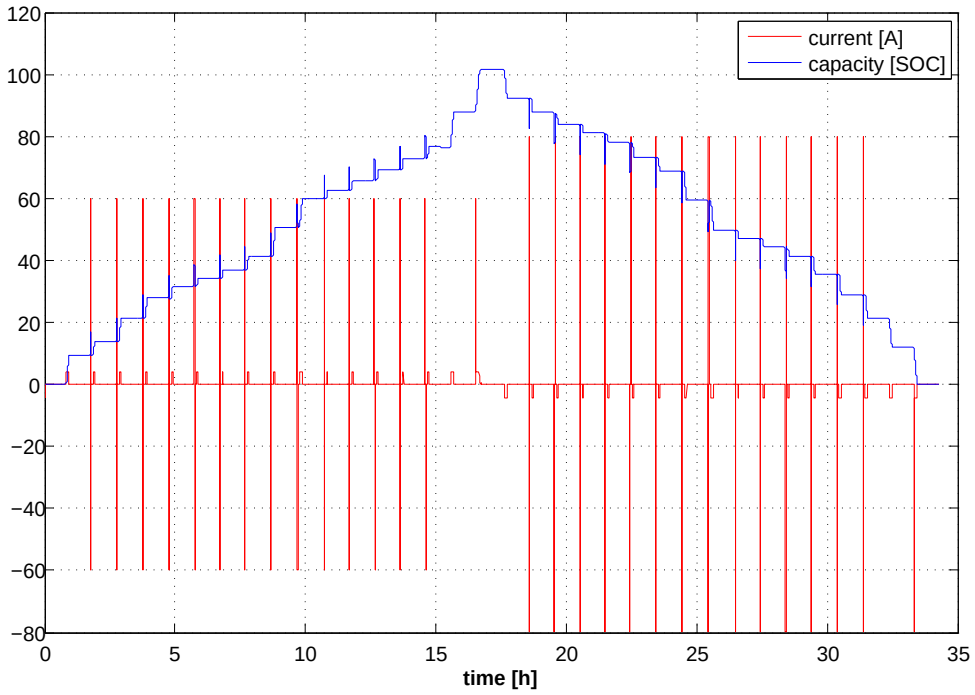

Figure 5.4: Raw data measured during the OCV-test of the LiFePO-pack at 40°C. The hysteresis pulses that turn the pack back to OCV-level are applied directly before the smaller charging and discharging pulses (red).

[5] Molecular Formula: $LiFePO_4$

[6] The 'missing' $0.5Ah$ form a buffer to make sure that no cell is overstressed (compare balancing methods on page 19).

5.2.2 Test-/Life-Cycle - Test

Test and the lifecycle data is available for 47°C. The load profile (i.e. the driving cycle, see section 5.3) was the same as in the case of the LiTipack. The test-cycle test covers two driving cycles, the lifecycle test seven cycles. Drift is again an issue. But in contrast to the other cell chemistry, a large negative drift can be observed when calculating the Ah-values directly from the input current, actually the values run below $0Ah$ as can be seen in Figure 5.5:

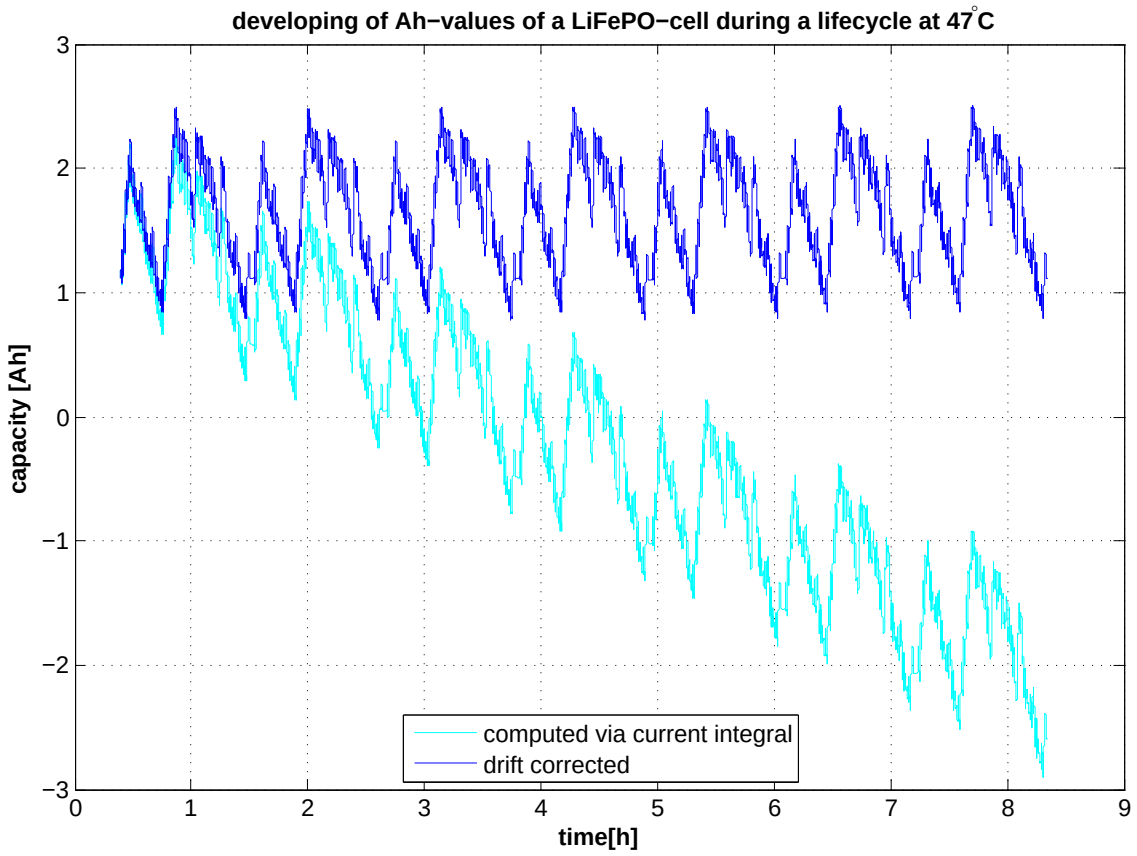

Figure 5.5: Life-cycle test of seven cycles. The Ah-values computed via the integral of the input current before (cyan) and after drift-correction (blue).

5.3 Load Profile of Driving Cycle

The driving cycle that was used as test cycle (two times repeated) as well as for the life-cycle test (seven times repeated) lasts about 4200 seconds and consists of four sub-cycles of different duration as listed in table 5.1.

Sub-cycle	Duration [s]
Cycle 1	144,2
Cycle 2	353,5
Cycle 3	789,4
Cycle 4	200,0

Table 5.1: The duration of each sub-cycle of the load profile which is used for test and lifecycle tests.

Cycles 1 to 3 describe predefined load values, at the end of cycle 2 a current reference value is provided to guarantee a neutral SOC-state regarding the higher-level sequence. This reference value depends on the temperature. Cycle 4 also consist of two current reference values which last 10 seconds each. The sub-cycles appear in the following order: 1, 1, 2, 2, 2, 1, 1, 3, 3, 2, 2, 4. The colored vertical lines in figure 5.6 indicate the begin of each sub-cycle.

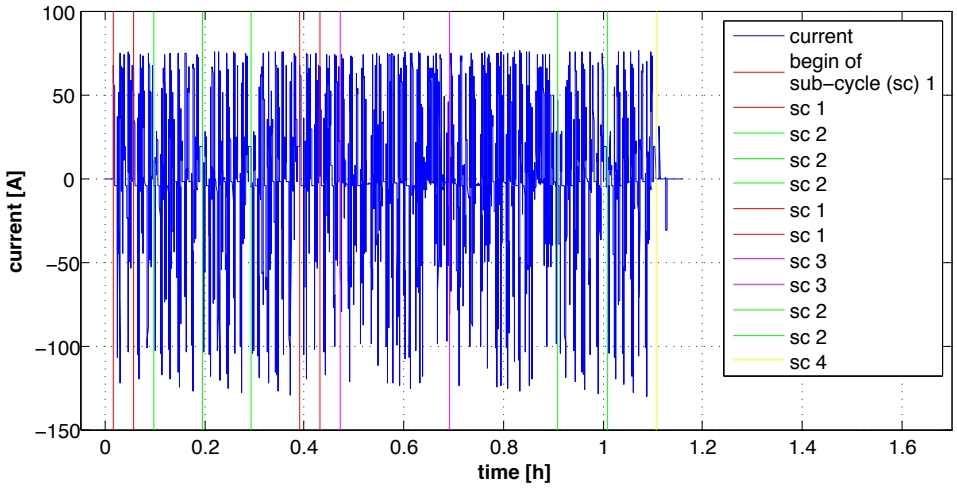

Figure 5.6: Load profile of a single test cycle. This is used in test cycle and life cycle tests for both cell types.

5.4 Preprocessing of Data

The naming of all workspaces supply information on type of the designated use, cell chemistry, origin of data (OCV, test-cycle, life-cycle), temperature (if data of same test is available at different temperatures), start-SOC (if differing from 'standard' values) and amperage (if various current settings are available as in the case of the OCV-test of LiFePO).

5.4.1 Open-Circuit Voltage Look-Up Tables

Data from OCV-tests was used to deduce the hysteretic behavior of the cells, i.e. the hysteresis legs. Further using these legs, the OCV-curves were determined.

The OCV characteristics are stored in workspaces that contain LUTs in the form of (m x 2) matrices for high and low temperatures (resolved with an accuracy of 0.1%), where m denotes the number of data points. The workspaces also contains the maximum polarization voltage read out from the hysteresis legs for both temperatures.

Since the resolution of the LUT is higher than achieved by only measured data, the missing corresponding voltage values for a vector x containing SOC-values from 0% to 100% (in steps of 0.1% SOC) are determined via linear interpolation.

The hysteresis legs needed to be smoothed for further calculations. This was done by a moving average window without zero padding to avoid distortions around 0% and 100% SOC. The smoothing starts with the $(\frac{\mathtt{ws}-1}{2}+1)$-th element, where ws denotes the window size.

In order to retrieve a reliable value for M, the maximum polarization is computed by searching the maximum difference between the hysteresis legs within the region of 25% to 75% SOC.

For the LiFePO-cell the OCV-test was accomplished at different amperages of charging and discharging currents. The results are nearly similar, for OCV computation we chose the data with the lowest amperages (i.e. $60A$ charging, $80A$ discharging pulses).

5.4.2 Training Sets

Training sets were generally generated from test-cycle data. When using this data (especially with regard to use the best data available for training sets) samples belonging to the first cycle were dismissed because of the evolution of the cell temperatures. The data is cleaned, that means its drift is corrected and samples that contribute to correction pulses during the cycle are neglected.

Drift was assumed to be linear. The data vector of a driving cycle contains as first and last element reference points of full discharge, i.e. of same value, namely $0Ah$. When data

is drift affected, these reference points show different values. Linear drift equals defining a straight line from the first to the last sample, i.e. a vector of the same size as the data vector with elements equally spaced from first to last sample value. Then test data can be cleaned by subtracting those drift values from the drift affected data.

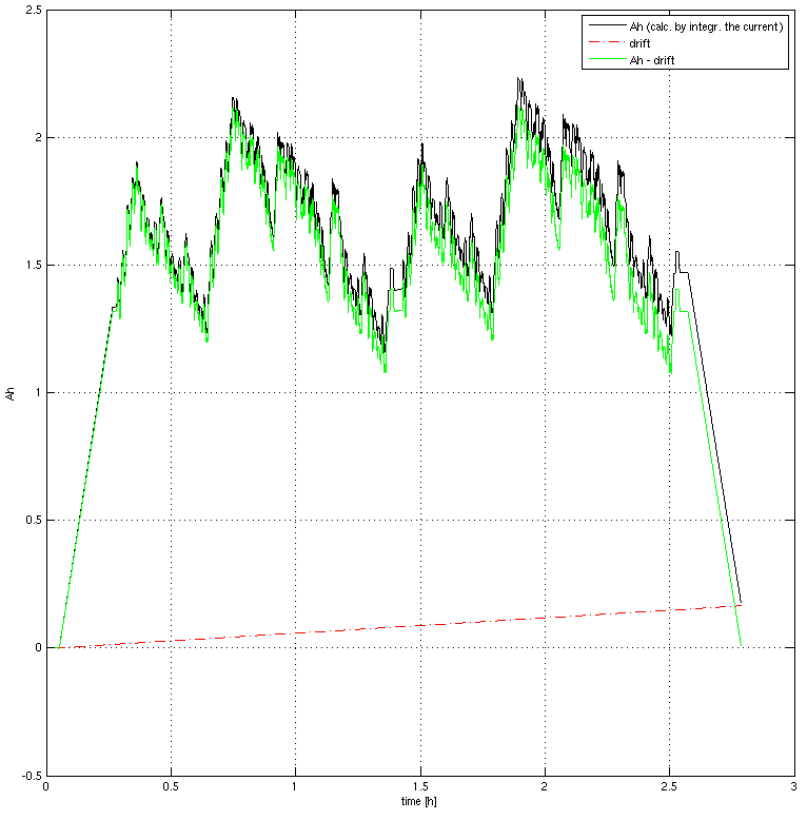

Figure 5.7: Drift affected data and same data corrected by subtracting the assumed to be linear drift values indicated by the straight line from the first to the last sample of the measured Ah values.

Furthermore the sets were built using the input current for Ah computation, since the Ah values determined by the Ampere-hour meter are derived from the current measured within the test plant (at the connectors of the battery) whereas the values of the input current directly come from the current sensor within the system itself, which equals also the 'real-life' scenario and usually is more accurate. The output voltage was set to the lowest

measured cell voltage[7] as by under-running first the threshold used for safe operations these cells were responsible for the switch off and can be regarded as matching best the corresponding SOC-level.

In the case of the LiTi-pack, test cycles were accomplished at various temperature ranges of the coolant (20°C, 25°C, 30°C, 35°C, 40°C, 42°C) and except for the latter also at three different levels of start SOC (33%, 43%, 53%), see also table 7.3. Training sets were built from all data sets with an initial condition of 43%. Thus system parameters can be identified for every temperature condition.

For the LiFePO-pack data is only available at 47°C.

5.4.3 Test Sets

Test sets were generated from the 2nd test-cycle as well as from life-cycle data. Data is drift corrected and includes correction pulses. Again the minimum cell voltage was chosen as system output. For every temperature of the coolant and every initial condition a separate test set was generated. When using life-cycle data, the cell temperatures were not taken into account.

Every set (training as well as test set) is provided as a matlab-workspace containing a (m x 3) data matrix `M` that holds m input-output triples of the form $\{y_k, i_k, z_k\}$ where y_k is the measured output voltage, i_k the input current and z_k the 'true' state of the cell, i.e. the corresponding SOC-value computed from the input current. Additionally the corresponding time-vector (`time_`) and a variable `cap_cell` that holds the measured nominal capacity is stored.

Both, training and test sets are drift corrected in their SOC-values. Moreover training sets do not contain any correction pulses that occur during the driving cycles. Current pulses in the beginning and in the end of the tests used for calibration and to approach a desired start-SOC are dismissed anyway.

For the life-cycle test sets we used drift corrected as well as drift affected data to be able to show the impact of drift on state and output estimation (which can not be seen as clear using shorter sequences).

[7] At the end of the test, when the pack is fully discharged again, the cell that first under-runs the threshold for switch off and states the pack as fully discharged, is in fact the cell that is the most discharged in comparison to the others and has therefore most likely the 'true' state of 0% SOC.

Chapter 6

Hysteresis and Open-Circuit Voltage

As already mentioned in chapter 2.2 the Open-Circuit Voltage (OCV)-curve reflects the characteristic behavior of a cell. In fact the measured samples $\langle voltage,\ ampere\ hours \rangle$ are not located on the OCV-curve directly but rather on the legs of the major hysteresis loop which evolves when cycling the pack from 0% to 100%SOC and back.

The OCV-characteristic itself is then computed as arithmetic mean of both legs. It is obviously monotonically increasing but not necessarily strictly monotonically increasing.

6.1 The Hysteresis Effect

A hysteresis effect can be observed in systems where the output not only depends on the independent variable input but also on its past environment. That means the system behaves according to path dependencies and may remain in different sates provided the same input. These states can also be regarded as several apparent *equilibria* of the system. To predict future outputs the current internal state (as it has emerged according to past inputs) or the system's history have to be known. If the system is provided an increasing followed by a decreasing input (or vice versa) the systems output will form a loop.

In the case of LIBs, the hysteresis effect describes a voltage gap at a certain point of SOC depending on if the system has been previously charged or discharged. Dreyer et al. [7, 8] investigated the hysteresis effect in batteries with focus on the behavior of LiFePO.

Conventional understanding of the hysteresis states that it is caused by the rates of charge and discharge, particle size, electrode thickness and so forth and could be minimized by i.e. minimizing the particle size. Hence the voltage gap between charge and discharge curve should become very small when decreasing the charging / discharging rates to sufficiently small values.

During experiments with preconditioned[1] electrodes they discovered a final voltage gap of a few millivolts to several tens of millivolts (depending on the electrode material) even when the charging/discharging currents approach zero. That implies that at least two equilibrium potentials do exist. According to Dreyer the hysteretic behavior is caused by the many-particle system and the fact that lithium can be exchanged between the connected particles.

Due to charging and discharging processes phase transitions take place that cause hysteretic behavior. Part of the particles transit to another phase while the others remain in the previous phase. The chemical potential and thus the localization of the equilibrium depends on the number of storage particles in each phase. The relation of the chemical potential and the lithium mole fraction is non-monotone which results in the hysteresis effect.

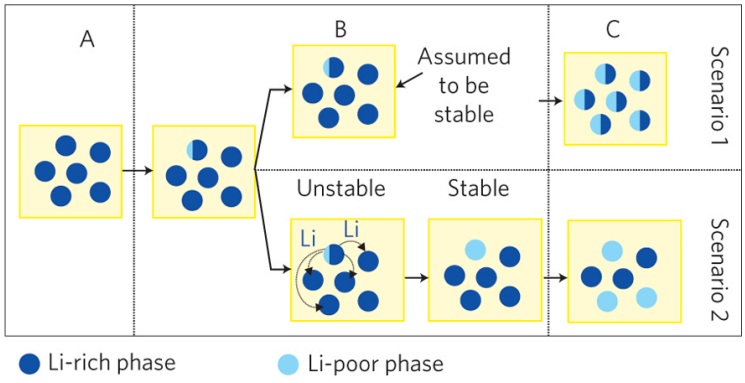

Figure 6.1: Phase transitions in a many-particle system: Scenario 2 where particles exchange lithium within their neighborhood is much more likely than scenario 1 since only the total amount of lithium of the whole ensemble can be controlled (from Dreyer et al. [7]).

Dreyer explains the basic mechanism of the phase transition by looking at a single $FePO_4$-storage particle [8]. If the lithium content of the particle is small it is in the so-called α-phase, a single-phase state. While discharging, the total amount of lithium increases. When exceeding a certain value the particle exhibits a coexistence of two phases: an inner shell with small and an outer layer with high lithium concentration which is likely to be unstable due to surface tensions between the two phases within the particle. For stability the amount of lithium of a single particle needs to be controlled (scenario 1 in Figure 6.1) which is impossible within an ensemble of a many-particle system where only the total amount of lithium within the ensemble can be controlled. In a multiple particle system the single particles can exchange lithium atoms, therefore two-phase particles can

[1] previously cycled

either absorb lithium from other particles in the neighborhood or release lithium in order to become a stable single-phase particle (Figure 6.1, scenario 2). The phase with high lithium concentration is called β-phase.

The chemical potential of the lithium-component is a function of lithium concentration, i.e. the particle composition[2] [7], where a particle itself exhibits a non-monotone chemical potential. This non-monotonicity with respect to the lithium concentration implies the hysteretic behavior of a many-particle system (provided that its members are single-phase particles) [8].

6.2 Computational Aspects

Using data from OCV-tests the significant samples needed for the computation of the hysteresis legs are found by taking the charge and discharge current onsets into account: Always the last sample before the next onset is chosen because at this time the pack is most relaxed and those samples represent most likely the hysteretic behavior as they are closest to (or rather assumed to be onto) the legs of the major loop. In the case of the Lithium Iron Phosphate cell, the sample right before the hysteresis correction pulses is chosen as sample that lies on the hysteresis leg. The correction pulses assure that the cell voltage returns to OCV-level from wherefrom the following charging / discharging pulse provokes the next 5% SOC-step.

Figure 6.2 shows which samples are selected (black crosses), the four subfigures represent the testing of both cell chemistries at low and high temperatures. Interpolation over those significant samples leads to the hysteresis legs of the major loop from 0% to 100% SOC with a precision of 0.1% SOC.

The OCV-characteristic is defined as arithmetic mean of the major hysteresis loop and is computed accordingly. It is used as mapping between terminal voltage and SOC, i.e. the value tuples are stored and used as Look-Up Table (LUT) for further computations (see also Section 5.4.1).

[2] see also chapter 2.1

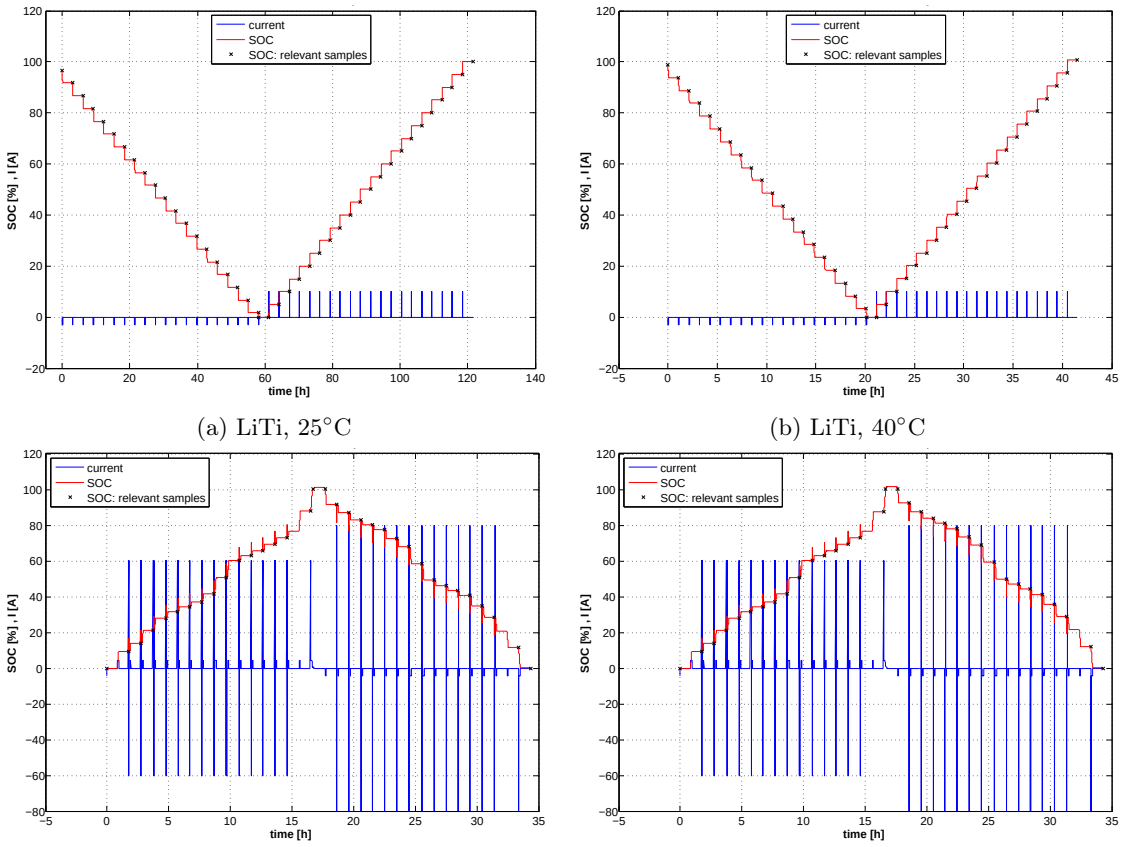

(a) LiTi, 25°C

(b) LiTi, 40°C

(c) LiFePO, 23°C

(d) LiFePO, 40°C

Figure 6.2: Charging and discharging currents (in blue) and SOC (in red) directly computed from Ah-values. The crosses mark the samples which are chosen in order to compute the hysteresis curves. (a) LiTi 25°C, (b) LiTi 40°C, (c) LiFePO 23°C, (d) LiFePO 40°C.

6.3 Polarization

With regard to the hysteresis legs, the maximum polarization can be determined as the maximum of half of the difference of the two legs (for logical reasons within a region of the two-phase-regime[3], i.e. between 25% and 70% SOC). Those values are listed in table 6.1, the corresponding graphs of the hysteresis legs are shown in Figure 6.4 and Figure 6.5.

[3]Particles are present in α- as well as in β-phase.

	Maximum polarization	Polarization at 50% SOC
$Li_4Ti_5O_{12}$		
25°C:	$0.3444mV$	$0.0092mV$
40°C:	$0.7331mV$	$0.5326mV$
$LiFePO_4$		
23°C:	$18.3387mV$	$8.6186mV$
40°C:	$18.1959mV$	$7.0732mV$

Table 6.1: The table above shows the maximum polarization values within the two-phase regimes and the polarization at 50% SOC for both cell chemistries.

6.4 Hysteresis and Open-Circuit Voltage of Lithium - Titanate cells

Lithium-Titanate (LiTi) shows very little hysteretic behavior. Due to inaccuracies of the measurements the legs of the hysteresis do slightly intersect within the upper regions of SOC which theoretically is not possible. For lower temperatures the intersection takes place around 50% SOC, at higher temperatures it starts between 55% and 60% SOC. This is shown in Figure 6.3. It is to stress, that as consequence the OCV-curve for SOC levels greater than 50% is not as trustworthy as for lower levels.

But from theory, at the very most in the case of no hysteretic behavior the legs may coincide, which is why for samples belonging to the charging leg but being their voltage smaller than the voltage of the corresponding sample of the discharging leg (at the same level of SOC), we used the arithmetic mean of both instead[4]. Thus in the case of the Lithium Titanate cell, the OCV-characteristic for higher levels of SOC is not as accurate as for lower levels.

The hysteresis curves for both temperatures at which the OCV-tests have been realized are shown in Figure 6.4a-b. Computation of the arithmetic mean leads to the OCV-characteristics which are shown in Figure 6.4c for both temperatures.

It has to be emphasized that the behavior of the OCV-characteristic in the case of LiTi is very appealing since it is strictly monotonically increasing and does not show any plateaus.

[4]According to the advice of Alexander Janek (Magna E-Car), personal conversation, 2011

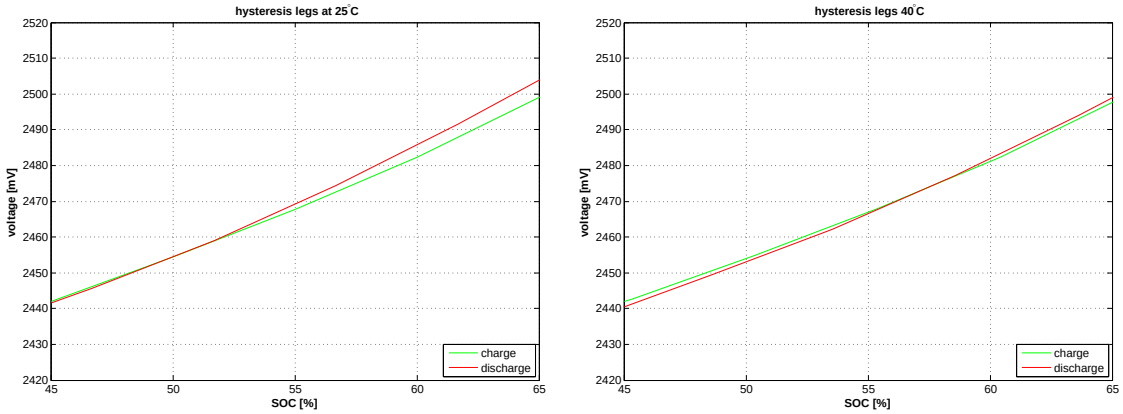

(a) Hysteresis legs at 25°C, without interpolation (b) Hysteresis legs at 40°C, without interpolation

Figure 6.3: LiTi: The legs of the major hysteresis loop are intersecting in higher regions of SOC for both temperatures of the coolant: (a) $25°C$ (b) $40°C$.

6.5 Hysteresis and Open-Circuit Voltage of Lithium - Iron-Phosphate - cells

Lithium-Iron-Phosphate (LiFePO) shows a greater polarization than LiTi. For this cathode material Dreyer [7] reveals a voltage gap of about $20mV$ within a region of 40% to 60% SOC. This matches the results shown in table 6.1, where LiFePO at 50% SOC exhibits a polarization up to $8.6mV$ which equals a voltage gap of $17.2mV$ at that point. The hysteresis curves are shown in Figure 6.5(a),(b).

The OCV-characteristics (Figure 6.5(c)) show a large plateau within the region of approximately 40% to 60% SOC and a smaller one around 80% SOC. These plateaus may lead to ambiguous results when searching the LUT for a certain voltage value.

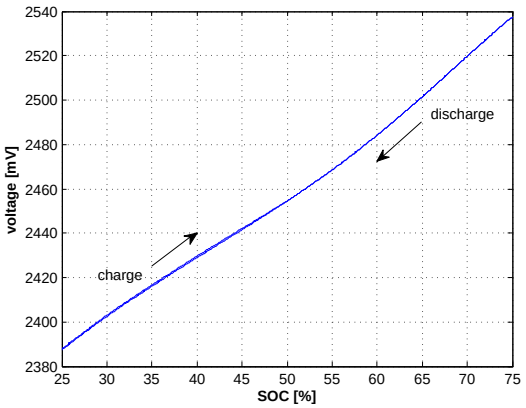

(a) Hysteresis loop at 25°C, maximum polarization within this region: $0.34438mV$

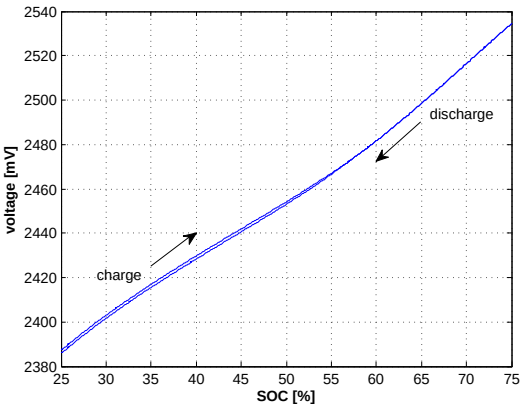

(b) Hysteresis loop at 40°C, maximum polarization within this region: $0.73311mV$

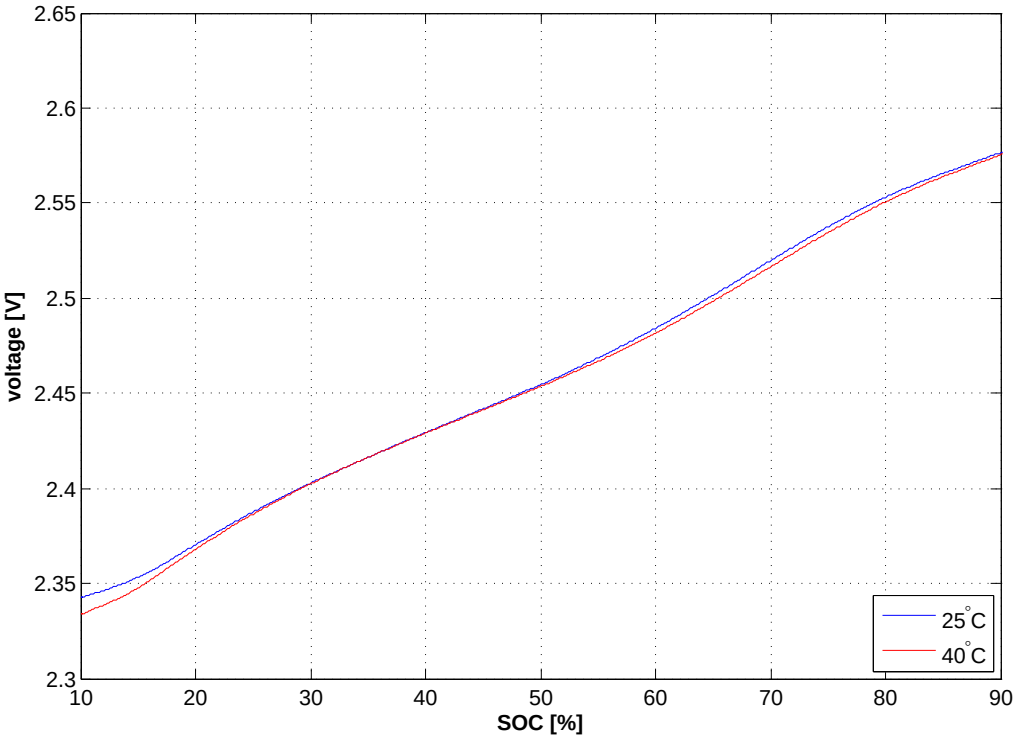

(c) OCV-characteristic of LiTi at low (blue line) and high temperatures (red line).

Figure 6.4: LiTi: OCV-characteristic and hysteresis curves within 10% to 90% of SOC for low and high temperatures. (a) $25°C$, (b) $40°C$, (c) OCV for both temperatuers.

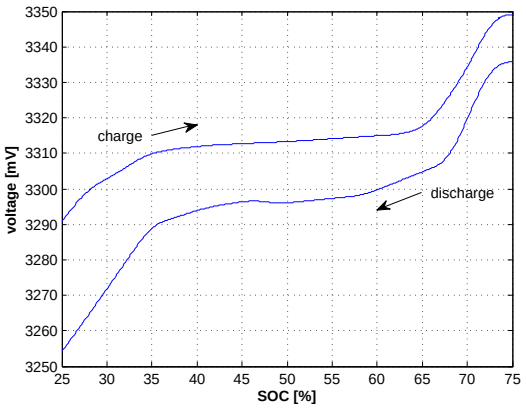

(a) Hysteresis loop at 23°C, maximum polarization within this region: 18.3387mV

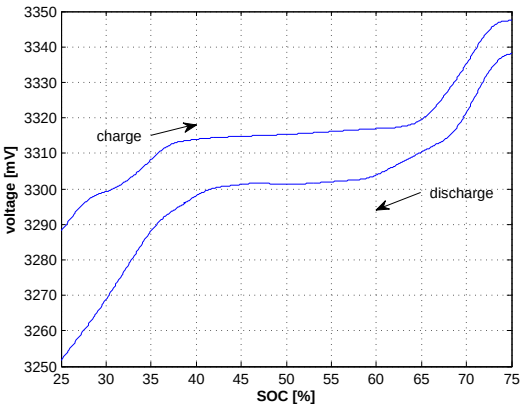

(b) Hysteresis loop at 40°C, maximum polarization within this region: 18.1959mV

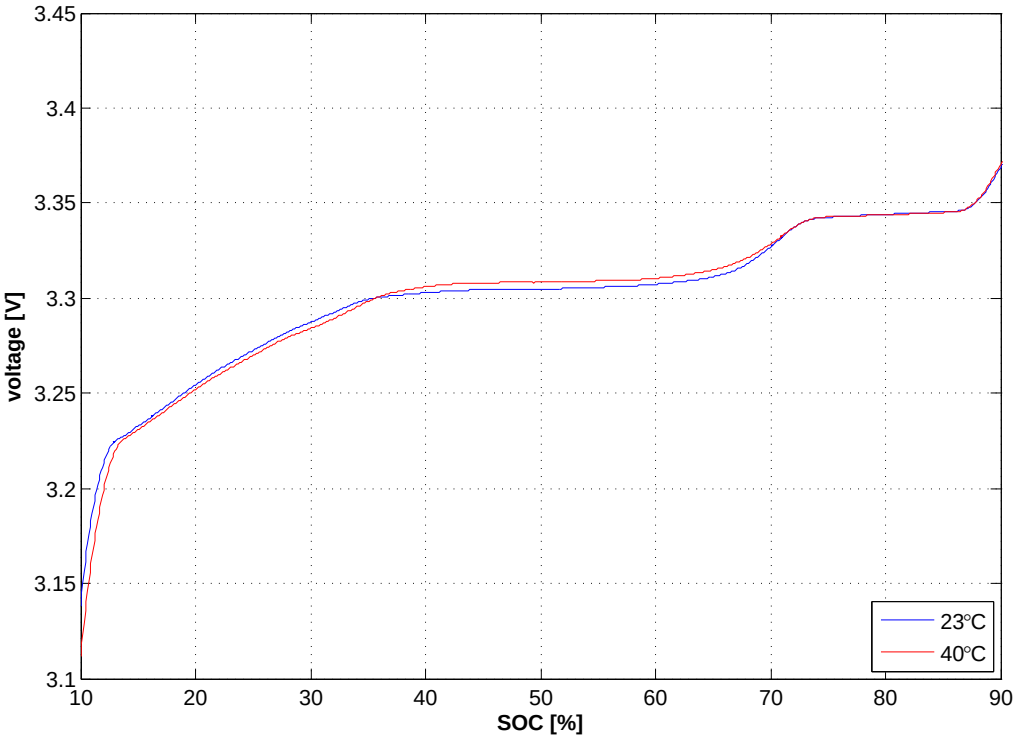

(c) OCV-characteristic of LiFePO at low (blue line) and high temperatures (red line).

Figure 6.5: LiFePO: OCV-characteristic and hysteresis curves within 10% to 90% of SOC. (a) 23°C, (b) 40°C, (c) OCV for both temperatuers.

Chapter 7

Implementation and Results

In the case of Lithium-Titanate (LiTi), for all experiments with data at temperature 20°C, 25°C and 30°C the OCV LUT at 25°C is used, for higher temperatures, the LUT at 40°C is used. In the case of Lithium-Iron-Phosphate (LiFePO), OCV-data at 40°C is applied, since test data is only available at 47°C.

7.1 System Identification

For system identification the training sets are used.

7.1.1 System Identification using Least Squares

In the case of the Simple Model (SM) and the Zero-State Hysteresis Model (ZSHM) least squares estimation[1] was applied.

Since in the case of the LiTi - pack data was available for several temperature ranges (of the coolant), parameters were estimated for every range. It can be seen that by increasing temperature the magnitude of the internal resistances decreases. Moreover the internal resistance for discharging is about $0.2m\Omega$ higher than the internal resistance for charging.

Training sets could be used en bloc, least squares estimation does not require separated charging and discharging data.

For the SM only the resistances are estimated, in the case of ZSHM the maximum polarization is estimated too. Figure 7.1 shows the trend of the estimated parameters for the LiTi - cell over the temperature range for both, for SM as well as for ZSHM.

The exact values for both cell chemistries are listed in Table 7.1.

[1] see section 4.6.1 for a detailed explanation

	Simple Model (SM)	Zero-State Hysteresis Model (ZSHM)
$Li_4Ti_5O_{12}$		**20°C**
R+:	$1.5127m\Omega$	$1.5621m\Omega$
R-:	$1.7760m\Omega$	$1.8227m\Omega$
M:		$2.5836mV$
		25°C
R+:	$1.4577m\Omega$	$1.5052m\Omega$
R-:	$1.7032m\Omega$	$1.7577m\Omega$
M:		$2.4853mV$
		30°C
R+:	$1.4166m\Omega$	$1.4464m\Omega$
R-:	$1.5897m\Omega$	$1.6237m\Omega$
M:		$1.5580mV$
		35°C
R+:	$1.3122m\Omega$	$1.3674m\Omega$
R-:	$1.5813m\Omega$	$1.6440m\Omega$
M:		$2.8686mV$
		40°C
R+:	$1.2862m\Omega$	$1.3315m\Omega$
R-:	$1.5172m\Omega$	$1.5684m\Omega$
M:		$2.3497mV$
		42°C
R+:	$1.2403m\Omega$	$1.2487m\Omega$
R-:	$1.3411m\Omega$	$1.3505m\Omega$
M:		$0.4335mV$
$LiFePO_4$		**47°C**
R+:	$1.5568m\Omega$	$1.5402m\Omega$
R-:	$1.5472m\Omega$	$1.5287m\Omega$
M:		$1.5675mV$

Table 7.1: Estimated parameter values for the SM and the ZSHM for both, LiTi and LiFePO cells. System identification was done using least squares. According to Plett's notation, R^+ denotes the internal resistance for discharge, R^- the internal resistance for charge.

7.1.2 System Identification using the Extended Kalman Filter

Identifying the parameters using the EKF requires treating charging and discharging data separately. The initial values for covariance matrices, noise, Θ etc. are chosen according to previous knowledge or in a neutral way.

The initial inner resistance is influenced by previous observations, the maximum polarization is determined during evaluation of the OCV-characteristic of the cell chemistry and gamma is initialized to a neutral value of 1.

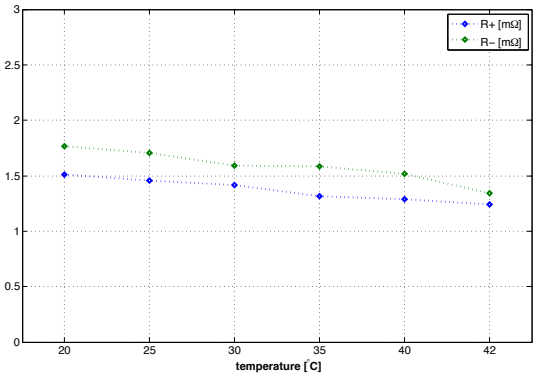

(a) Internal resistances for SM, determined by least squares.

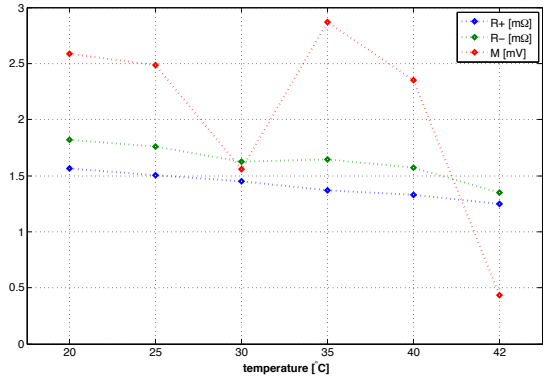

(b) Internal resistances and maximum polarization for ZSHM, determined by least squares.

Figure 7.1: Estimated parameters of the LiTi-cell at various temperatures of the coolant.

The error covariance matrices need to be initialized as diagonal matrix with plausible values, i.e. a roughly estimated deviation of 0.0001Ω for the inner resistance. Its size is specified by the length of the Θ-vector. It is a diagonal matrix because any dependencies of parameters among each other are unknown and the entries of the main diagonal only represent the variances of the parameters themselves.

The derivative $\frac{\mathrm{d}x_0}{\mathrm{d}\theta}$ is initialized to zero unless side information gives a better estimate of its value [15].

The fictitious process noise Q is necessary to model slow changes of the parameters and the infidelity of the model itself. Furthermore it allows the filter to adapt Θ. Thus it is initialized to very small values non equal zero. The sensor / measurement uncertainty is supposed to be about $0.1V$, thus the measurement noise R is initialized accordingly.

The initial values of SOC z_0 and hysteresis voltage h_0 are set to the 'true' measured SOC-value of the first sample within the training set and the maximum polarization value, respectively.

Issues that may arise when implementing a Kalman Filter on a real system

When implementing a KF/EKF on a real system various kinds of difficulties such as divergence or instability may occur and it may not work even if its theory is correct. The main reasons for that are finite precision arithmetic (which theoretically should be infinite and thus leads to round-off errors) and modelling errors [17]. When talking about modelling errors this includes that in real life applications the system model is not precisely known. In this work neither the measurement noise nor the process noise is known. They are not pure white, zero-mean noise either which however is another assumption as well as that the noise sequences are supposed to be completely uncorrelated. Not violating any of these

assumptions seems impossible in real implementations.

Advantage of various strategies can be taken into account to make the filter work. Increasing arithmetic precision would be the most obvious at first glance but it is costly, tackles only symptoms and doesn't get to the root of the problem. Moreover this isn't always realizable in real systems.

We used the following configurations from [17, p. 140] to realize a stable behavior:

- Appropriate initializing to avoid large changes (especially in P).
- Symmetrizing P at each time step: $P = (P + P^T)/2$.
- Using fictitious process noise.
- Using a rewritten form of the covariance measurement update equation (Joseph form, Equation 7.1), thus reducing computational complexity and improving robustness.
- Defining boundaries for the parameters to estimate and resetting them when exceeding the limits (plus updating the error covariance accordingly).

The Joseph Form assures that the covariance matrix is positive semi-definite. It replaces the common covariance measurement update equation (see Equation 3.21)

$$P^+ = (I - K * C) * P^- \qquad \text{by}$$

$$P^+ = (I - K * C) * P^- * (I - K * C)' + K * R * K' \quad . \tag{7.1}$$

For better readability indexes are omitted.

Moreover it may be useful to set limits for the estimated values in order to avoid them to diverge. Physical limits are obvious, others may be predicted from previous knowledge of the cell-type, like values that can be expected for inner resistances of the cell. This is particularly important when using EKF for system identification. In-depth explanations can be found where the models are discussed in detail. The parameter values used for initializing the EKF for parameter identification are shown in Table 7.2.

	One-State Hysteresis Model (OSHM)	Enhanced Self-Correcting Model (ESCM)
$Li_4Ti_5O_{12}$/$LiFePO_4$		
Θ (if no other information on theta is provided):		
R:	0.0016Ω	0.0013Ω
g1:	—	0
g2:	—	0
g3:	—	0
$\beta 1$:	—	0
$\beta 2$:	—	0
$\beta 3$:	—	0
$\beta 4$:	—	0
M:	maximum polarization	maximum polarization
γ:	1	1
P^+:	$\begin{bmatrix} 0.0001 & 0 & 0 \\ 0 & 0.0001 & 0 \\ 0 & 0 & 0.2 \end{bmatrix}^2$	$\begin{bmatrix} 0.0001 & 0 & 0 & 0 & 0 & 0 & 0 & 0 & 0 & 0 \\ 0 & 0.0001 & 0 & 0 & 0 & 0 & 0 & 0 & 0 & 0 \\ 0 & 0 & 0.0001 & 0 & 0 & 0 & 0 & 0 & 0 & 0 \\ 0 & 0 & 0 & 0.0001 & 0 & 0 & 0 & 0 & 0 & 0 \\ 0 & 0 & 0 & 0 & 0.0001 & 0 & 0 & 0 & 0 & 0 \\ 0 & 0 & 0 & 0 & 0 & 0.0001 & 0 & 0 & 0 & 0 \\ 0 & 0 & 0 & 0 & 0 & 0 & 0.0001 & 0 & 0 & 0 \\ 0 & 0 & 0 & 0 & 0 & 0 & 0 & 0.0001 & 0 & 0 \\ 0 & 0 & 0 & 0 & 0 & 0 & 0 & 0 & 0.0001 & 0 \\ 0 & 0 & 0 & 0 & 0 & 0 & 0 & 0 & 0 & 0.2 \end{bmatrix}^2$
$\frac{dx_0}{d\theta}$:	$\begin{bmatrix} 0 & 0 & 0 \end{bmatrix}$	
Q:	$q * q'$	
q:	$\begin{bmatrix} 0.0001 & 0.0001 & 0.0001 \end{bmatrix}$	
R:	$0.1 * 0.1$	
z_0	SOC of first sample	SOC of first sample
h_0	maximum polarization value of the particular cell chemistry	maximum polarization value of the particular cell chemistry

Table 7.2: The paramter values that are used to initialize the EKF for parameter identification are the same for both chemistries except the value of maximum polarization.

7.2 State-space equations for output estimation (Simple Model, Zero-State Hysteresis Model)

To get a glimpse whether the identified parameters are appropriate or not, they can be fed into the state space equations and be tested using the known initial condition of the system's state.

Both models, SM as well as ZSHM, use the current integral to determine the state of the next time step. This equals the procedure the Ah-values of the test-set itself have been determined. Therefore to some extend a correct state estimate can be expected. But the estimated SOC won't match the 'true' values exactly, since these are drift corrected and the 'estimates' of the state equations are not (just integrating the current leads to the same amount of drift that has been corrected in advance when generating the training and test sets).

A correct initial state value is needed because a state-space model itself is not able to adapt or correct its estimates to any measurements[2].

Nevertheless, the comparison of the estimated output voltage to the measured output voltage gives evidence if the magnitudes of the internal resistances lie within plausible ranges or not.

7.2.1 Lithium - Titanate cell

Figure 7.2 shows the results for a single test set at 35°C with a start SOC of 53%. 7.2(a) shows the whole sequence whereas (b) and (c) zoom in for details.

Looking at the trend of SOC in (a) the drift starts to become evident after about 25 minutes.

Retrieving the to the system state (i.e. SOC) corresponding voltage values from the OCV-LUT leads to the first rough estimate that output equations of all models have in common. It is represented by the blue solid line that can be seen in the second plot in (a). An output equation is generally composed of the rough estimate taken from the LUT and improved by additional terms that take the actual input current and possible additional system states into account:

$$\underbrace{y_k}_{\text{red solid line}} = \underbrace{\mathrm{OCV}(z_k)}_{\text{blue solid line}} - \underbrace{Ri_k \quad \ldots}_{\text{additional terms}}$$

An interpretation from a different point of view would be that the blue line represents the system at rest and the additional terms model the dynamics of the system.

[2]To recall the models see the sections 4.1 and 4.2 on page 27f.

In Figures 7.2(b) and (c) a timeframe is picked where the drift does not play a role yet as can be seen in the first plot of (b). Investigating the positive and negative peaks of the voltage it turns out that sometimes the estimated value matches the true value pretty accurate and sometimes the differences of the amplitudes are quite big. On the one hand this is caused by inaccurate values of the internal resistances, but on the other hand universal and accurate magnitudes do not exist. The internal resistances do not only depend on temperature but also on the condition of the input current: Amplitude as well as duration of a current pulse do have influence on the internal resistance of a cell.

The characteristic of the input current is opposed to a (greater) zoom of the output voltage in Figure 7.2(c). While first the resistances seem to be too small for charge and too large for discharge, a minute later the values get very close.

Another interesting observation can be made around minute 2,2: A longer period of constant input current close to zero causes a nearly constant estimate of the output voltage while the true voltage slowly decays to OCV (i.e. the blue line). This phenomenon is referred to as relaxation. Since the SM doesn't take it into account[3], the output estimate proceeds with a step instead of a smooth decay. This step can also be noticed in (b) around minute 1, 1.2, 3.4 and 4.6. For data at 35°C the OCV-characteristic at 40°C was used.

Figure 7.3 shows the root mean squared errors of output voltage and the SOC. Since SM and ZSHM only differ in their output equations, the SOC-error stays the same. The error of the output voltage is in the case of ZSHM slightly higher than in the case of SM. This can be explained by the fact, that ZSHM adds / subtracts the maximum polarization value i.e. the 'worst case' hysteretic behavior in form of the constant parameter M. The model 'thinks' that the cell's voltage constantly deviates from OCV-level about $1 - 2mV$. But the real hysteresis is far smaller up to zero, so augmenting the OCV-value by M may lead to worse results in that specific case.

Moreover it appears that with increasing temperatures the voltage error diminishes. From this the conclusion can be drawn that the smaller internal resistance values that have been identified for higher temperatures, fit the model and thus model the cell better than greater values.

Training sets were built from data with 43% SOC as initial condition. Even though best results are gained using test sets with 33% start SOC (Figures 7.3(a), (c)). Since the OCV-characteristic of LiTi has nearly the same gradient for every of the three initial conditions, it can not be responsible for the divergence. A plausible explanation is the assumption that also the current state of the cell has an impact on the internal resistance. That means that the internal resistance at 53% SOC differs, due to differing proportions

[3]The relaxation effect is modeled within the Enhanced Self-Correcting Model, for implementation details and results see 7.3.1 and 7.3.2

of the chemistries inside the cell, from the internal resistance of the same cell (at the same temperature and age) at 33%.

Figures 7.3(b) and (d) are not very meaningful since the state is not really estimated but computed and therefore inaccurate due to drift. Thus the magnitude of the bars only states how much the data drifts. The current sensor that has been used was a hall effect sensor whose drift depends on the magnetic field it was exposed to during recently past measurements. Remarkable is the fact that the RMSE of the test set an 42°C almost doubles the RMSE of SOC of the other data sets: This data was recorded weeks before and the remaining data sets during consecutive experiments.

Equivalent to Figure 7.2, Figure 7.4 shows the results when testing the ZSHM with the same test set. Figures 7.4(a) and (b) are directly comparable to Figures 7.2(b) and (c).

Using life-cycle data for testing makes the drift obvious. In Figures 7.5(a) and (b) the SM has been used and has not been altered, merely the test set has been exchanged by its drift affected pendant. Thus it is evident, that the error of the estimated output voltage is due to drift caused by the current sensor. Moreover this is the proof that data (training sets and test sets) need to be drift corrected.

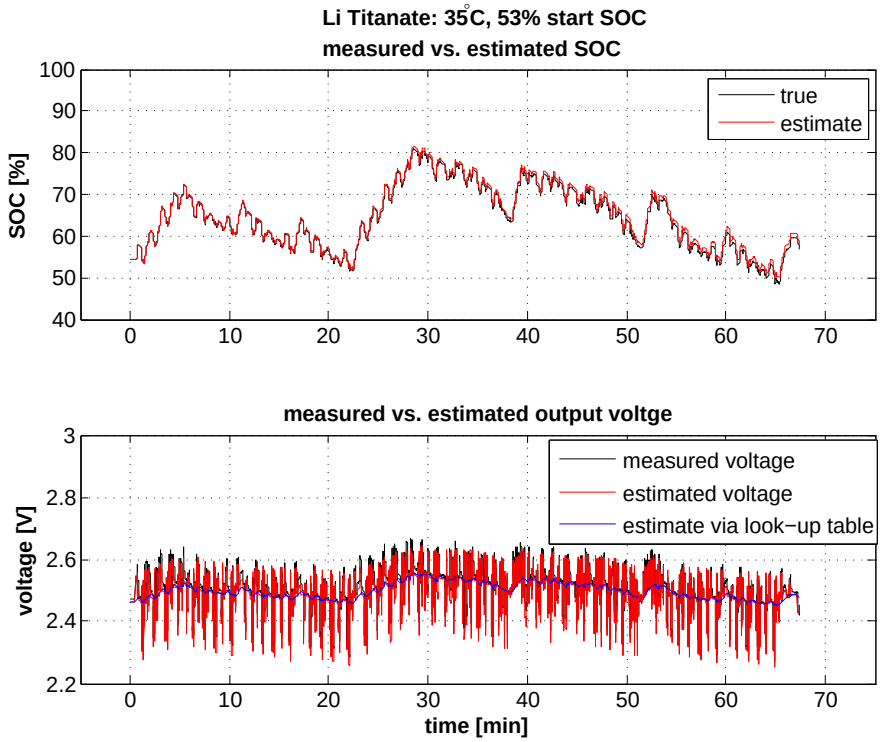

(a) SOC and output voltage of the whole cycle. The first plot shows the true SOC-values in comparison to the estimate of the state equation. The blue solid line in the voltage plot marks the crude estimate by the LUT. This estimate added up with the voltage computed from internal resistance and input current results in the red line and represents the estimate of the output equation.

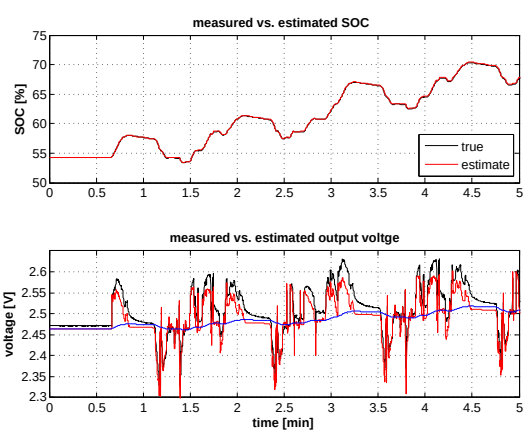

(b) Zoom of first 5 minutes (drift has no serious impact yet).

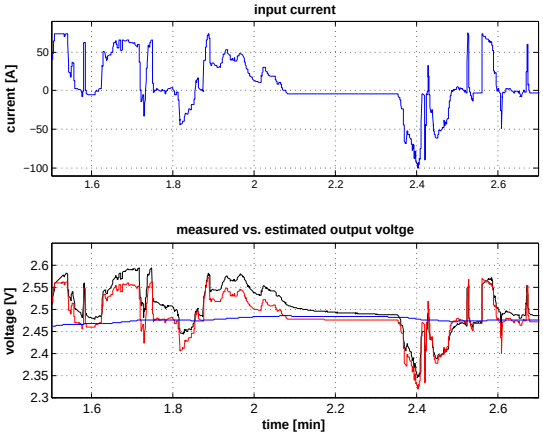

(c) Detailed zoom lined up with corresponding input current.

Figure 7.2: Simple Model (SM). Test-cycle at 35°C with initial condition of 53% SOC. Internal resistances: $1,3122m\Omega$ (charge), $1,5813m\Omega$ (discharge). Red lines represent the 'estimates' by the state-space equations, black lines the true values. (b) and (c) zoom in on same data as shown in (a).

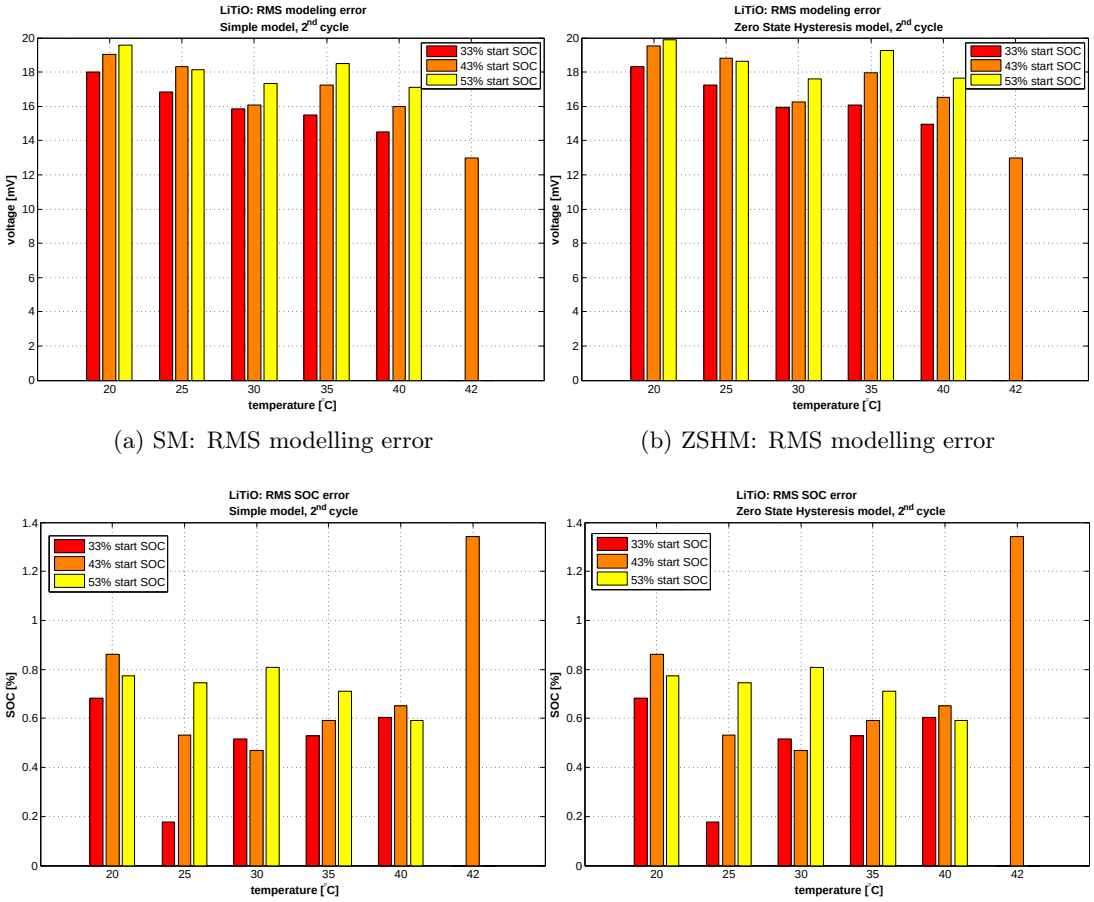

(a) SM: RMS modelling error

(b) ZSHM: RMS modelling error

(c) SM: RMS SOC error

(d) ZSHM: RMS SOC error

Figure 7.3: Root mean squared errors of output voltage and SOC for the LiTi-cell when only using the state-space equations for prediction.

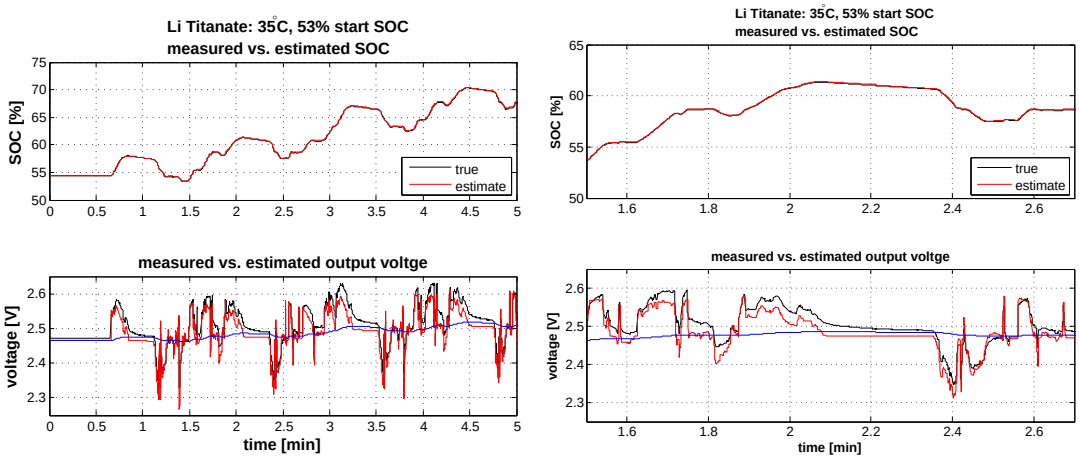

(a) Zoom of first 5 minutes (drift has no serious impact yet).

(b) Detailed zoom.

Figure 7.4: Zero-State Hysteresis Model (ZSHM). Test-cycle at 35°C with initial condition of 53% SOC. Internal resistances: $1.3674m\Omega$ (charge), $1.6440m\Omega$ (discharge). Maximum polarization M: $2.8686mV$. Red lines represent the 'estimates' by the state-space equations, black lines the true values.

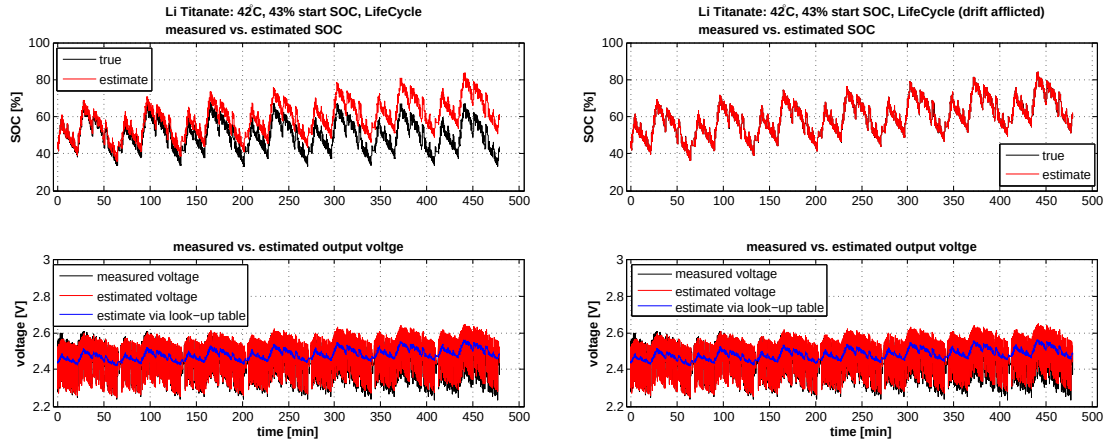

(a) drift corrected

(b) drift affected

Figure 7.5: Simple Model (SM). (a) Drift corrected data of the life-cycle at 42°C, (b) same data as in (a) but including the drift.

7.2.2 Lithium - Iron - Phosphate cell

In the case of Lithium-Iron-Phosphate (LiFePO), the drift caused by the current sensor is worse than in the case of Lithium Titanate. When using the state-space equations without the possibility of correcting the state itself it quickly decays to 0% SOC (and would fall below, what is physically impossible.). This is shown in Figure 7.6 together with the corresponding zoomed details in (c) and (d).

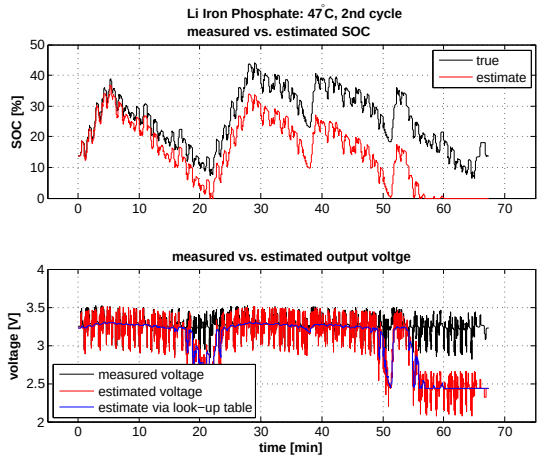

(a) LiFePO, SM.

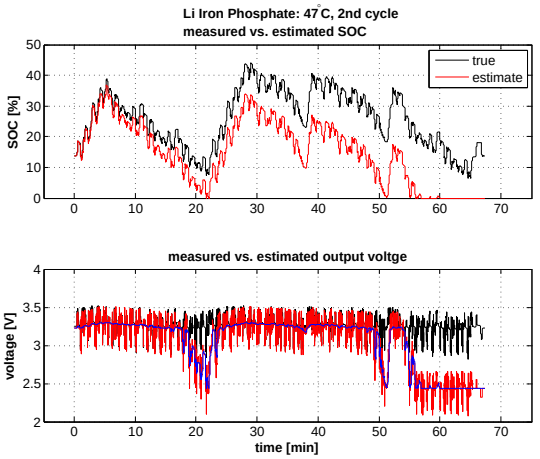

(b) LiFePO, ZSHM.

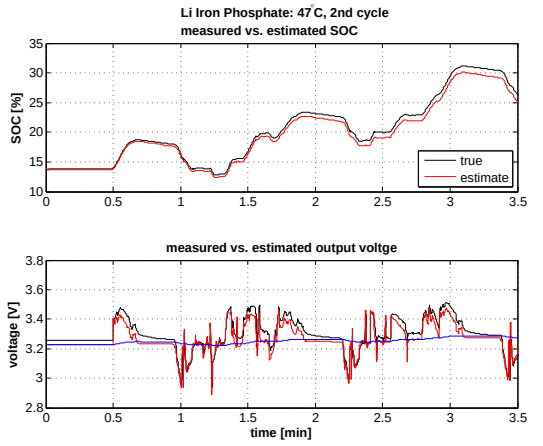

(c) SM, zoomed details

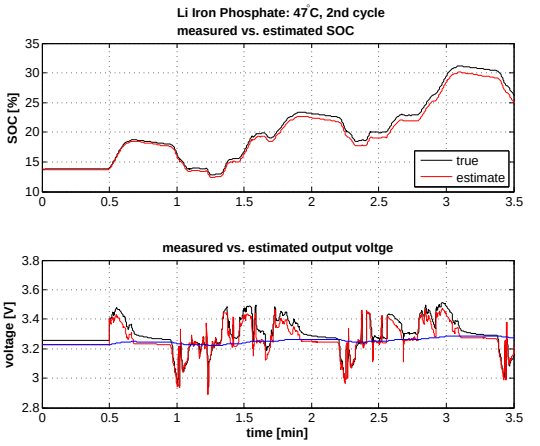

(d) ZSHM, zoomed details

Figure 7.6: LiFePO: Parameters for SM: $1.5568m\Omega$ (R+), $1.5472m\Omega$ (R-); for ZSHM: $1.5402m\Omega$ (R+), $1.5287m\Omega$ (R-), $1.5675mV$ (M).

7.3 The Extended Kalman Filter for state estimation

Once parameters are determined, every model can be fit into an EKF for state estimation. Even in the case of SM and ZSHM an EKF is necessary, since in the output equations z_k occurs as parameter of the function OCV(z_k) and is not only associated with a linear coefficient.

Process noise and measurement noise are assumed to be zero-mean white Gaussian stochastic processes and can therefore be considered as invariant and chosen within plausible ranges (see section 3.1). The process noise Q is defined as diagonal matrix of same size as the state vector. The measurement noise R is important to select well, since it determines how much the filter 'trusts' the actual measured value compared to it's own prediction.

The measurement was carried out using a hall effect sensor. Thus the measurement noise would in fact be depending on the current and diminish if it is constant over a period of time. But this is neglected within the modelling. The characteristic of these sensors that must not be neglected is that they are prone to temperature and cause significant drift which has to be compensated.

7.3.1 Lithium - Titanate cell

For the Lithium Titanate cell test sets for various temperatures with different initial SOC were available (Table 7.3). For each temperature the corresponding training set was loaded and the system parameters were determined using least squares or EKF like already explained in sections 7.1.1 and 4.6.2. Since OCV is only available at 25°C and 40°C, the OCV-characteristic with temperature closer to the temperature of the training set was used[4].

	33%	**43%**	**53%**	**lifecycle, 43%**
20°C	✓	✓	✓	
25°C	✓	✓	✓	
30°C	✓	✓	✓	
35°C	✓	✓	✓	
40°C	✓	✓	✓	
42°C		✓		✓

Table 7.3: Available data sets for the Lithium Titanate cell, used for cell testing.

In order to be able to compare the results directly (and since the data was the same

[4]The OCV characteristic at 25°C was used for 20°C, 25°C and 30°C data; the OCV characteristic at 40°C was used for 35°C, 40°C and 42°C data sets.

for each test) for each model the same process noise and measurement noise were chosen: Q = a diagonal matrix of same size as θ, with 0.001^2 as main entries; $R = 0.5^2$.

Preliminary the state variable z_{k-1} was initialized to a random SOC-value between 20% and 80%. This is the range, the SOC of a battery pack of a HEV is expected to lie within.
The corresponding error covariance can only be a guess since no 'a priori' measurement exists. The only prior knowledge ready at hand is that data sets start at 33%, 43% or 53% of SOC. The first sample of the state variable z will therefore lie within the interval on which z_{k-1} has been initialized before. It is likely that between two samples the state variable does not make large changes.
In practice initialization errors of more than 20% are not very realistic and mainly depend on the shape of the OCV-characteristic.

60% SOC is the difference of the maximum and minimum value of the desired range mentioned above and is used as kind of worst case guess for initializing the error covariance value of z: $P^+_{k-1} = 60^2$. The random number for z and the first sample of the data set (which roughly can also be interpreted as real value of z_{k-1}) will not differ more than 60%, this holds true for every data set and is used for initializing the corresponding error covariance.
The sampling rate for the 'preceding' output sample was set to 20ms in order to fit the data characteristics.

In order to avoid the estimated state values to run out of physical boundaries, their reasonability is verified after each iteration of the filter. In the case of SOC the value is reset to 50%, if the value of z was beyond its boundaries of 0% reps. 100%.

As showcase, test runs at 30°C with start-SOC of 33% are used. Taking into account the estimated inner resistances and root mean squared error values, performance can be expected to be quite good.

Simple Model

When feeding the SM into the EKF the parameter set determined through least squares estimation (Table 7.1) was used. The state variable was initialized as declared in the beginning of this Section (7.3.1). Results are shown in Figure 7.7. Jumps regarding the trend of the values from 30°C to 35°C may very likely refer to the use of different OCV LUT. Figures 7.8 and 7.9 show the performance of the model for data at $30C$.

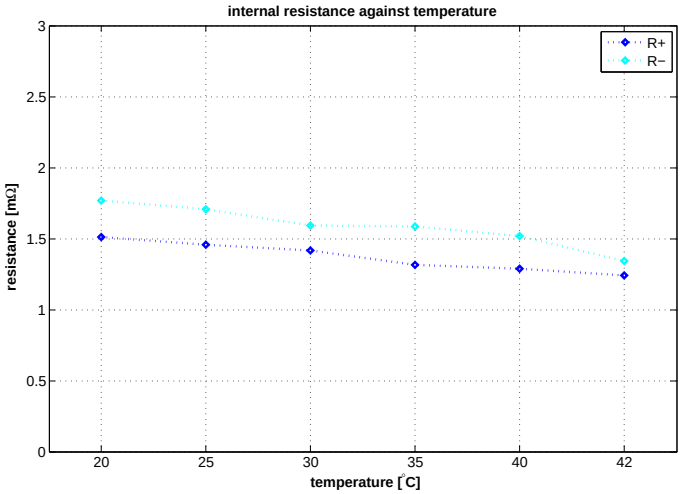

(a) Estimated parameters.

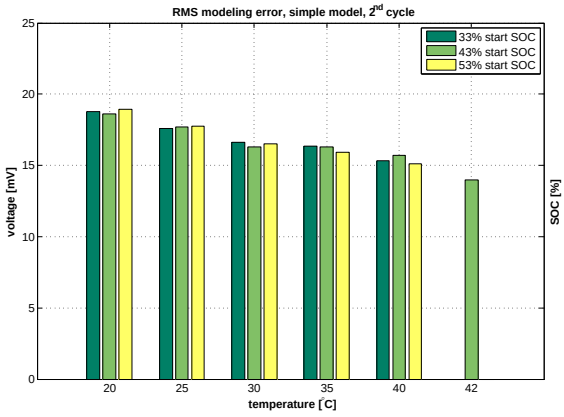

(b) Modelling error.

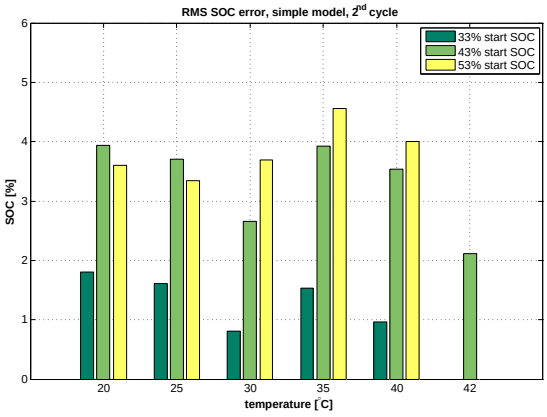

(c) SOC error.

Figure 7.7: Simple Model (SM), (a) Parameters estimated via least squares estimation, (b) and (c) RMS errors regarding the output voltage and estimated SOC value for each available test-set.

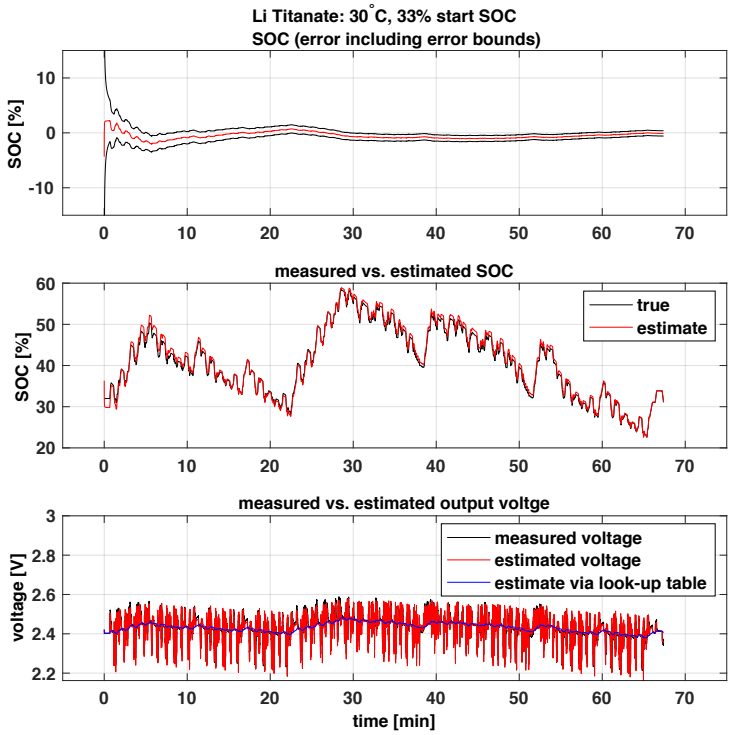

Figure 7.8: LiTi, test data at $30°C$, 33% start SOC: Measured and estimated output voltage and SOC for 2^{nd} cycle of a test-cycle, using EKF and SM for state estimation. Figure 7.9 shows the first five minutes of same data.

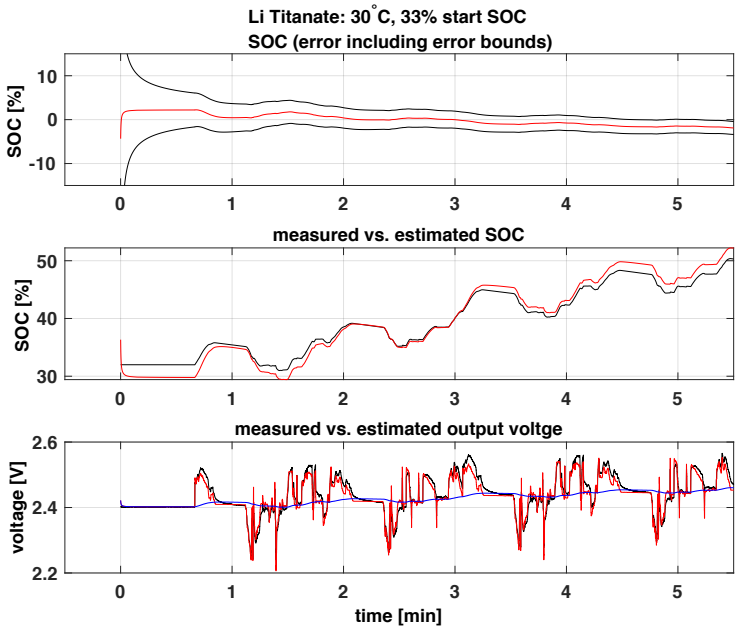

Figure 7.9: SM. Detailed zoom of Figure 7.8

Zero-State Hysteresis Model

Though another parameter M is added, the model is still linear in its parameters. Thus they are determined via least squares as in the case of the SM (Table 7.1). Initialization of the single state variable was the same as explained earlier (7.7). Jumps regarding the trend of the values from 30°C to 35°C may very likely refer to the use of different OCV LUTs. The estimated parameters together with the results are shown in Figure 7.10.

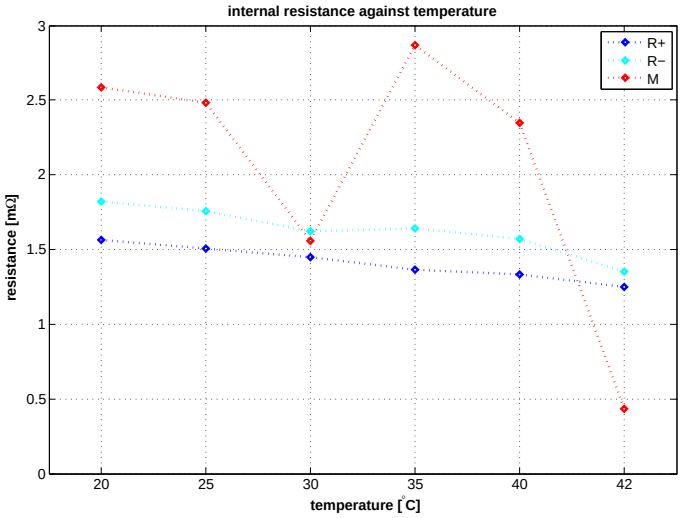

(a) Estimated parameters.

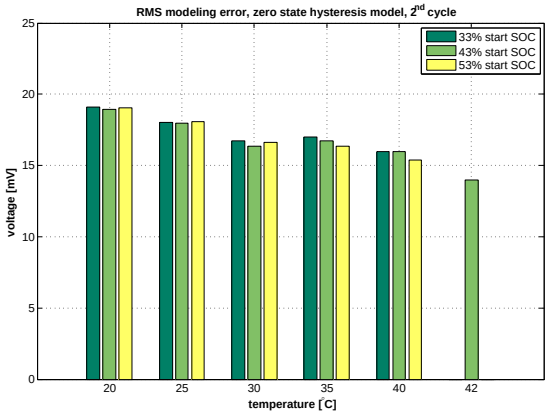

(b) Modelling error.

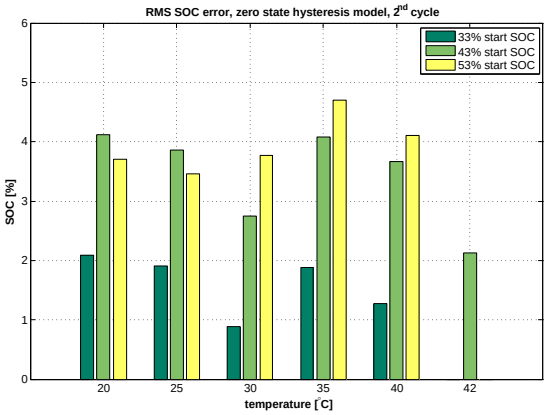

(c) SOC error.

Figure 7.10: Zero-State Hysteresis Model (ZSHM), (a) Parameters estimated via least squares estimation, (b) and (c) RMS errors regarding the output voltage and estimated SOC value for each available test-set.

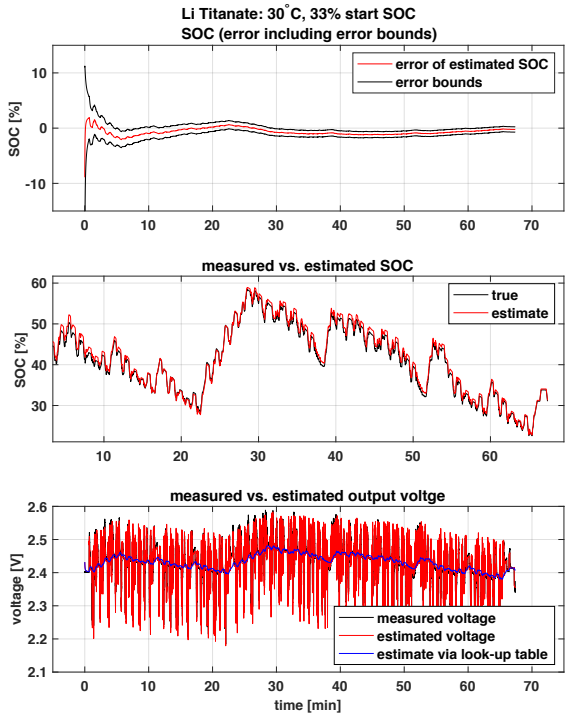

Figure 7.11: LiTi, test data at $30°C$, 33% start SOC: Measured and estimated output voltage and SOC for 2^{nd} cycle of a test-cycle, using EKF and ZSHM for state estimation. Figure 7.12 shows the first five minutes of same data.

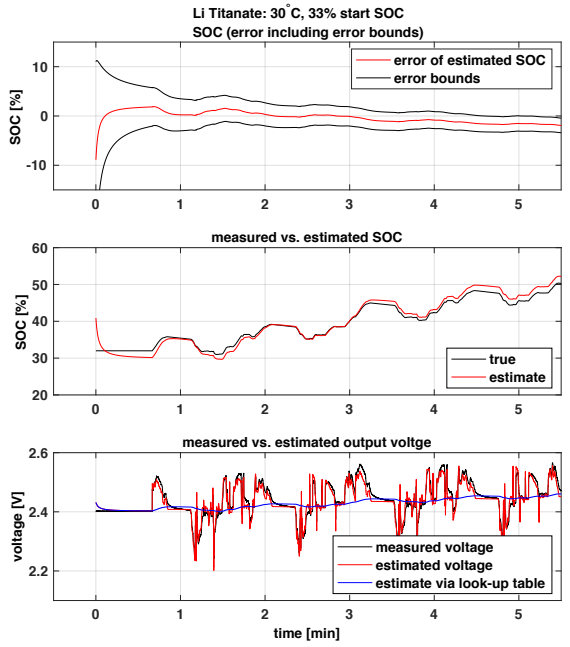

Figure 7.12: ZSHM. Detailed zoom of Figure 7.11

Comparison of models (SM, ZSHM) that are linear in parameters by means of test data at $30°C$ and start SOC of 33%.

Both models have the same inner resistances identified (see Figures 7.7(a) and 7.10(a)). They have similar performance, ZSHM seems to lead to a little worse results than SM. This may refer to the characteristics of the LiTi-cell which hardly shows hysteresis effects, thus very small maximum polarization values are identified which still may be too large. Also recall that OCV data is not very accurate at least for SOC-levels greater than 50%. The hysteresis legs are interleaving which is theoretically impossible and may cause faulty values of maximum polarization (see Chapter 6.4 and further discussion within Chapter 7.2.1). Recall when using the state equations of SM and ZSHM for state estimation, data is prone to drift (Chapter 7.2.1, Figure 7.5), whereas feeding them into an EKF, the model corrects itself and adapts appropriately.

Figure 7.11 and 7.8 show data from the 2^{nd}cycle of the test-cycle at 30°C and start SOC of 33%[5]. As mentioned before, OCV-data seems to be more trustworthy for smaller SOC-values and with regard to parameter estimation the lower temperatures seem to yield not the best, neither the worst results but a balanced compromise.

[5]This cycle is used for demonstration for all models using EKF

One-State Hysteresis Model

The OSHM is not linear in its parameters ($\theta = [R^{\pm}, \pm M, \gamma]$), thus they need to be estimated using an EKF. It turned out to be necessary to estimate separated parameters sets for charging and discharging. Otherwise the filter would not converge. The longer a sequence of charging / discharging is, the more reliable the result of the parameter set will be.
Unfortunately the training data consists of short sequences of charging and discharging stringed together. Thus the training set is parsed for sequences of continuous input current values of the same sign for at least 8 seconds which equals a subset of data consisting of 400 samples or more. Each subset is provided to the filter where the results of a processed subset are used as initial values for the subsequent set. The parameters of the very first subset are initialized to $R^{\pm} = 1.6m\Omega$ (see Table 7.1), $\pm M = \pm$*maximum polarization value* derived from the OCV-characteristic and $\gamma = 1$ (positive constant, neutral element).
This approach may be more time consuming but cannot be avoided. The testing using all available test sets including parameter estimation for each temperature takes about 7 minutes[6].
Again, the estimations of the filter need to be restricted to reasonable boundaries, namely: R has to be positive, $3m\Omega > R > 0\Omega$; M has to have the correct sign and should not exceed the maximum polarization two times, γ has to be positive. It is substantial for the modelling that those restrictions are well-considered. If they are too loose or too strict, parameter estimation leads to unreasonable values which has bad influence on the performance of the model later on.
If it is necessary to reset the estimated values, the error covariance needs to be updated accordingly. Furthermore it may happen, that due to round-off errors, the covariance matrix does not stay symmetric, which is also prevented programatically.

Figures 7.13 and 7.14 show the estimated parameters and the performance of the model if the inner resistance R is limited to $3m\Omega$ compared to a strict limit of $1.8227m\Omega$ which is the highest inner resistance that has been identified earlier using least squares (see Table 7.1). A loose restriction for R during parameter identification leads to larger inner resistances in general. But the ratio between charging and discharging values stays roughly constant and values decrease over increasing temperature. Compared with the result from least square estimation (Figure 7.1 and Table 7.1, the maximum values for the inner restitances are $R+ = 1.5621m\Omega$ and $R- = 1.8227m\Omega$ estimated for ZSHM at 20°C. It can be assumed that with increasing temperatures of the coolant, the values of the inner resistances decrease, as it happens, if the filter is allowed to converge somewhere between zero and double the value that is expected.

[6]Platform: MacBook Pro, 2.4 GHz Intel Core i5, 4 GB 1333 MHz DDR3, OS X 10.7.5

It seems that parameters within more severe restrictions do not evolve correctly, even though the model gives the impression to perform better with smaller inner resistances. Nevertheless for all computations less severe restrictions were chosen. Parameter identification using EKF seems to work fine. If it does not converge to exactly the expected values - like in the particular case of the inner resistances - it may be caused by the fact, that the EKF is not provided all data but subsequences and / or the data is not optimal for accurate parameter estimation.

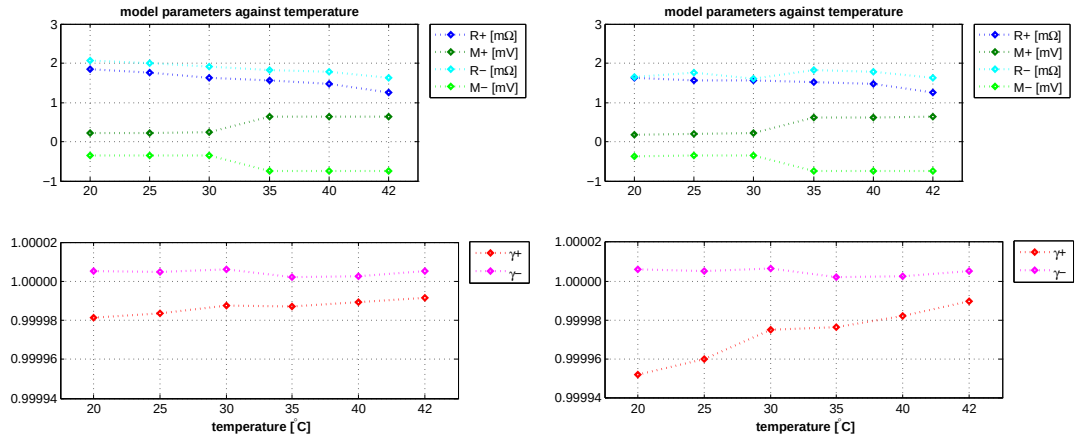

(a) R limited to $3m\Omega$. (b) R limited to $1.8227m\Omega$.

Figure 7.13: LiTi: Estimated parameters for OSHM (via EKF).

The additional state variable h is initialized to $0.5mV$, which is the approx. mean of the maximum polarization values at both temperatures where OCV- data is available (see Table 6.1). To limit the value of h it is tested against the doubled maximum polarization value. If it fails, it is reset to the (positive or negative) maximum polarization value. Testing against the maximum polarization value itself seemed to be too restrictive to let the filter evolve, thus the doubled value is used instead.

Figure 7.14 shows the results using parameter sets from Figure 7.13 (a) and (b). Jumps regarding the trend of the values from 30°C to 35°C may very likely refer to the use of different OCV LUTs. As expected since LiTi does not show much hysteretic behavior, the results are similar to the results of SM (Figure 7.7) and ZSHM (Figure 7.10). Figures 7.15 and 7.16 using parameters from Figure 7.13(a) (Figures 7.17 and 7.18 using parameters from Figure 7.13(b)) show the performance of the model using data at $30°C$ of the coolant.

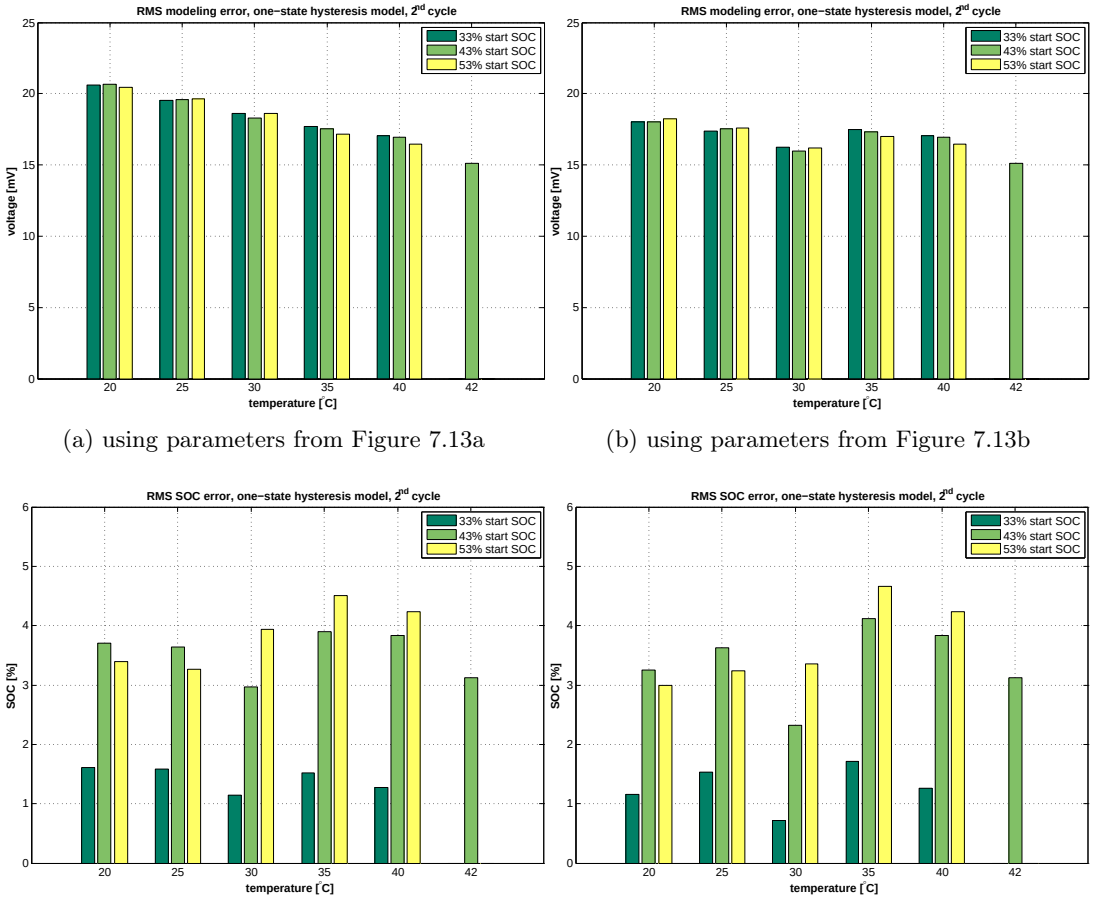

(a) using parameters from Figure 7.13a

(b) using parameters from Figure 7.13b

(c) using parameters from Figure 7.13a

(d) using parameters from Figure 7.13b

Figure 7.14: LiTi: Modeling error of the OSHM, using parameter sets obtained with different restrictions (see Figure 7.13).

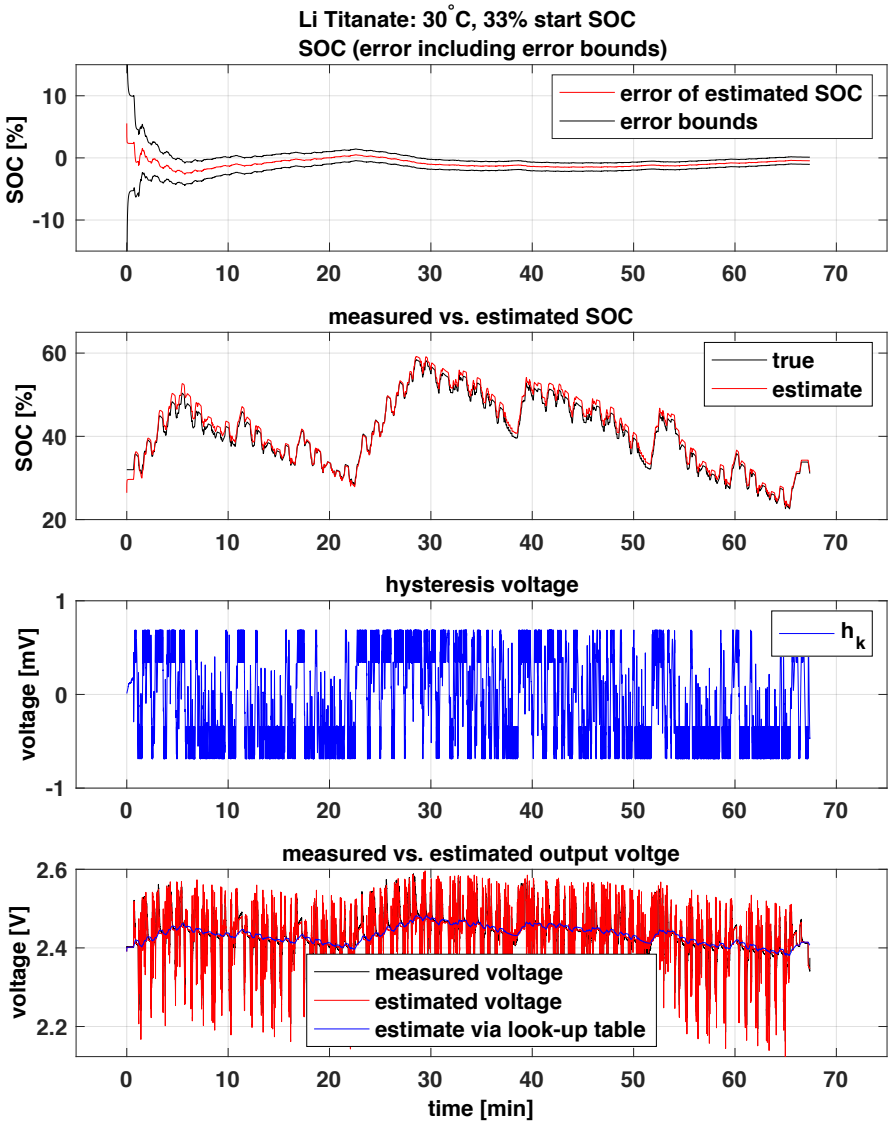

Figure 7.15: LiTi, data at 30°C and 33% start SOC: Measured and estimated output voltage and SOC for 2^{nd} cycle of a test-cycle, using EKF and OSHM for state estimation. Identified parameters as in Figure 7.13(a). Figure 7.16 shows the first five minutes of the same data in detail.

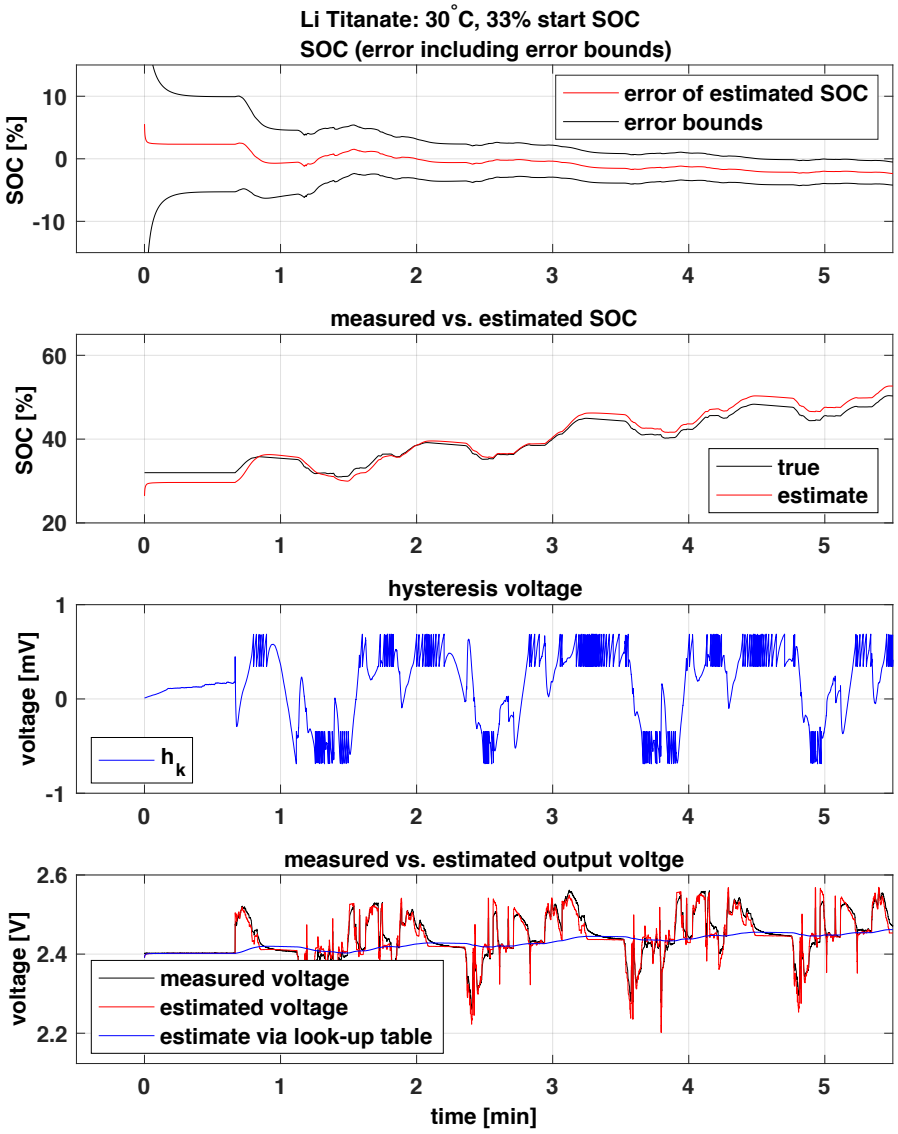

Figure 7.16: OSHM. Parameter setting: Figure 7.13(a). Detailed zoom of Figure 7.15

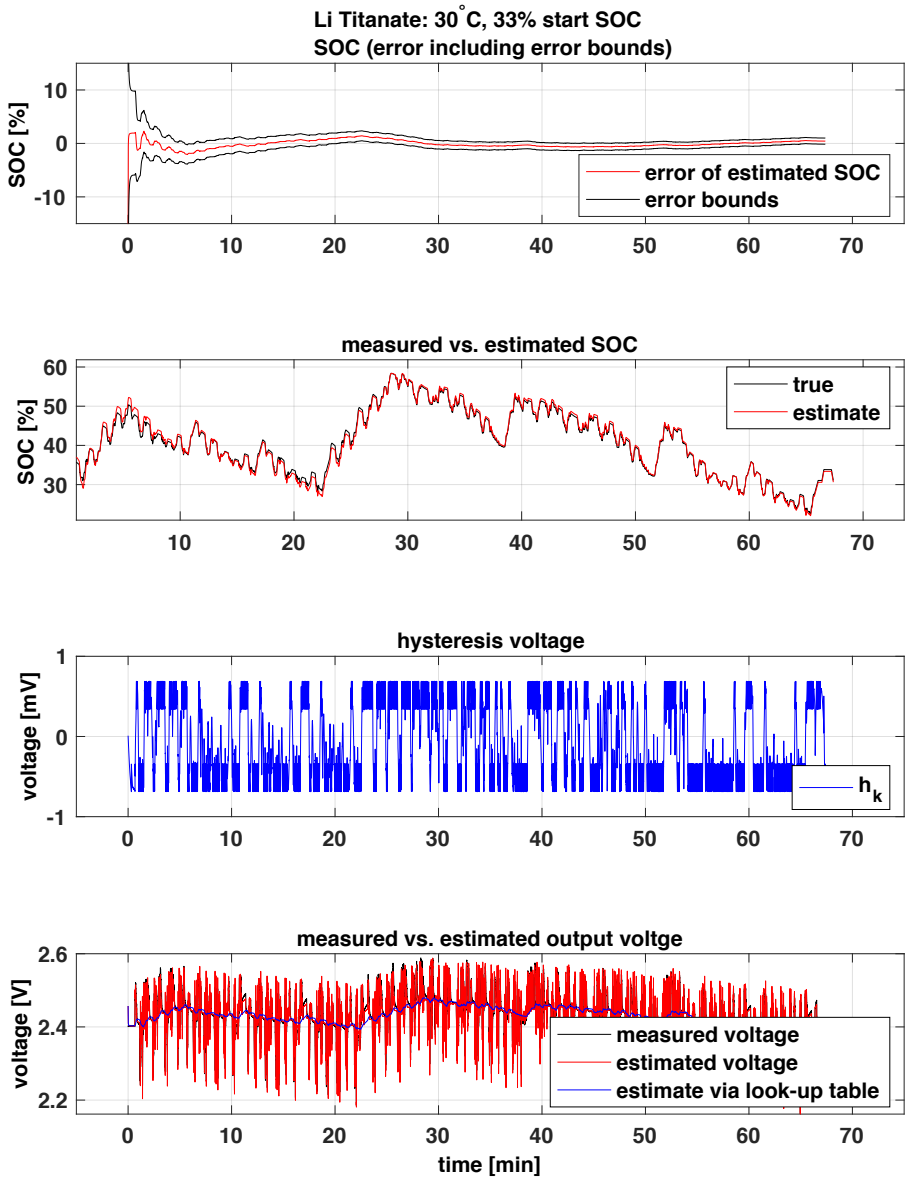

Figure 7.17: LiTi, data at 30°C and 33% start SOC: Measured and estimated output voltage and SOC for 2^{nd} cycle of a test-cycle, using EKF and OSHM for state estimation. Identified parameters as in Figure 7.13(b). Figure 7.18 shows the first five minutes of the same data in detail.

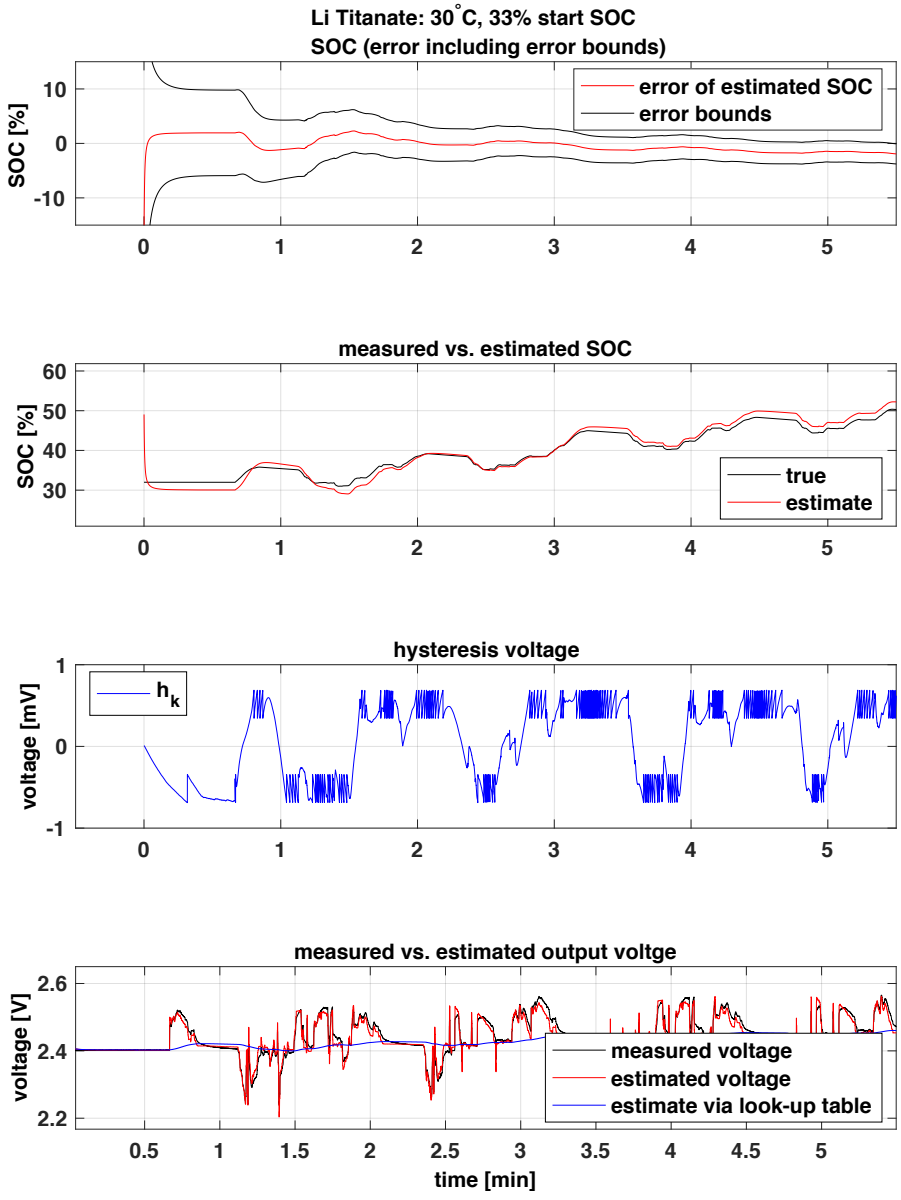

Figure 7.18: OSHM. Parameter setting: Figure 7.13(b). Detailed zoom of Figure 7.17

Enhanced Self-Correcting Model

For the ESCM not only the parameters R, M and γ have to be determined but also the filter weighting factors $g_1, \cdots, g_3$ and the poles $\beta_1, \cdots, \beta_4$ (see 4.6.2).

It seems that the more complex the model gets, the harder it is to determine the correct parameter setting. Again training data is split in charging and discharging subsets like it was already done for the parameter identification of the OSHM. The parameters both models have in common - $R^{\pm}, \pm M, \gamma$ - are initialized to the same values due to the consideration of the ESCM being an upgrade (i.e. an enhancement) of the OSHM. Thus the models can be directly compared to each other.

The remaining parameters that represent the gain of the filter, g_1, g_2, g_3, are initialized around 1 $(0.9, 1, 1.1)$, thus the diagonal matrix G would resemble the identity matrix. The parameters $\beta_1, \beta_2, \beta_3, \beta_4$ are initialized to arbitrary complex values such that a pole is located in each quadrant and none of them are complex conjugate $(0.1 + 0.1i, 0.7 - 0.3i, -0.3 + 0.04i, -0.4 - 0.6i)$. Since the EKF is robust to poor initialization the exact values are not that crucial.

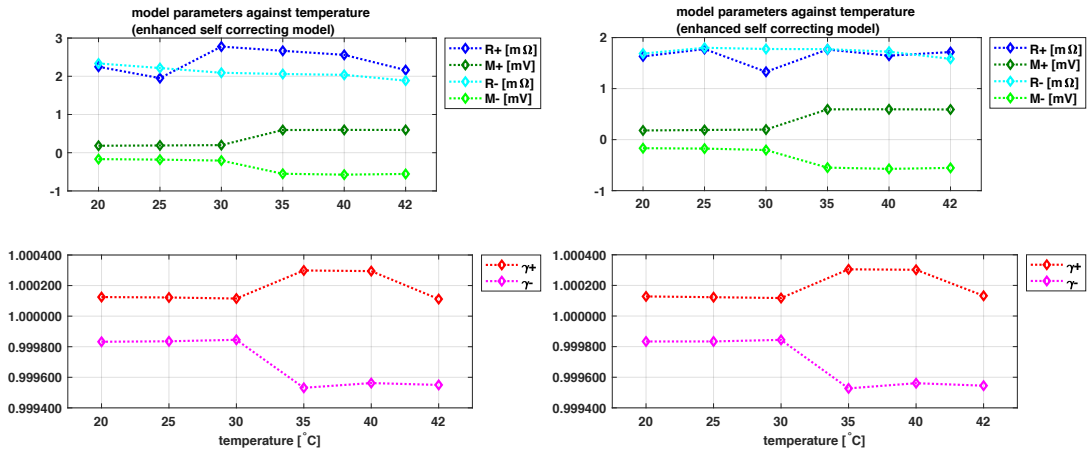

(a) R limited to $3m\Omega$.

(b) R limited to $1.8227m\Omega$.

Figure 7.19: LiTi: Estimated parameters for ESCM (via EKF).

During identification the parameters R, M, γ are tested against boundaries as already described in subsection 7.3.1. The parameters g_i may evolve freely, but β has to be forced within boundaries too. The reason for that are round-off errors during computation. Even when α stays within its bounds $-1 < tanh(\beta) < 1$ (according to the definition of the tangens hyperbolicus), α would not only approximate but become 1 if only β would be a sufficient large number. Matlab evaluates $tanh(5)$ to 0.9999 [7], $tanh(5.2) = 1.0000$. The

[7] assuming datatype short

latter would lead to division by zero when deriving g_4. Therefore it is crucial to ensure that each $|\alpha| < 1$ and therefore force each β to stay within $|\beta| = \pm 5$ (see also the definition of α: 4.23).
In order to avoid bad values of the remaining parameters, they are verified to be real numbers and reset to their real part if necessary.
If the correction of parameters is necessary, the error covariance matrix is updated accordingly. The identified parameters are shown in Figure 7.19. Looser restrictions for R during parameter identification lead to larger inner resistances as already noticed before, but in comparison to system identification using the OSHM (Figure 7.13) they've increased even more.

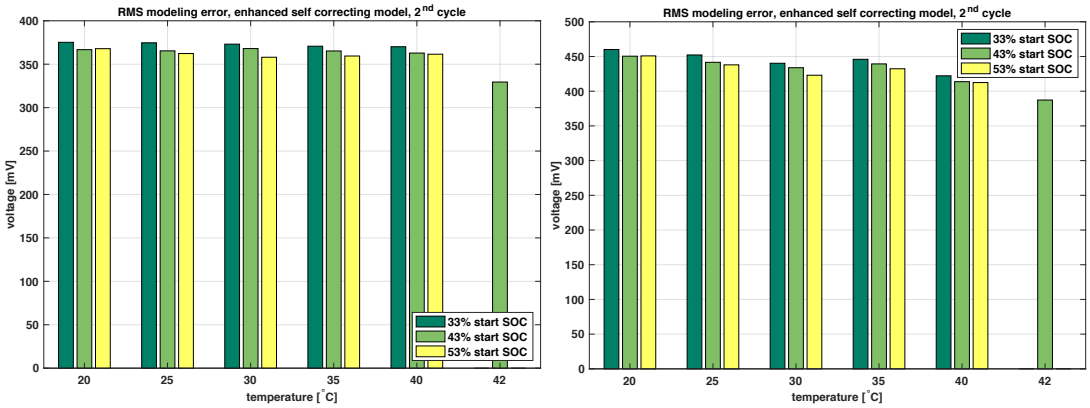

(a) using parameters from Figure 7.19a

(b) using parameters from Figure 7.19b

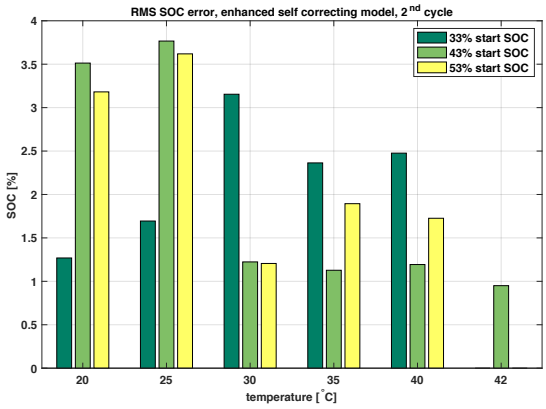

(c) using parameters from Figure 7.19a

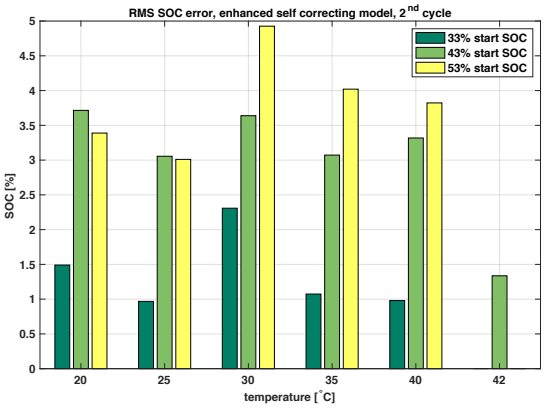

(d) using parameters from Figure 7.19b

Figure 7.20: LiTi: Modeling error of OSHM, parameter sets with different restrictions (see Figure 7.13).

When using the identified parameters to run the EKF model with, the state variables SOC and hysteresis voltage need to be tested with regard to their real numbered nature

too. To keep the state variables within physical boundaries the same checks as described for the OSHM in Section 7.3.1 are applied.

The parameter determination in this case identifies much greater values for the inner resistances than the other models (see Figure 7.19). It is obvious that those values cause oversized voltage peaks when comparing the estimated to the measured output value. This can be seen in 7.20(a) and (b) - the resulting RMS modelling error is more than ten times higher than for the OSHM. But the estimation of the state variable seems to be very accurate and the EKF converges with more ease when restrictions are not too rigorous. ESCM yields the best result for the life-cyle though. Figures 7.21 to 7.24 show the performance of the model using the same test data at $30°C$ as for the previous models. The oversized voltage peaks of the estimated output voltage can clearly be seen in the corresponding subplots of the figures.

In the case of ESCM parameter identification and testing using all available test sets lasts about 16 minutes.

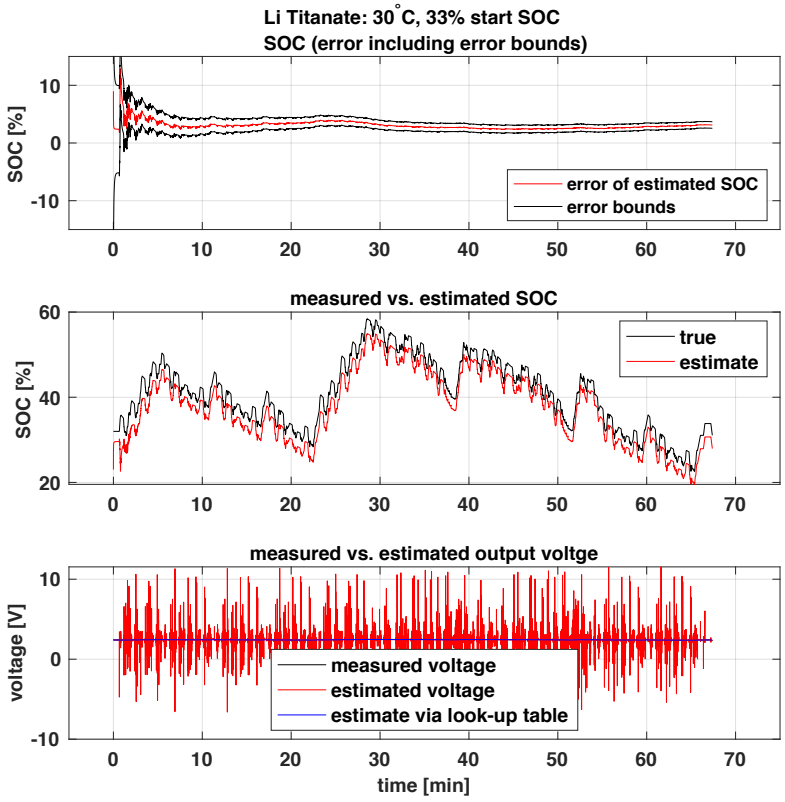

Figure 7.21: LiTi, ESCM, test-cyle at $30°C$ and 33% start SOC. Measured and estimated output voltage and SOC. Identified parameters as in Figure 7.19(a). Figure 7.22 shows the first five minutes of the same data in detail.

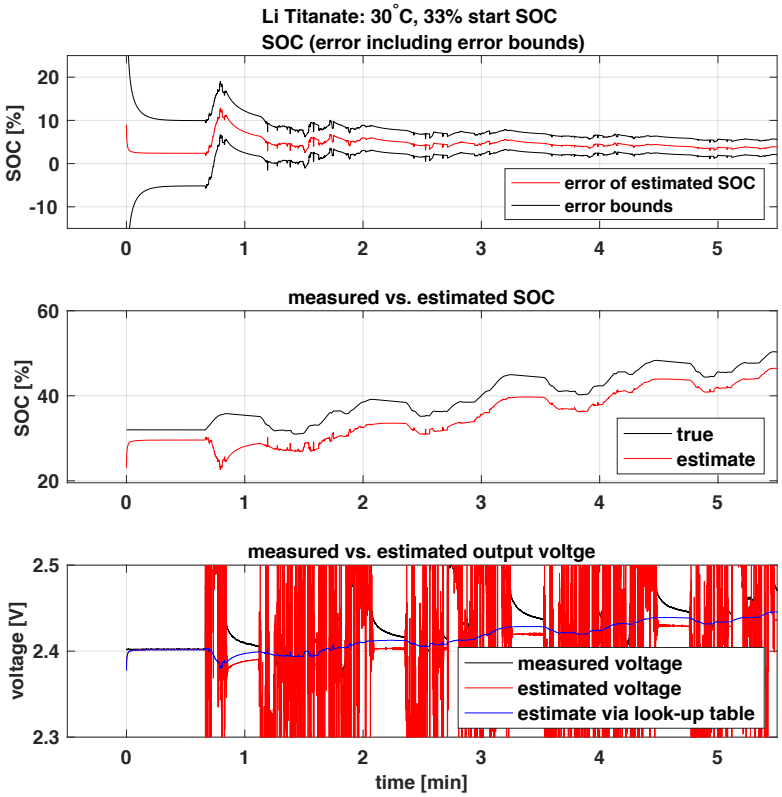

Figure 7.22: LiTi, Detailed zoom of Figure 7.21

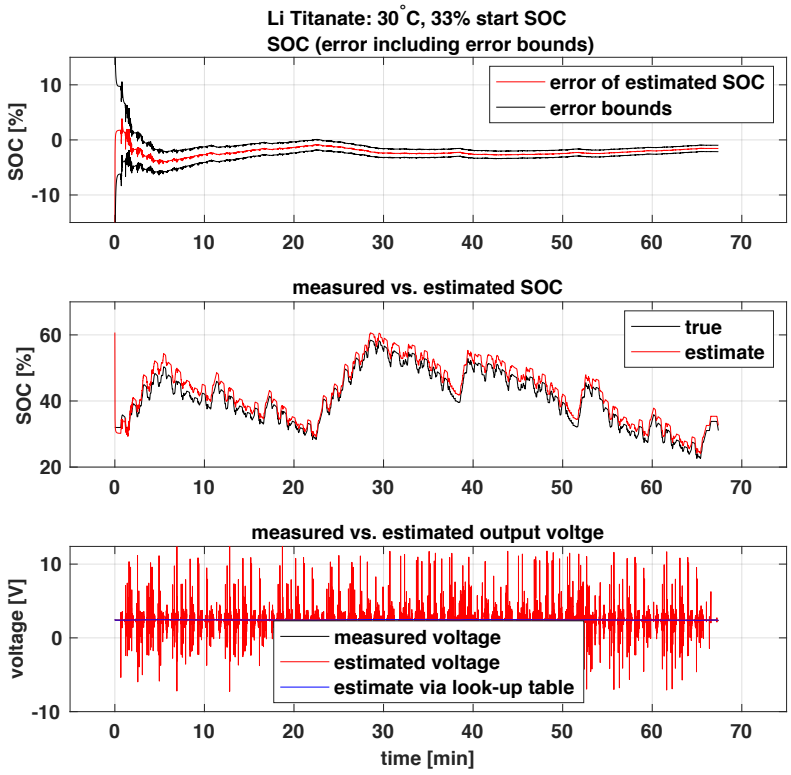

Figure 7.23: LiTi, ESCM, test-cyle at $30°C$ and 33% start SOC. Measured and estimated output voltage and SOC. Identified parameters as in Figure 7.19(b). Figure 7.24 shows the first five minutes of the same data in detail.

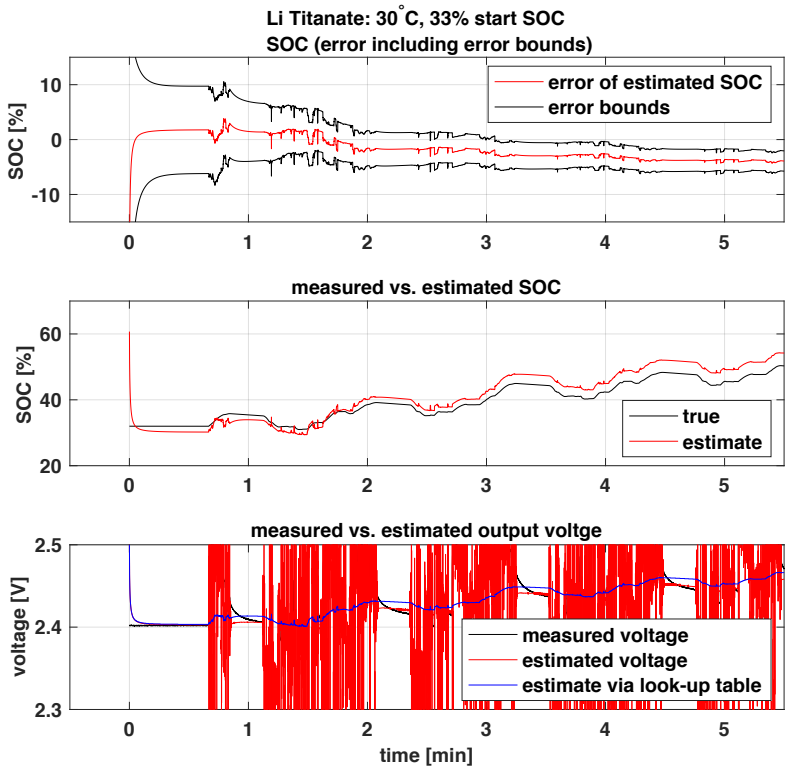

Figure 7.24: LiTi: Detailed zoom of Figure 7.23

7.3.2 Lithium - Iron - Phosphate cell

For the LiFePO-cell the same scripts were applied as for the LiTi-cell. Since only test data at 47°C is available, the OCV characteristic at 40°C was used. For lack of further insights, nearly the same settings as for the LiTi-cell were applied except for the measurement noise $R = 0.1^2$ (the process noise stays the same: $Q = 0.001^2$). For details see section 7.3.1.

One major difference to the data of the LiTi-cell are the initial values of the SOC: the test-cycle test starts at approximately 14% SOC, whereas the life-cycle test starts at approximately 25% SOC, which are very small numbers regarding the fact that usually the cells are tried to keep in the range of 20% to 80% SOC in order to avoid overstressing of the cell. But taking the OCV-characteristic in account (see Figure 6.5), these values lie within a range where the curve shows the highest gradient and is almost linear which is ideal for using the characteristic as LUT, since no ambiguous values will occur as they would in higher regions. Therefore the state variable representing the SOC will be initialized accordingly to a random number $10\% \leq z \leq 40\%$ SOC during testing.

Simple Model

Parameter estimation and testing for the SM model takes about 90 seconds. The internal resistances for discharge, R^+, and charge, R^-, are identified using least squares. The parameters are listed in Table 7.1.

Keeping in mind that the OCV-characteristic isn't that much reliable for LiFePO due to noisy data, the rough estimate by the corresponding LUT isn't reliable either. Since that given estimate plays a huge role for all models this can be regarded as systematic bias or error the EKF is likely to compensate. Compare the OCV curve of the LiFePO-cell(Figure 6.5, Section 6.5) to the performance of the model in Figures 7.25 and 7.26. Notice the bend of the OCV-characteristic close to 10% SOC and oppose it to the resulting values of the estimated output voltage by the LUT represented by the blue line of the bottom plot. Inaccuracies of the OCV- characteristic for low SOC-values can be seen in the voltage plot by the blue line which represents the estimate from the OCV LUT: for SOC-values significantly smaller than 20% the curve which is in general smooth shows unusual big changes and jumps. The bottom plot of Figure 7.26 shows that the identified inner resistances seem to fit the model since the estimated output voltage matches the measured output voltage well (especialy the peaks).

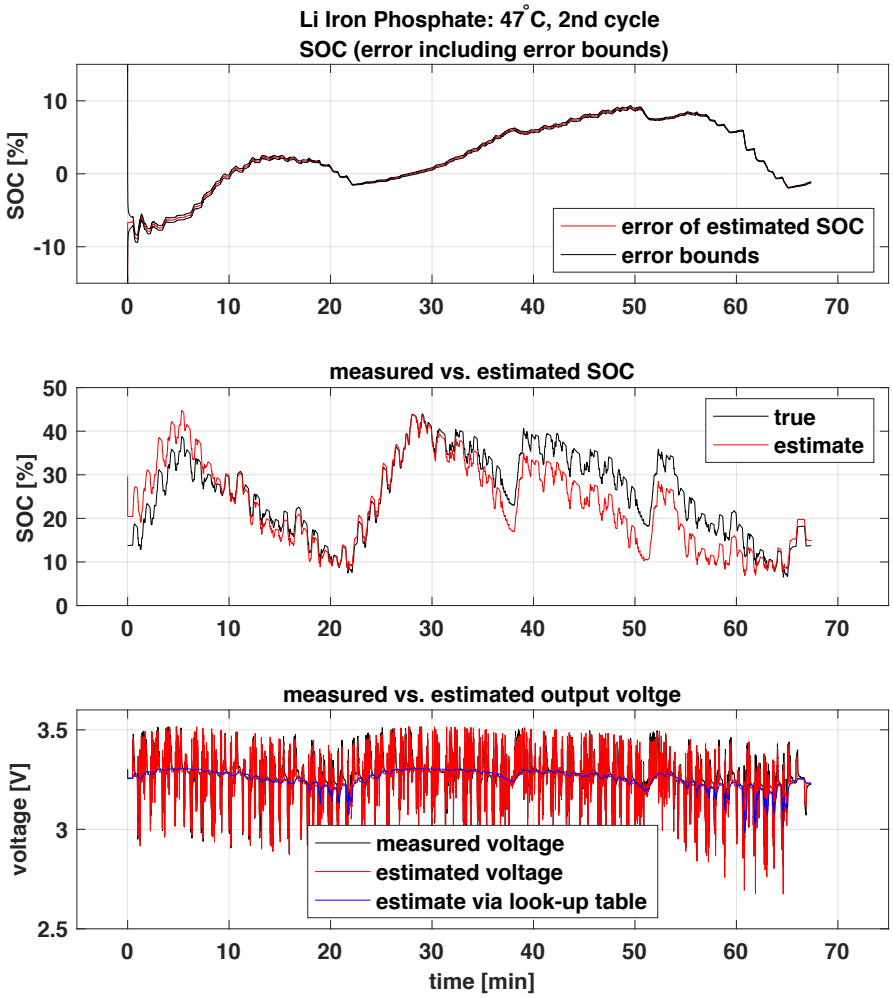

Figure 7.25: LiFePO, SM, test-cycle. Measured and estimated output voltage and SOC. Figure 7.26 shows the first five minutes of the same data in detail.

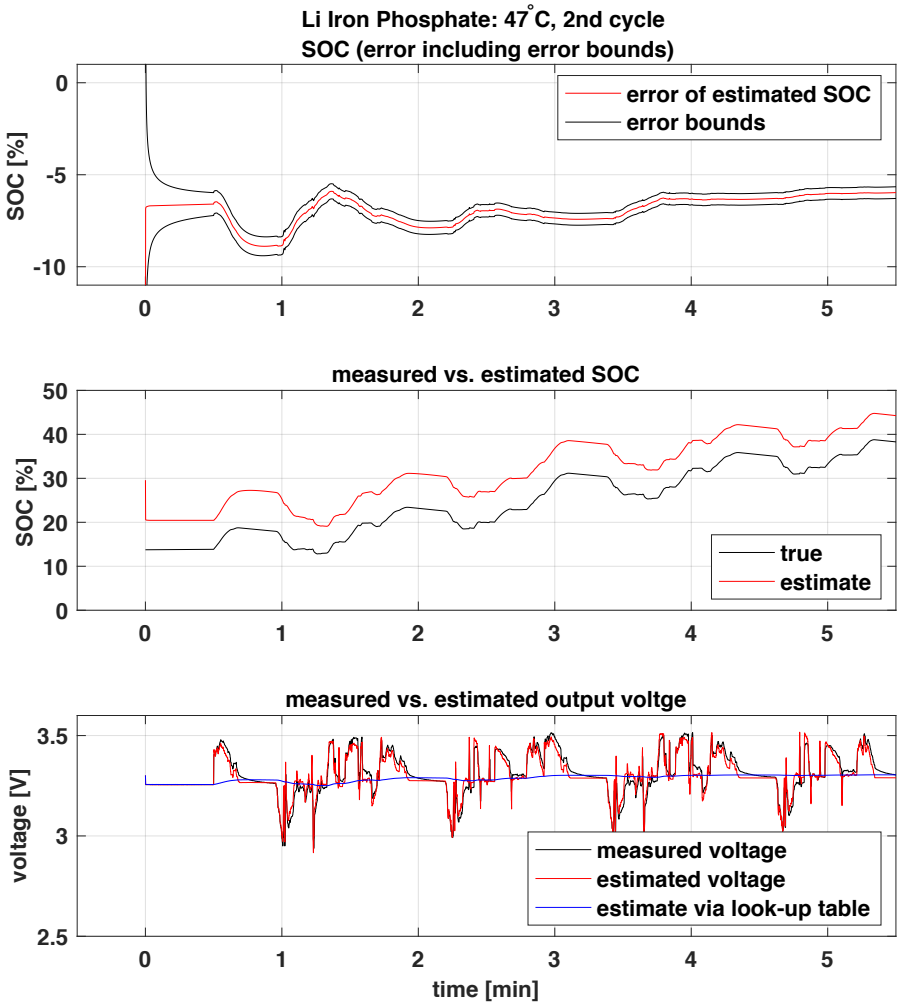

Figure 7.26: LiFePO: Detailed zoom of Figure 7.25.

Figure 7.27 shows that the simple model doesn't take hysteresis effects into account. The estimated output voltage results in a constant value (red line of the bottom plot) between minute 0.7 and minute 0.9 whereas the measured output (black line) is slowly declining to that voltage level. SOC stays constant within that interval.

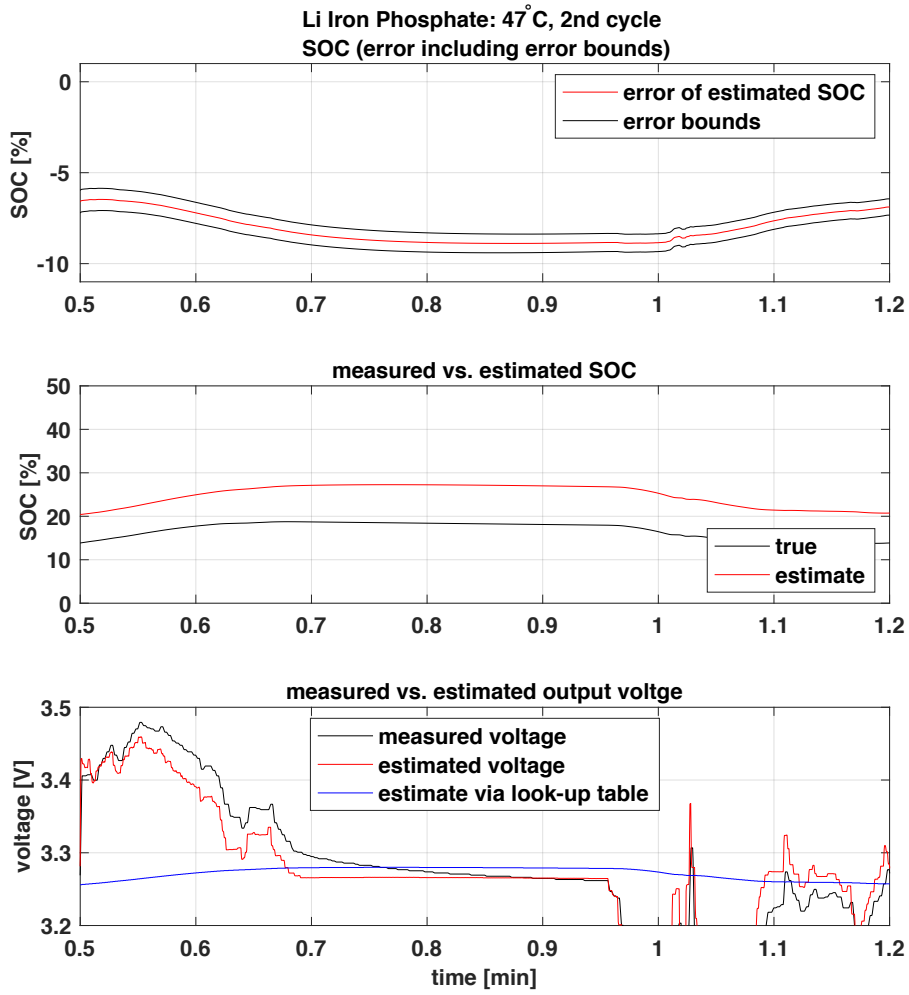

Figure 7.27: LiFePO: Measured and estimated output voltage and SOC. No hysteresis effect modeled.

Zero-State Hysteresis Model

Parameters are identified using least squares estimation, for the identified values see Table 7.1. Process and measurement noise of the EKF are set to: $Q = 0.001^2, R = 0.1^2$. There's no significant improvement to the SM from the previous section evident.

During testing the state variable is monitored and reset to 50% SOC if it exceeded its physically reasonable bounds of 0% resp. 100% SOC. Parameter estimation and testing for the ZSHM model takes about 100 seconds.

Figures 7.28 and 7.29 show the second cycle of the test-cycle at $47°C$, where in the latter only the trend during the first five minutes is shown. In the case of the LiFePO pack, the filter converges much slower than with LiTi (see Figure 7.12). This may be caused by inaccuracies of the OCV LUT and the shape of the OCV characteristic which shows a plateau from 35% SOC to about 70% SOC.

In order to avoid the plateau and its ambiguous values from the LUT, the intend was to shift the load profile to lower capacity regions of the battery pack where the OCV characteristic is linearly increasing. Compare Figure 6.5 in Section 6.5. The favorable interval to this intend would lie within approximately 13% SOC to 35% SOC. But in Figure 7.28 it can be seen, that the load of the test-cycle exceeds this interval, namely from lower than 10% SOC to more than 40% SOC.

Close to 0% SOC and close to 100% SOC, data isn't reliable anyways[8], that's why battery packs typically are used within a range from 25% to 75%. In Figure 6.5 this can be deduced from the steeply sloping OCV-characteristic for SOC-levels lower than approximately 13% and may cause estimation errors of the SOC (since the bias i.e the estimate from the LUT is less reliable). Ambiguous SOC values for $y_k > 3.3V$ may also provoke bad state estimates.

[8] Personal conversation at Magna E-Car.

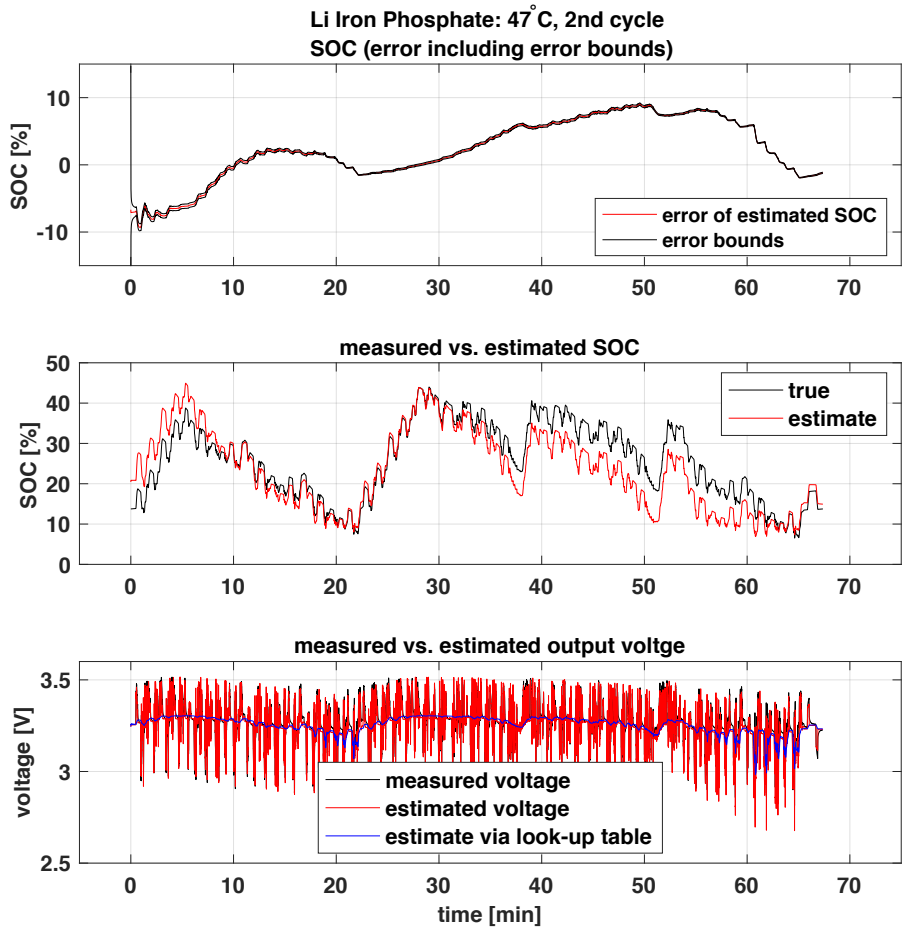

Figure 7.28: LiFePO, SM, test-cycle. Measured and estimated output voltage and SOC. Figure 7.26 shows the first five minutes of the same data in detail.

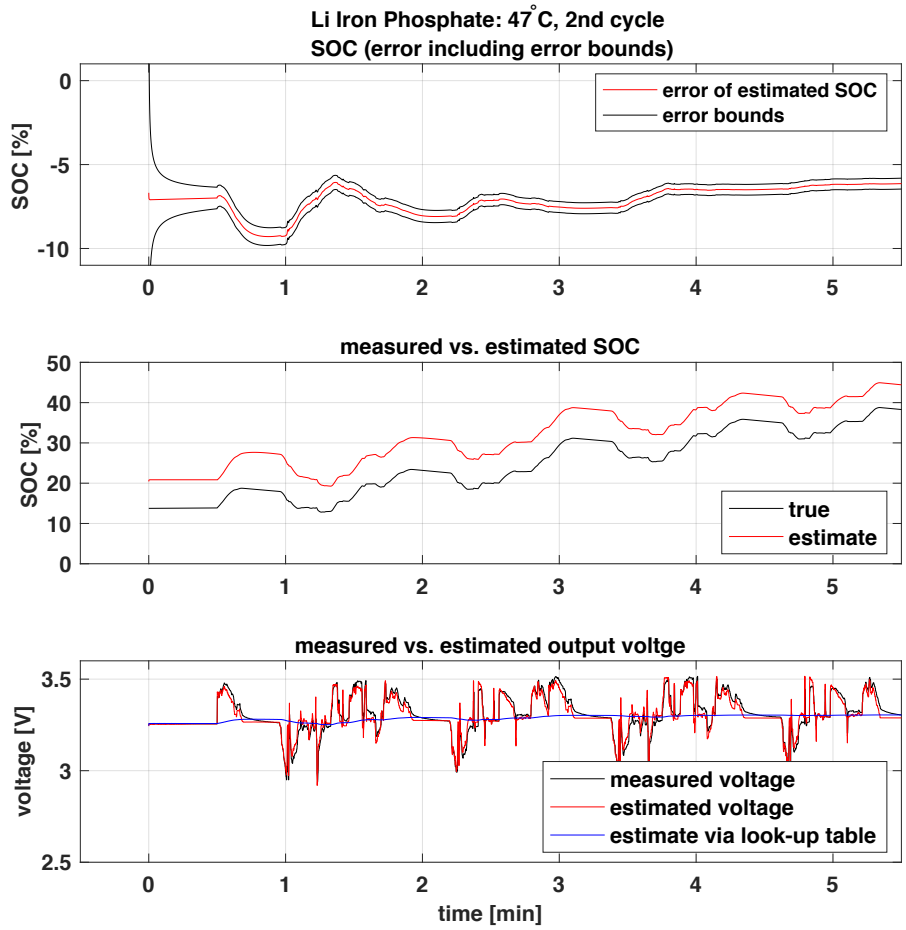

Figure 7.29: LiFePO: Detailed zoom of Figure 7.28.

One-State Hysteresis Model

The OSHM parameters are initialized and identified like earlier described for the LiTi-cell (section 7.3.1), except the measurement noise and process noise which are set to $R = 0.1^2$, $Q = 0.001^2$ for state modeling (system identification: $R = 0.5^2$).

The maximum polarization M of the LiFePO-cell is much greater than the maximum polarization of the LiTi-cell, thus during parameter identification it is only restricted to $\pm 10\%$, R is supposed to stay within $1m\Omega \leq R \leq 2m\Omega$. During modelling, the hysteresis voltage is limited to two times the maximum polarization.

Parameter estimation and testing takes about 110 seconds. The performance of the model is shown in Figures 7.30 and 7.31. Since LiFePO shows hysteretic behavior, the hysteresis state takes plausible values in contrast to modeling the LiTi-cell with the same model (see Figure 7.15). Possible causes of inaccuracies of the estimate are discussed in the previous paragraphs on SM and ZSHM.

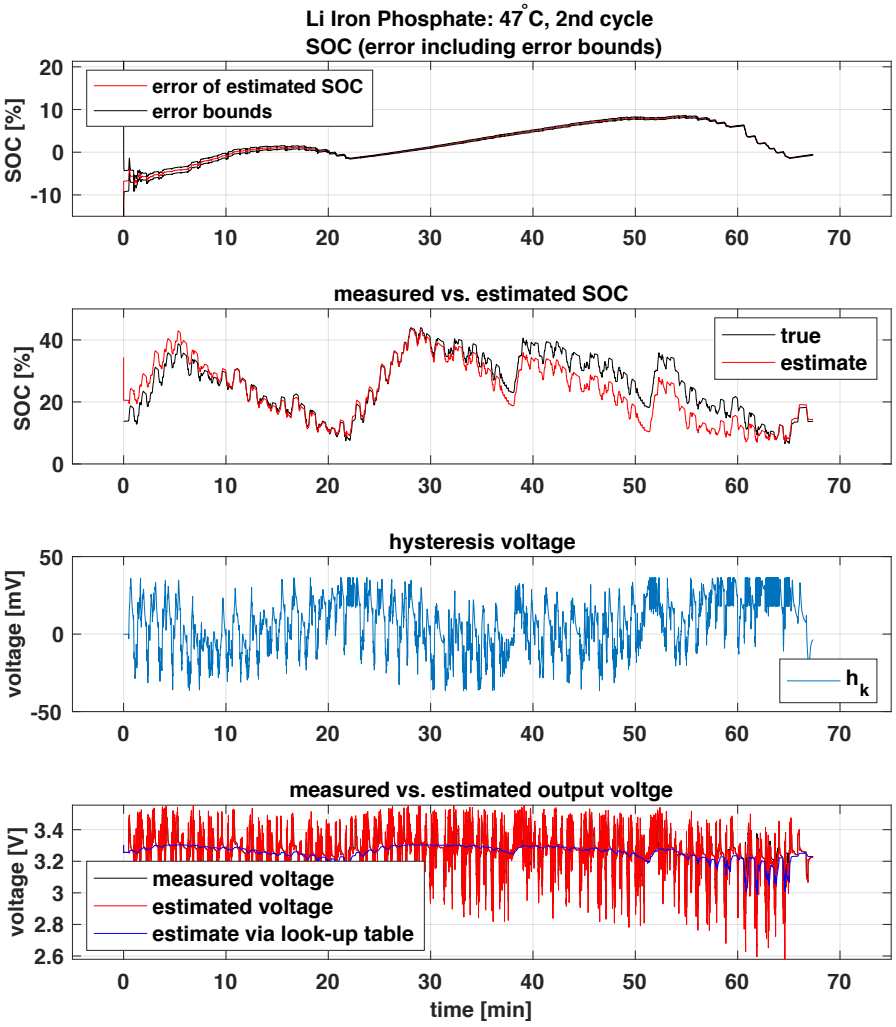

Figure 7.30: LiFePO, OSHM, test-cycle. Measured and estimated output voltage and SOC. Figure 7.31 shows the first five minutes of the same data in detail.

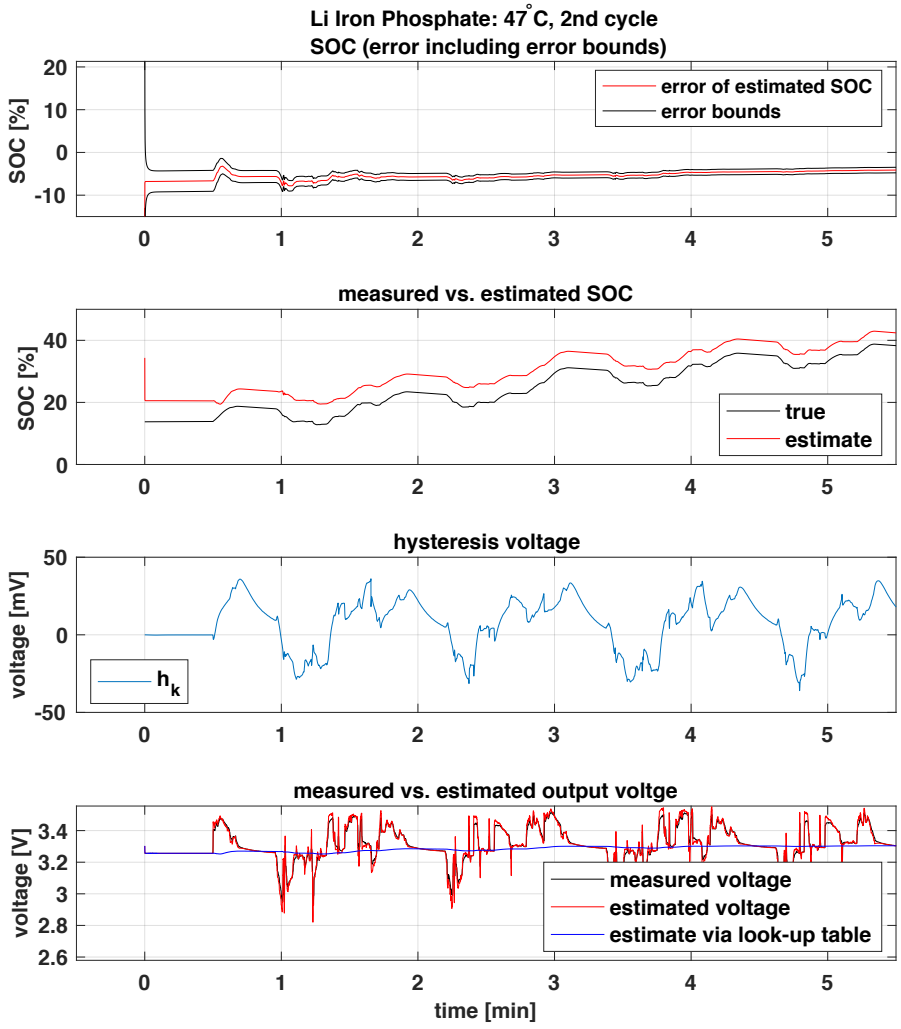

Figure 7.31: LiFePO: Detailed zoom of Figure 7.30.

The success of modeling the hysteresis effect can be seen in Figure 7.32 which is a detailed zoom of Figure 7.30 and covers the same interval as Figure 7.27. The estimated output voltage declines similar to the measured output voltage within the interval of 0.7 to 0.9 minutes. The estimate of the LUT is constant during that interval, but the hysteresis voltage is decreasing which causes the estimated output to decrease as well. Compare Figure 7.27 which shows the behavior of the output voltage when modeling was done using a model (i.e. the SM) which doesn't take hysteresis effects into account.

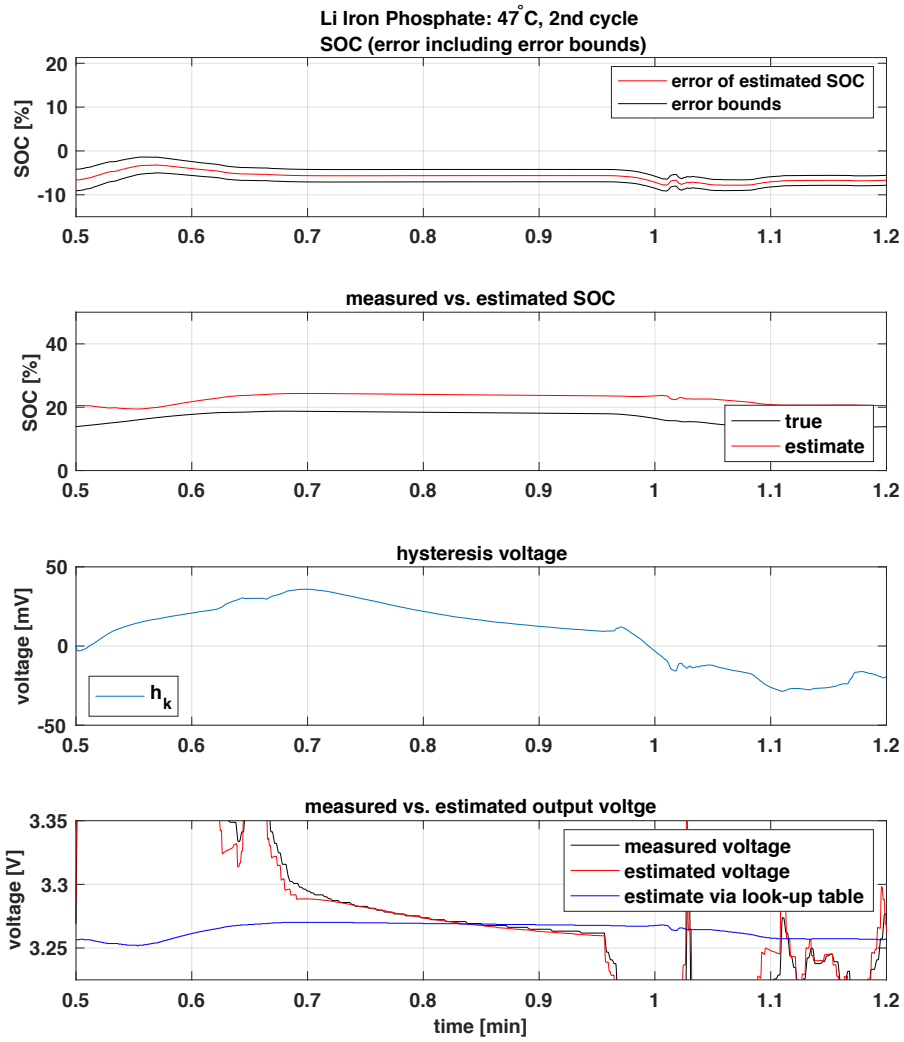

Figure 7.32: LiFePO: Measured and estimated output voltage and SOC. Hysteresis effect modeled.

Enhanced Self-Correcting Model

System identification is done as described for the LiTi-cell in section 7.3.1. For parameter estimation a measurement error of $R = 0.5^2$ was assumed, during testing, the measurement error was set to $R = 0.1^2$.

The ESCM converges fast to a good estimate of SOC but faces the same issues as the other models due to erroneous training / test / OCV data. It is to point out that this model predicts the SOC best but at the same time the predicted output value y_k overshoots the measured output value multiple times. This can be seen in Figure 7.33 and Figure 7.34 where the performance of the model is shown.

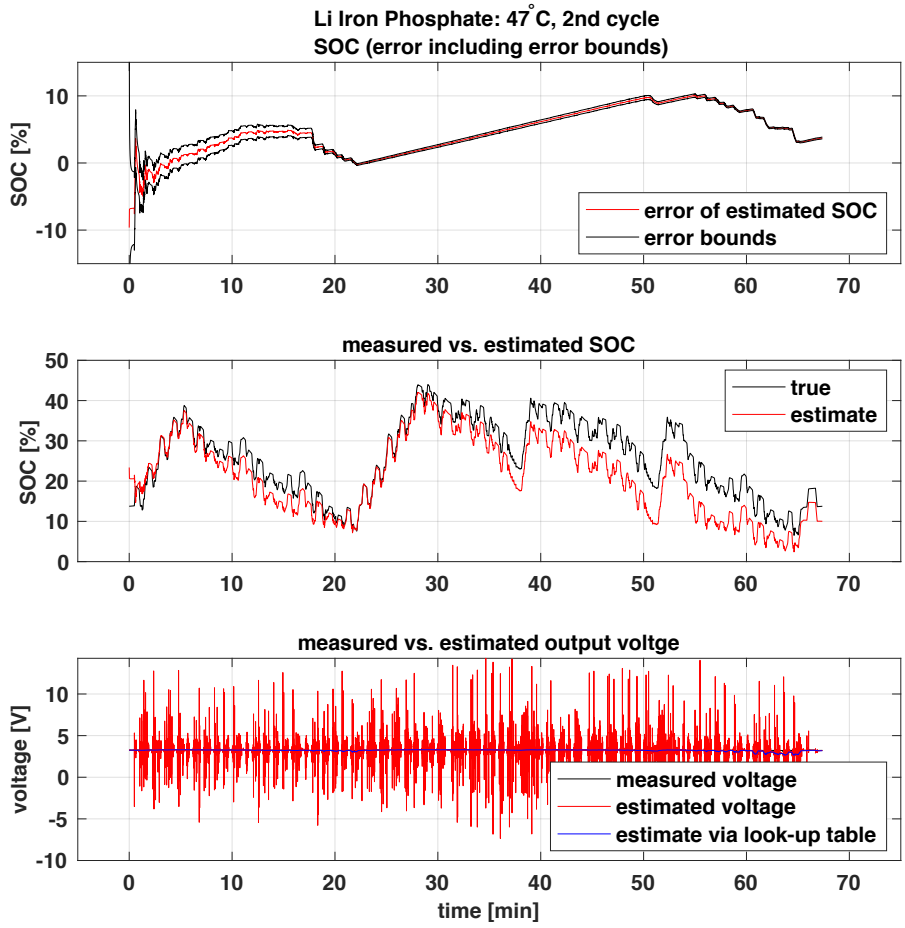

Figure 7.33: LiFePO, ESCM, test-cycle. Measured and estimated output voltage and SOC. Figure 7.34 shows the first five minutes of the same data in detail.

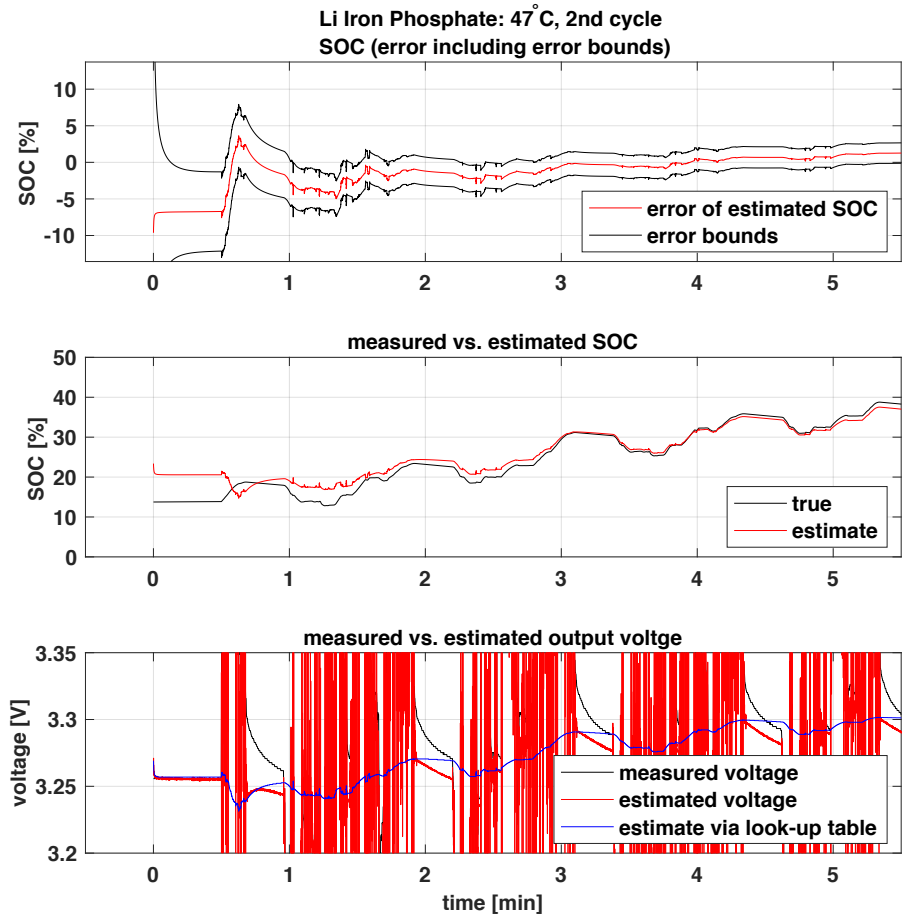

Figure 7.34: LiFePO: Detailed zoom of Figure 7.33.

Chapter 8

Discussion and Future Work

This work shows that battery modeling by means of statistical models is a promising approach for SOC estimation. Especially within the field of HEV where a battery pack is constantly charged and discharged during use, an accurate estimate of SOC is required for the BMS to operate safe. Battery modeling by means of statistical models can fulfill that requirement. Dynamic effects like hysteresis can easily be factored in and lead to better estimates.

It also demonstrates the importance of reliable data for system identification. If the identified model parameters are appropriate, the EKF is robust even to poor initialization and converges fast.

Basic prerequisite is good knowledge of the cell's behavior and an accurate OCV-characteristic. That knowledge can be drawn from interpreting data from standard cell tests, detailed insights on the cell are not necessary. As this is the only information needed and to rely on, it emphasizes the importance of reliable cell data.

Basically this approach is feasible for every cell type, but not all cell types are equally well suited. Cell types that show a monotonically increasing OCV-characteristic within the middle range of SOC seem to be the best choice.

Since the main part of all models consists of the rough estimate by looking up the OCV-characteristic, the models only differ in the way they are able to enhance this estimate. Furthermore not every possible enhancement seems to provide the expected improvement. For example in the case of the LiTi-cell which does not show much hysteretic behavior, adding an additional state variable to adapt hysteretic voltage does not have big influence on the resulting estimate but makes the model way more complex, where on the other hand the same model is promising for the LiFePO-cell.

For further investigation it would be interesting to set up a model for LiTi, which emphasizes the relaxation effect but ignores the hysteresis effect. Moreover, since system identification via least squares seems to lead to more reliable values of the cell's internal

resistances for charge and discharge, it could be of interest, forcing the EKF to those resistance values when doing system identification using the EKF. Another approach would be treating the internal resistance in general not as constant values for charge and discharge but dependent on temperature (those measurements are available) and SOC.

For the LiFePO-pack, acquisition of new test and OCV data would be good in order to serve as proof of the assumptions that have been made in this work concerning the performance of the EKF. If a highly accurate OCV-test is feasible, it would be worth a try using test cycle data which load profile is located within a higher range of SOC. Based on this new insights, better assumptions concerning the models and parameter identification could be made.

And last but not least, generating training sets from data from different driving cycles i.e. load profiles would lead to better parameterization of the models. Thus potentially over-fitting to a certain test-cycle behavior could be eliminated. For the LiTi-pack at least test data at different temperatures with different initial conditions was available (but always of the same cycle), but for the LiFePO-pack test data and life-cycle data was only recorded at 47°C.

Bibliography

[1] D. Andrea, *Battery Management Systems*. ARTECH HOUSE, 2010.

[2] H. J. Bartsch, *Taschenbuch Mathematischer Formeln*, 17th ed. Fachbuchverlag Leipzig im Carl Hanser Verlag, 1997.

[3] R. Bauer, "Zustandsschätzung und Filterung," Arbeitsblätter zur Vorlesung, Institut für Regelungs- und Automatisierungstechnik, TU Graz, 2007.

[4] J. Cao, N. Schofield, and A. Emadi, "Battery balancing methods: A comprehensive review," in *Vehicle Power and Propulsion Conference, 2008. VPPC '08. IEEE*, sept. 2008, pp. 1 –6.

[5] N. Chaturvedi, R. Klein, J. Christensen, J. Ahmed, and A. Kojic, "Algorithms for Advanced Battery-Management Systems," *Control Systems, IEEE*, vol. 30, no. 3, pp. 49 –68, june 2010.

[6] R. Cope and Y. Podrazhansky, "The art of battery charging," in *Battery Conference on Applications and Advances, 1999. The Fourteenth Annual*, 1999, pp. 233 –235.

[7] W. Dreyer, J. Jamnik, C. Guhlke, R. Huth, J. Moskon, and M. Gaberscek, "The thermodynamic origin of hysteresis in insertion batteries," *Nat Mater*, vol. 9, no. 5, pp. 448–453, 05 2010.

[8] W. Dreyer, C. Guhlke, and R. Huth, "The behavior of a many-particle electrode in a lithium-ion battery," *Physica D: Nonlinear Phenomena*, vol. 240, no. 12, pp. 1008 – 1019, 2011.

[9] E. Hering, M. Stohrer, and R. Martin, *Taschenbuch der Mathematik und Physik*, 5th ed. SrpingerLink (Online service), 2009.

[10] M. Horn and N. Dourdoumas, *Regelungstechnik. Rechnerunterstützter Entwurf zeitkontinuierlicher und zeitdiskreter Regelkreise*, 1st ed. Pearson Studium, 2004.

[11] E. Kreyszig, *Advanced Engineering Mathematics*, 8th ed. John Wiley & Sons, Inc., 1999.

[12] B. Y. Liaw, G. Nagasubramanian, R. G. Jungst, and D. H. Doughty, "Modeling of lithium ion cells - A simple equivalent-circuit model approach," *Solid State Ionics*, vol. 175, no. 1âĂŞ4, pp. 835 – 839, 2004, fourteenth International Conference on Solid State Ionics.

[13] S. Piller, M. Perrin, and A. Jossen, "Methods for state-of-charge determination and their applications," *Journal of Power Sources*, vol. 96, no. 1, pp. 113 – 120, 2001, proceedings of the 22nd International Power Sources Symposium.

[14] G. L. Plett, "Extended Kalman filtering for battery management systems of LiPB-based HEV battery packs: Part 1. Background," *Journal of Power Sources*, vol. 134, no. 2, pp. 252 – 261, 2004.

[15] ——, "Extended Kalman filtering for battery management systems of LiPB-based HEV battery packs: Part 2. Modeling and identification," *Journal of Power Sources*, vol. 134, no. 2, pp. 262 – 276, 2004.

[16] ——, "Extended Kalman filtering for battery management systems of LiPB-based HEV battery packs: Part 3. State and parameter estimation," *Journal of Power Sources*, vol. 134, no. 2, pp. 277 – 292, 2004.

[17] D. Simon, *Optimal State Estimation: Kalman, H[infinity], and nonlinear approaches*. Jon Wiley & Sons, 2006.

[18] R. M. Spotnitz, "Battery Modeling," *Interface, ECS (The Electrochemical Society)*, vol. 14, no. 4, pp. 39 – 42, winter 2005.

[19] G. Welch and G. Bishop, "An Introduction to the Kalman Filter," *Design*, vol. 7, no. 1, pp. 1–16, 2001.